EXPERIMENTAL INVESTIGATION OF THE EFFECT OF ETHANOL AND BIO-DIESEL BLENDED DIESEL FUELS ON COMBUSTION BEHAVIOR AND EMISSION CHARACTERISTICS OF COMMON RAIL DIRECT INJECTION DIESEL ENGINE

PHYO WAI

A THESIS REPORT SUBMITTED IN PARTIAL FULFILLMENT

OF THE REQUIREMENTS FOR THE DEGREE OF

MASTER OF ENGINEERING IN AUTOMOTIVE ENGINEERING

SCHOOL OF ENGINEERING

KING MONGKUT'S INSTITUTE OF TECHNOLOGY LADKRABANG

YEAR 2023

KMITL-2023-EN-M-047-011

THESIS TITLE	Experimental Investigation of Effect of Ethanol and Biodiesel on Combustion Behavior and Emission Characteristics of Direct Injection Diesel Engine
STUDENT	Phyo Wai
STUDENT ID	63601184
DEGREE	Master of Engineering
PROGRAM	Automotive and Advanced Transportation Engineering systems
THESIS ADVISOR	Assoc. Prof. Dr. Preechar Karin
CO-THESIS ADVISOR	Dr. Nuwong Chollacoop
CO-THESIS ADVISOR	Prof. Dr. Hidenori Kosaka

ABSTRACT

Fossil fuel shortage and greenhouse gas emissions have forced to increase research efforts on liquid renewable biofuels like bioethanol and biodiesel as partial replacement of diesel fuel. Moreover, the blending of three fuels (diesel, biodiesel and ethanol) referred as ternary blends are also popular due to the compensatory effects of one to another and its more renewable portion in the blend. Therefore, this work aims to study the impact of biofuels (biodiesel and ethanol) over the combustion, emissions, and thermal efficiency of diesel engine.

Ten different fuel blends are tested on a common rail direct injection diesel engine coupled with the eddy current dynamometer. The tested engine is a four-cylinder, three-liter direct injection diesel engine. The engine was not modified for the experiment. The tested fuel blends are B10 (10%vol biodiesel with 90%vol diesel), B20 (20%vol biodiesel with 80%vol diesel), B100 (100% biodiesel), B10E5 (5%wt ethanol with 95%wt B10), B10E10 (10%wt ethanol with 90%wt B10), B20E5 (5%wt ethanol with 95%wt B20), B20E10 (10%wt ethanol with 90%wt B20), B20E20 (20%wt ethanol with 80%wt B20), B100E5 (5%wt ethanol with 95%wt B100) and B100E10 (10%wt ethanol with 90%wt B100). The experiment was performed under three engine speeds of 1000 rpm, 1500 rpm, and 2000 rpm corresponding with four constant engine torques of 56 Nm, 84 Nm,112Nm, and 140 Nm.

The findings demonstrate that the premixed combustion pressure and heat release rate peaks of ethanol-biodiesel-diesel ternary blended fuels are higher. The cumulative heat release of ethanol blended fuels is also higher for ethanol blended fuels despite of the shorter combustion duration. The fuel consumption increased with the ethanol and biodiesel portion in the blended fuels while there were no losses of brake thermal efficiency. The air fuel equivalent ratio increased with ethanol and biodiesel portion in blends. The exhaust temperatures of based fuels are higher than that of blended fuels. It's clearly observed that the particle emission could be reduced while nitrogen oxides emission increased with the ethanol and biodiesel percent increased. Moreover, when ethanol is added to the diesel fuel, the emitted soot particles are easy to oxidize, and the agglomerate size is smaller because of the increased oxygen availability in the exhaust.

Keywords: Biofuel, Diesel-biodiesel-ethanol blends, Combustion, Emission, Diesel engine.

ACKNOWLEDGEMENTS

Firstly, I would like to acknowledge to my parents, the Ministry of Industry, Myanmar, and Thailand for giving a chance of further study in abroad to study automotive engineering course for the Master of Engineering.

I would like to express the deepest appreciation to my thesis main advisor, Assoc. Prof. Dr Preechar Karin, who kindly supported me for providing great academic advice during the whole thesis period, and genuinely thankful for everything.

I would like to express special thanks to my co-advisors, Prof. Dr. Hidenori Kosaka from School of Engineering, Tokyo Institute of Technology, Japan and Dr Nuwong Chollacoop from National Science and Technology Development Agency (NSTDA), Thailand, really appreciate for kindly advised me to meet great research.

Finally, I would like to thank all KMITL Laboratory members and special thanks to My friends (Mr. Ban-Seok Oh and Mr. Liu Hai) for giving me suggestions and helping during the experiments.

Phyo Wai
16/11/2022.

TABLE OF CONTENTS

LIST OF TABLES

LIST OF FIGURES

Chapter 1

INTRODUCTION

1.1 Background and Challenges

There are two kinds of energy sources like renewable and non-renewable energy source. The term non-renewable energy sources include coal, petroleum, and natural gases, but on the other hand, the renewable energy sources are solar, winds, hydro energy and green biofuels which produced from animal fats and crops. Nowadays, energy consumption around the world is increasing dramatically because of rising population. However, this book is especially subject to reduce fossil fuel usage by on-road vehicles by partially substitution with ethanol and biodiesel. This research challenge originated from the depletion of fossil fuels around the world and emissions of greenhouse gases especially carbon dioxide from the production and burning of fossil fuels. According to the report of the Department of Alternative Energy Development and Efficiency (DEDE) Thailand, around 40% of total energy consumption was consumed by the transportation sector. In 2020, the demand for diesel fuel increase 5.7% in Thailand than diesel demand in 2016. In addition, the road vehicles consumed around 50% oil and it is increased 19% from 1973 to 2018 within 45 years. Therefore, to recover energy shortage problem became one of the big challenges around the world.

Because of the former problems, the liquid biofuels which derived from the edible and non-edible feedstocks was become popular among the researchers of energy related fields because of its renewability and emissions reduction. For example, the di-methyl esters biodiesel could be fueled in CI engines by partially or totally (100% biodiesel) without reducing the engine efficiency. This was proved by many researchers. Nevertheless, biodiesel could not produce as much as demand due to losing of human food stocks and higher cost of production. Therefore, bioethanol, which production cost is much cheaper than the biodiesel production and can be produced from the variety of feedstocks such as sugarcane, cassava, and molasses, was added to the diesel fuel. In addition, the ternary blended fuels (diesel-biodiesel-bioethanol blends) increased the renewable energy portion of blends and reduced the emissions of smokes and particulate matters emissions.

In addition, the biofuels show negative carbon dioxide emissions because of carbon neutral process (**Figure 1-1**). The biodiesel and ethanol are produced from the plants, and these are burned out inside the internal combustion engines. The main products form the ICE engines are carbon dioxide, water, and nitrogen. Then, the plants used carbon dioxide, water, and sun light to growth again. Finally, the leaves or fruits or seeds of plants (e.g., grasses, algae, and jatropha) are used to produced biodiesel and ethanol.

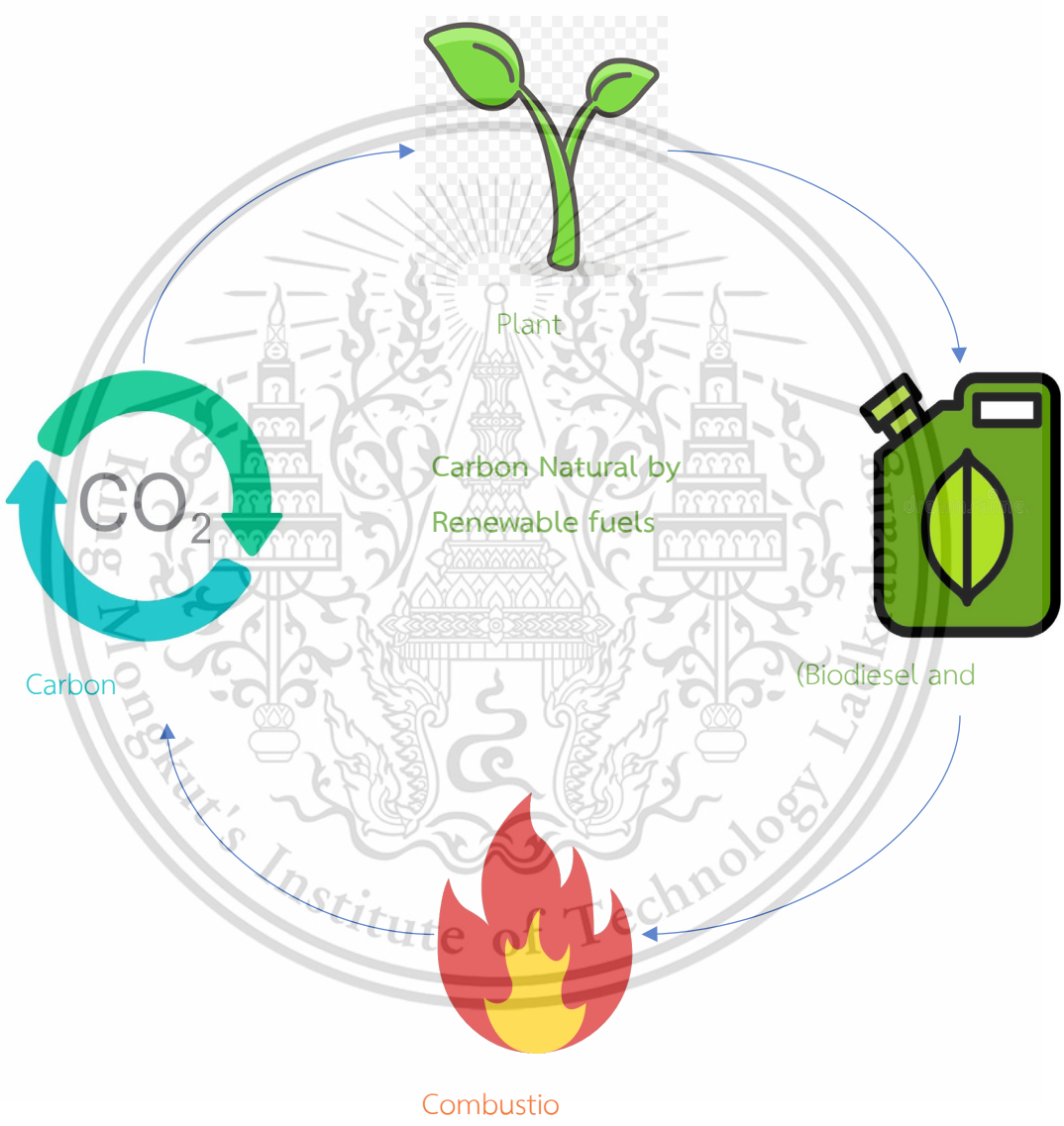

Figure 1-1 Carbon neutral process

1.2 Objectives

- To investigate feasibility to use ethanol in a compression ignition engine by blending it with diesel fuel, called diesohol,

- To facilitate biofuel market management by increasing biofuel (both ethanol and biodiesel) from diesel sector, and,
- To analyze the impact of ethanol on the compression ignition engine's combustion and emissions fueled with ternary blended (diesel- biodiesel-ethanol) fuel.

1.3 Scope of the Work

This study mainly subjected on the impact of ethanol and biodiesel from ternary blended fuels on the combustion, engine performance and emissions of common rail direct injection diesel engine. The ten different blends were prepared in different portions of diesel, biodiesel and ethanol and tested on the ISUZU D-max engine and eddy current dynamometer test bed. Engine load, revolution, and fuel consumption are recorded to analyze the engine performance parameters and moreover, in-cylinder pressure and crank angle degree are measured to study combustion. On the other hand, emissions were measured by AVL exhaust gases analyzer and PMs are collected on the filter paper and measured smoke intensity with the help of BOSCH smoke intensity meter. Then, particle size analysis was also performed.

CHAPTER 2

Literature Review

2.1 Renewable Biofuels

The term "renewable biofuels" includes biofuels that are derived from the renewable sources of both edible feedstocks (palm, sugarcane, animal fats, etc.) and non-edible feedstocks (jatropha, used cooking oil, etc.). Generally, the type of biofuel can be distinguished into three groups, such as gaseous (biogas), liquid (biodiesel, ethanol, and so on) or solid, based on the physical states. Among renewable energy sources, liquid biofuels provide several noteworthy benefits:

1. They are portable, easy to store and readily available [1],
2. They could significantly diminish emissions of carbon dioxide and particulate matter when compared to petroleum fuels [2], [3],
3. They could aid nations in varying their energy supplies, boosting energy security, and stabilizing energy markets [4], and,
4. With their cyclical process from energy crop farming to production, they might create a new circular economy [5], [6].

Until present time, three generations of biofuels had had been emerged depend on the type of feedstocks. The first-generation biofuels are directly produced from the food crops such as soybeans, sugar cane, corn, wheat, and vegetable oils ([7], [8]). The second-generation biofuels differ from the former that their feedstocks are non-edible, nevertheless these are lignocellulosic biomasses or other biomass wastes ([9], [10]). Switchgrass, miscanthus, Indian grass, seed crops (jatropha and camelina, oil palm, and rapeseed), waste vegetable oil (WVO), and municipal solid waste (MSW) (including landfill gas, excess sludge from wastewater purification, grass, and yard clippings) are some of the most widely used second generation feedstocks ([11], [12]). The most popular and updated third-generation biofuels are derived from the algae and microalgae and hence sometimes called as algae-derived biofuels. However, the major downside of algae-derived fuels is that they need a huge amount of water and

nutrients to grow [13]. Yang et al. calculated that 3726kg of water as well as 0.33kg and 0.71kg of N and P are required to get 1kg of biodiesel from microalgae [13].

The two primary first-generation biofuels that are widely employed as additives in the global transportation sector are biodiesel and bioethanol [14]. Biodiesel mainly contains fatty acids methyl-esters which could be produced from both edible and non-edible oils. It could be applied to conventional diesel engine as directly or blending with diesel fuel because its physical and chemical properties are similar to those of conventional diesel. Moreover, it is more environmentally sustainable than fossil fuels, due to lower carbon dioxide and PMs emissions ([15], [16]). In Thailand, biodiesel is produced from plum oil by transesterification process [17].

One of the most promising alcohol-based biofuels on the market right now is bioethanol because it can be produced from agricultural crops, and it emit fewer toxic by-products (i.e., acetaldehyde, acetic acid) during the incomplete combustion than other alcoholic biofuels [18]. The basic chemical formula of bioethanol is CH_3CH_2OH, and its main feedstocks is sugarcane. Ethanol, which contain oxygen molecules, could promote combustion to cleaner combustion although its energy content is lower than fossil fuels [19]. Therefore, it was utilized as common additive to gasoline fuel in different concentrations. In addition, the production of ethanol from sugarcane includes three steps which are sugar extraction, fermentation, and product purification (**Figure 2-1**). The fermented ethanol from sugarcane juice is purified commonly by distillation, followed by the rectification and dehydration processes [18].

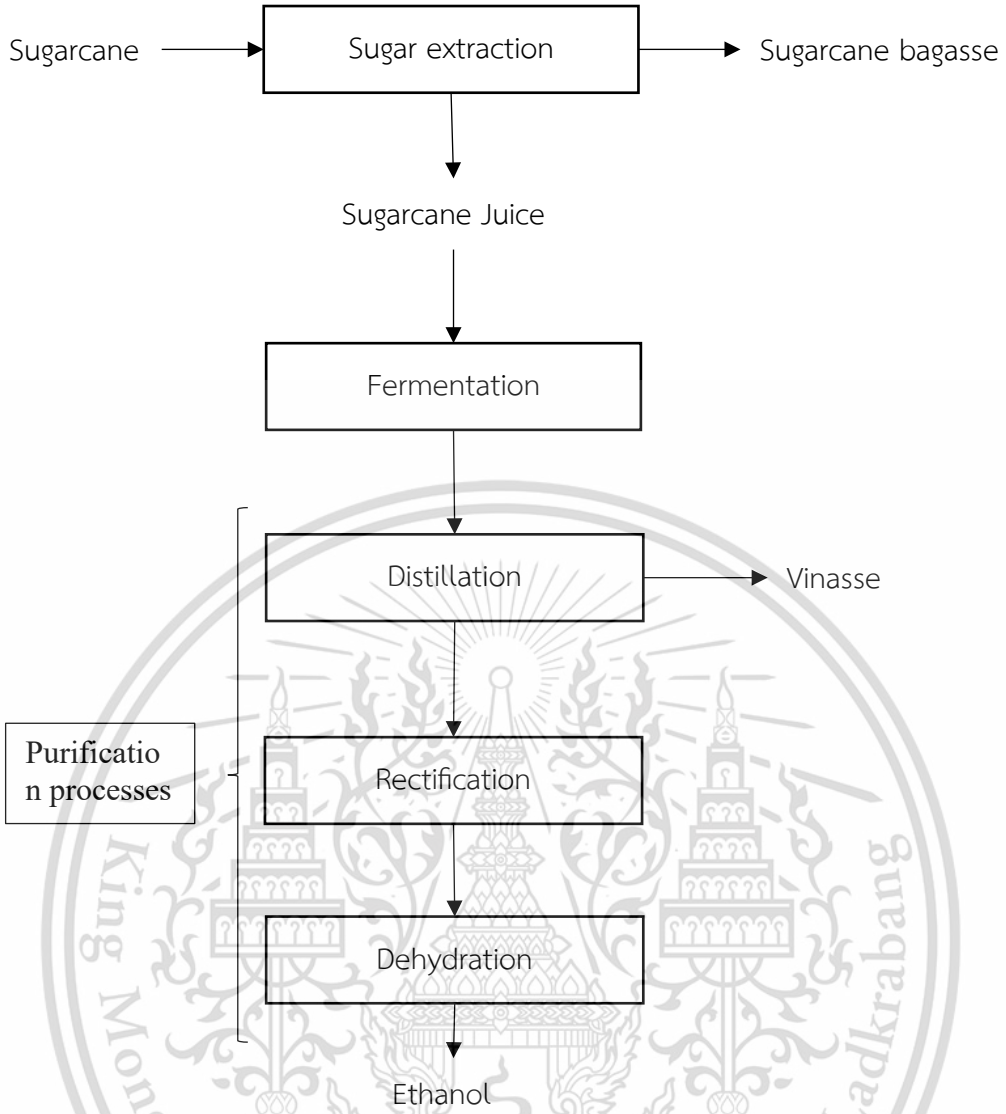

Figure 2-1 Scheme of ethanol fermentation from sugar cane

2.2 Direct Injection Common Rail Diesel Engine

The term engine can be defined as a mechanism which convert chemical energy from hydrocarbon fuels into mechanical energy by combusting the fuels. Fundamentally, there are two types of combustion engine such as internal combustion engine and external combustion engine. The internal combustion engine generates the mechanical power from the burning of hydrocarbon fuel inside the engine. The most popular internal combustion engines, in the transportation sector, are spark ignition gasoline engine and compression ignition diesel engine because of their simplicity, ruggedness, high power to weight ratio, efficiency and low cost [20].

The internal combustion engine which are subject of this book is compression ignition diesel engine. Although it emits significantly higher amounts of nitrogen oxide

and particulate matters than gasoline engine, the demands of diesel engines remain considerable due to its higher power output and higher thermal efficiency. To pass the increasing stringency of the emission standards, emissions from the diesel engine could be lowered by three typical methods such as 1. Pre-treatment method (using oxygenated green fuels), 2. Engine combustion control method (using common rail injection system, pray pressure, swirl mixing, HCCI engine, etc.) and 3. Exhaust gases after treatment method (using DOC, DPF, catalytic DPF, etc.). Development of injection system to be more precise fuel delivery might reduce engine noise, exhaust gas emissions and fuel consumption [21]. Therefore, most of the modern diesel engine, which are used in automobiles, use common rail injection system.

2.2.1 Combustion behaviors in diesel engine

The combustion characteristics of DI diesel engines can be discussed with the analysis of in-cylinder pressure data. To understand the Internal combustion engine (ICE) combustion, the heat release rate analysis from the in-cylinder pressure is one of the important factors. The relationship between injection rate, in-cylinder pressure and net heat release rate (NHRR) are shown in **Figure 2-2**. The figure represents for multi-spray injection system. The start of injection (SOI) and the start of combustion (SOC) are identified by the variation in slope of the pressure profile. Around 5 crank angle degree (CAD) after the start of injection, the slope of pressure rises steeply for a few crank angle degrees, after that the pressure rise gradually to a peak value. The typical heat release rate curve is generally in that shape (**Figure 2-2**) for the multi spray direct injection engine. The interval between SOI and SOC is the ignition delay period which took around 5 CAD. Within that interval, 15CAD (SOI) to 20 CAD (SOC), the negative NHRR is observed due to heat transfer to the liquid fuel droplet, vaporizing and evaporating it, and heat transfer to the cylinder walls as well.

When the injected fuel droplets reach their combustible temperature, combustion starts. **Figure 2-3** presents the three phases of combustion on the Log P versus Log V graph as well as on the heat release rate versus crank angle graph. The phases are as follows:

I. Premixed combustion phase: it is from a to b. Some fuel droplets are already mixed with the air during the ignition delay period before start of combustion, then these are burnt when the mixture temperature reach to auto-ignition

temperature, as the first premixed combustion phase. The peak of heat release rate is occurred in this phase because of the combustion of fuel-rich mixture.

II. Diffuse combustion phase: it is from b to c. The flame of former premixed combustion phase is situated around each jet of the fuel spray and towards the downstream. During this period, however, the flame grows to enclose the jets, which later burn as a turbulent diffusion flame.

III. Late combustion phase: it is from c to d. Into the expansion stroke, heat release still going, but at a slower and decreasing rate. This is due to the burning of residual fuel which may not have burned or the soot which keep a fraction of fuel energy or fuel rich combustion products. This phase can promote to more complete combustion and cleaner engine out gases. The rate of this combustion phase also depends on the residual availability of oxygen molecules.

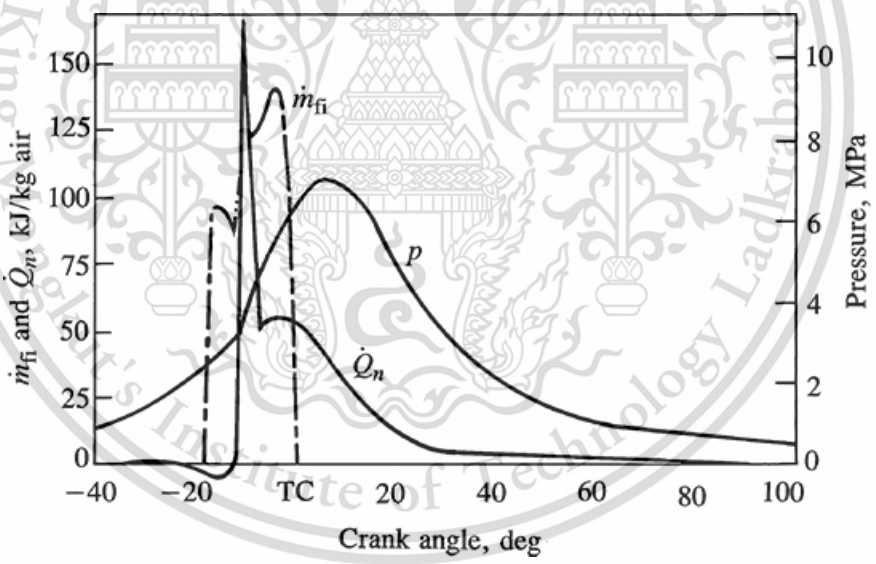

Figure 2-2 The relation between mass fuel injection, in-cylinder pressure and net heat release rate [20].

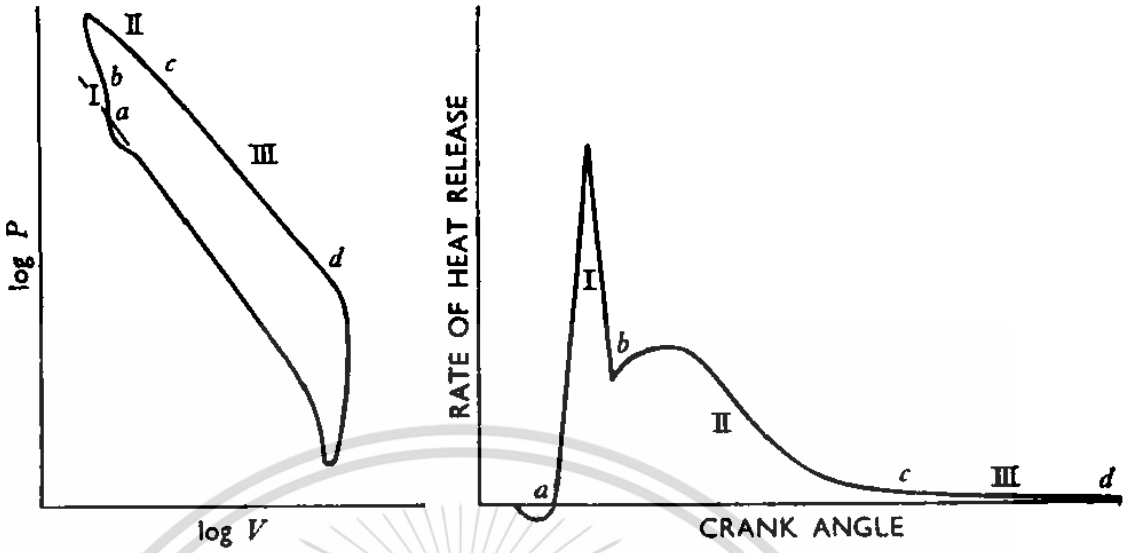

Figure 2-3 Phases of combustion in a DI diesel engine [22].

2.2.2 Emissions from the ICE engine

The products from the complete combustion of hydrocarbon fuel are carbon dioxide and water. However, as the byproducts of incomplete combustion, pollutant emissions were occurred. **Figure 2-4** reveals the estimated composition of diesel engine exhaust gases. It includes 67% of nitrogen (N_2) as the highest element in exhaust gases because of lean combustion. Then, it is followed by 12% of carbon dioxide (CO_2), 11% of water vapor (H_2O), 9% exceed oxygen (O_2) and approximately 1% of pollutant emissions. The pollutant emissions include carbon monoxide (CO), hydrocarbons (HC), nitrogen oxide (NO_x), Sulphur dioxide (SO_2), and particulate matter (PM).

The concentration of CO and HC is minimal in the pollutants of diesel engine exhaust gases. Both are mainly come from incomplete combustion. Carbon monoxide forms from the incomplete oxidation processes. In the fuel-rich zones, there is no insufficient oxygen to convert all the carbon into carbon dioxide and be formed CO concentration. However, CO is emitted under lean combustion as well due to the chemical kinetic effect [23]. On the other hand, HC emissions is a result of unburned fuel droplets. It might be because of two reasons generally. The injected fuel droplets are too big and hence cannot burn completely. The second is the fuel cannot burn completely in the low temperature zones which occur near the cylinder wall. HC emissions occur mainly at low load engine conditions. This is due to the lean fuel-air

mixing. In lean mixture, it's possible that the flame speeds are too slow to complete combustion during the power stroke, or combustion doesn't take place [24].

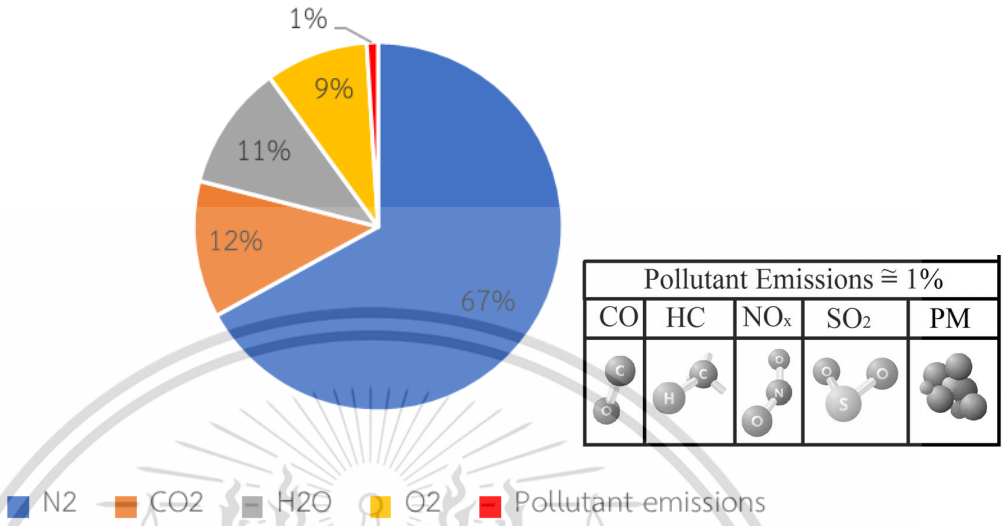

Figure 2-4 Estimate composition of DI diesel engine exhaust gases [25].

The air is composed of 79% nitrogen and 21% oxygen. Nitrogen is an inert gas normally, but it can react with oxygen and form NOx at high temperatures above 1600 °C. Therefore, the formation of NO_x depends on the combustion temperature, oxygen availability and reaction time [26]. NO_x consists of both NO and NO_2. As the first step of reaction, the oxygen combines with nitrogen and formed NO at high temperature, hence in the cylinder, 85 to 95 percent of NOx is made up of NO. It can then be oxidized to NO_2 in the atmospheric air. In addition, NO is a colorless and odorless gas, while NO_2 is a reddish-brown gas with the pungent odor [27].

PMs are originated from the accumulation of very tiny particles of fuel and lubricant that has partially burned, fuel oil's ash content, cylinder lube oil, or sulfates and water [28]. These are generally spherical shape with the diameter of 15-40 nm. The causes of PMs emissions in DI diesel engines are the sulfur and ash content of fuel, the quality and consumption of lubricant oil, combustion temperature and exhaust gases cooling, and so on [29].

Although diesel engine emits significant amounts of pollutants, these emissions can be reduced by applying emission control systems such as diesel oxidization

catalyst (DOC) to control CO and HC, diesel particulate filter (DPF) to filter PMs from exhaust gases and selective catalytic reduction (SCR) to control NO_x emissions [25].

2.3 Blending of diesel, biodiesel, and ethanol

Adding ethanol to the diesel fuel has several advantages over the combustion and emissions of DI diesel engine due to the oxygen content of ethanol. However, the major drawback of diesel and ethanol blending is the phase separation of two liquid. The blending temperature and water content of ethanol are the two key factors which degrade diesel-ethanol miscibility [30]. Therefore, a surface-active agent like Fatty acid methyl ester (biodiesel) can be used as co-solvents to avoid splitting of two liquids [31]. Less additive is needed to keep homogeneous mixture of diesel-ethanol blends in summer than winter.

Prommes Kwanchareon et al. studied the effects of ethanol purity on a diesel-biodiesel-ethanol blend at room temperature (**Figure 2-5**). In the investigation, different purities of ethanol (95% ethanol, 99.5% ethanol, and 99.9% ethanol) were used. In **Figure 2-5.a**, the 95% ethanol can also be referred to as hydrous ethanol, and fossil diesel cannot mix homogeneously because of the 5% water content in the ethanol. However, in the case of 99.5% and 99.9% purity ethanol, they could be blended into a clear one-phase liquid in any ratio (**Figure 2-5 b and c**). However, after three months, the mixtures that do not include biodiesel separate into two phases, while the mixtures with biodiesel content as a co-solvent are still in a homogeneous state. Biodiesel, which has polar heads and non-polar tails, can serve as an amphiphile by orienting its polar head with the ethanol and its non-polar tail with the diesel [32].

Different kinds of biodiesels can be applied as an emulsifier, a surfactant, or a surface-active agent to keep diesel and ethanol blends stable for long periods of time and at low temperatures. Moreover, the biodiesel has high cetane number, high viscosity, and high heating value. Therefore, adding biodiesel to the diesel-ethanol blend will compensate for the degradation of cetane number, fuel lubricity, and heating value and make it standard to use this ternary blend in the existing CI engines without any modification.

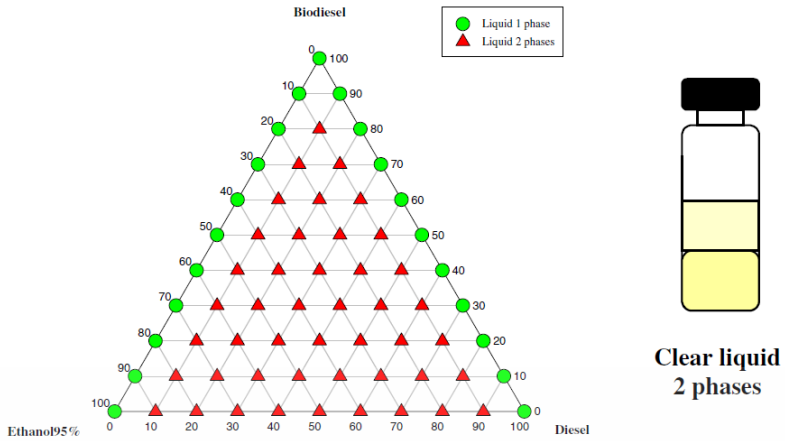

(a) Diesel-biodiesel-95%Ethanol at room temperature

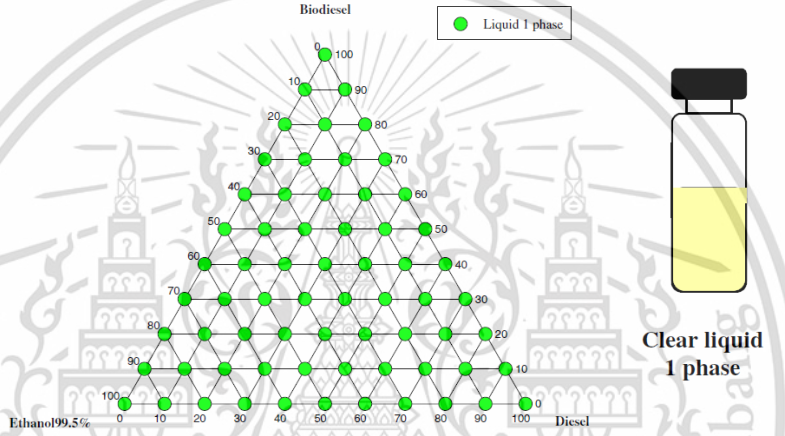

(b) Diesel-biodiesel-99.5%ethanol at room temperature

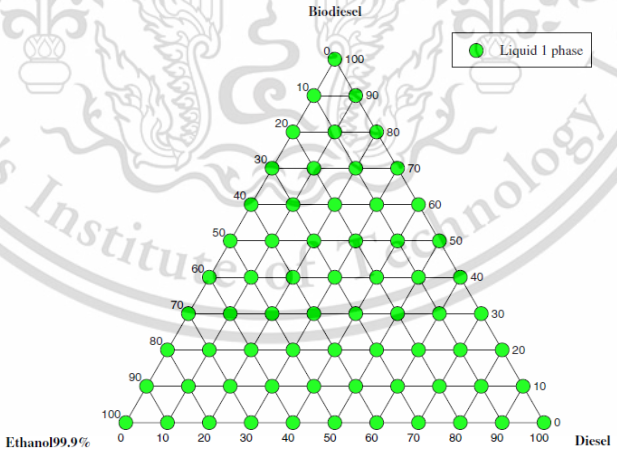

(c) Diesel-biodiesel-99.9%ethanol at room temperature

Figure 2-5 Phase triangle diagram of diesel, biodiesel and ethanol blends at room temperature using different purity of ethanol (a)95%, (b) 99.5% and (c) 99.9%. [32].

CHAPTER 3

RESEARCH METHODOLOGY

3.1 Research Apparatus

3.1.1 Engine

The engine used for the experiment is the ISUZU 4JJ1 TC engine. The **Figure 3-1** shows the actual photograph of tested engine after installed on the foundation of engine test room. The engine's specifications are listed in **Table 3.1**. It was produced by ISUZU motor company in 2005. And it is an in-line four-cylinder diesel engine. The total capacity of the engine is three liters, and it can produce maximum power of 107 kw at 3600 RPM and peak torque of 294 Nm within the engine speed range of 1400 RPM to 3400 RPM. The common rail injection system is mounted to get the high injection pressure. Moreover, the injection timing and pressure are controlled by electrically from Engine Control Unit (ECU). Therefore, the injection parameters could be varied according to engine speed and loads. It is included four valves per cylinder as two intake and two exhaust and open and closed by double overhead camshaft.

Figure 3-1 ISUZU 4JJ1 TC engine after installation for testing

The valve timings are also mentioned in **Table 3.1**. The Exhaust Gas Recirculation system reduced the NOx emissions by reducing the temperature of combustion. The output power of the engine is boosted by turbocharger by enhancing the intake air pressure. EGR could reduce the engine output power because of reducing maximum temperature of engine cycle. On the other hand, it is recovered back by turbocharger. The performance of tested engine is shown in **Figure 3-2** as power, torque, and engine speed graph.

Table 3.1 Tested engine specification

Parameter	**Value**
Model	Isuzu 4JJ1 TC
Model year	2005
Engine type	Diesel, four stroke
Cylinder layout and number	In-line, four cylinders
Firing order	1-3-4-2
Bore x Stroke (mm)	95.4 x 104.9
Total displacement (cc)	3000
Maximum power output	107kw@3600rpm
Maximum torque output	294Nm@1400-3400rpm
Injection System	Common rail
Injection Nozzle	Electrical controlled injector
Injection pressure	Eclectically control
Valve layout	Double Overhead Camshaft
Intake Valve Open at BTDC (°CA)	13
Intake Valve Close at ABDC (°CA)	41
Exhaust Valve Open at BBDC (°CA)	52
Exhaust Valve Close at ATDC (°CA)	6
Addition devices	EGR, Turbocharger

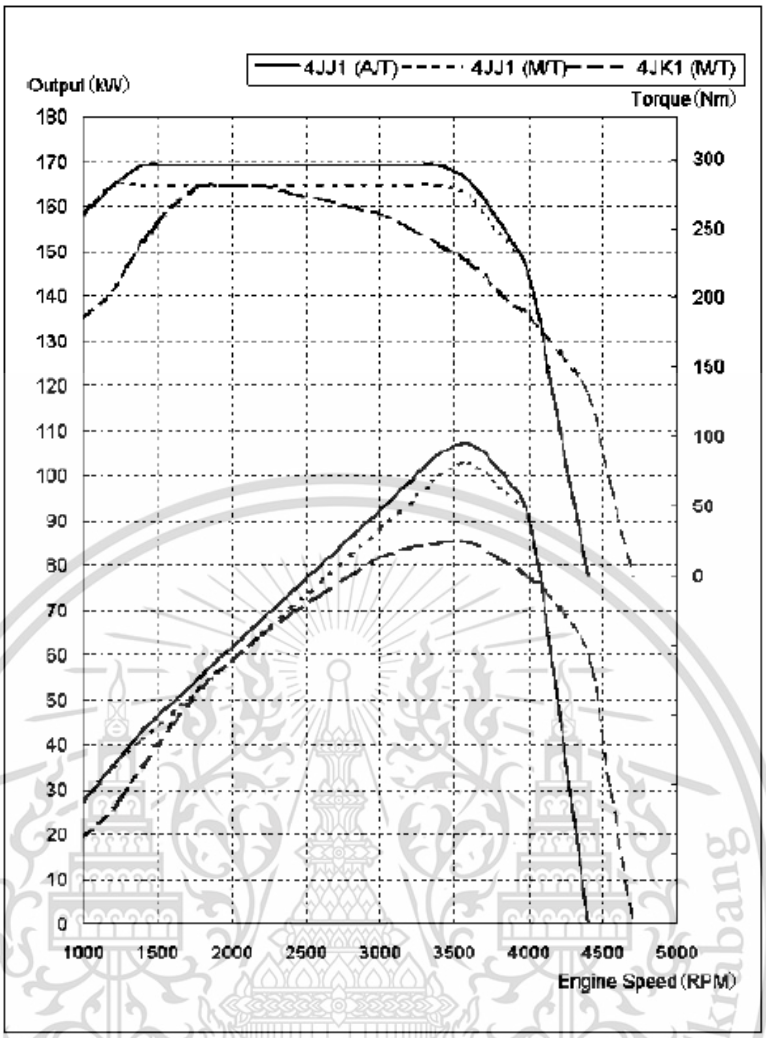

Figure 3-2 Engine's performance curve

3.1.2 Eddy current dynamometer

An eddy current dynamometer is connected to the engine flywheel to apply the load on the engine. The **Figure 3-3** shows the schematic diagram of an eddy current dynamometer. The rotator shaft is connected to the engine flywheel by which power is delivered from engine to dynamometer. It is surrounded by the stator coil which apply mechanical friction on it. When the rotator rotates through the electromagnetic field of stator coil, an eddy current will be produced. This current is flowing through the short circuit around the stator coil and dissipated into heat. That heat will be transferred to water medium. Moreover, the current produced is read by the load cell and converted to torque.

In this study, the eddy current dynamometer was used to apply the load on tested engine and **Figure 3-4** show the actual photo of dynamometer after installation on the experimental test bed.

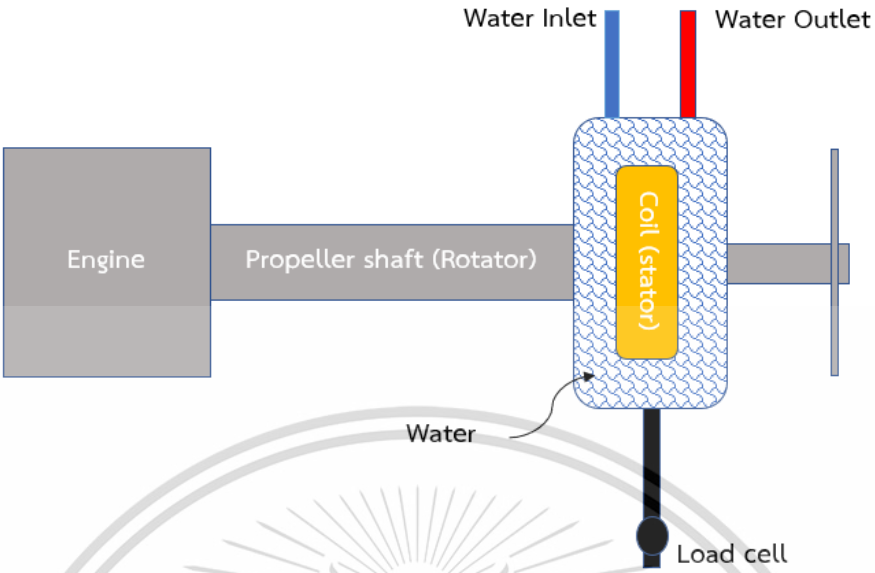

Figure 3-3 Schematic diagram of eddy current dynamometer

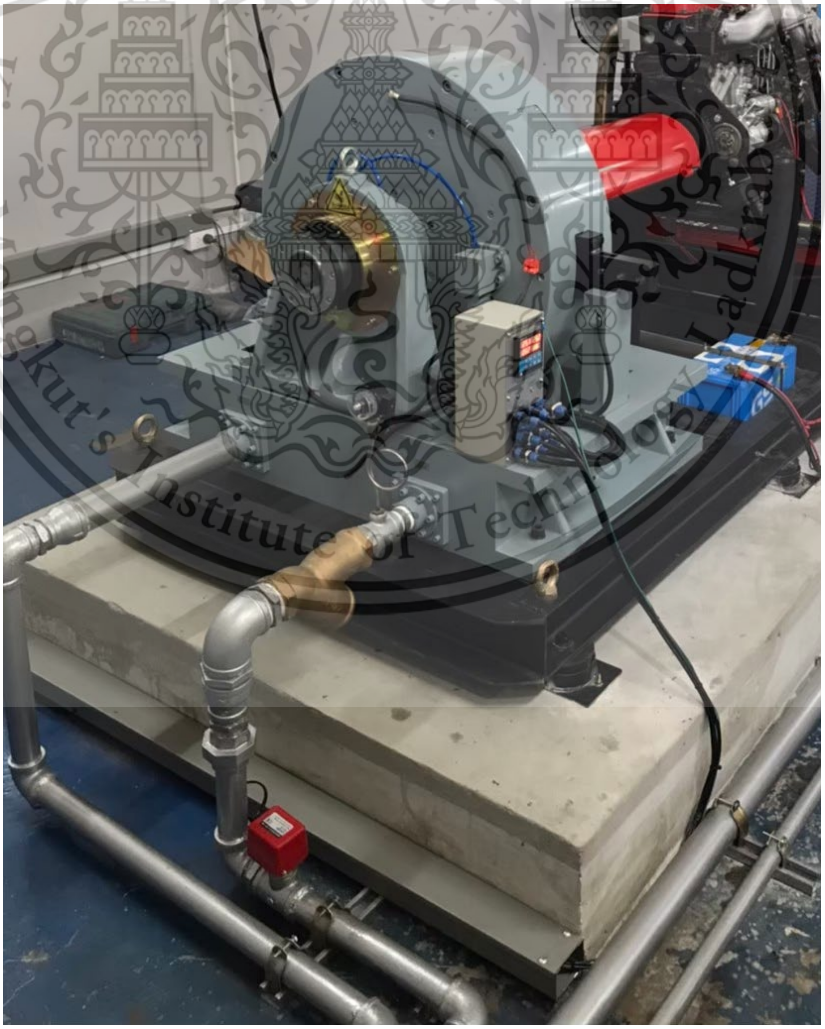

Figure 3-4 Eddy current dynamometer

3.1.3 Cooling Tower

Both the engine and dynamometer were cooled by water by connecting with the cooling tower. **Figure 3-5** shows the schematic diagram and **Figure 3-6** shows the actual photo of water-cooling tower which is connected with the experimental test bed. The cooling tower is placed outside of the building and the water is cooled by ambient air. The tower has the two shells as lower and upper shells. The upper shell has filter and flow guide to pour down the water, which was elevated by water pump, from all the area of upper shell gradually and equally distributed. In the lower shell, the water is stored to supply to engine and dynamometer. The water is circulated from the lower shell to upper shell by electric water pump. In this study, the cooling water temperature is maintained within the temperature range of 75 to 90 degree Celsius.

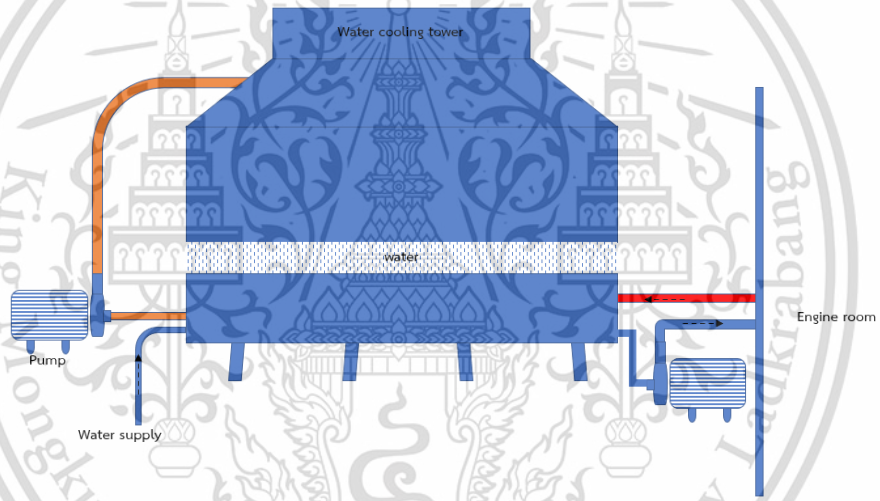

Figure 3-5 Schematic diagram of water-cooling tower

Figure 3-6 Actual photo of water-cooling tower

3.1.4 Pressure Sensor

The high thermal resistance pressure sensor was used to measure the combustion pressure by mounting inside the engine's cylinder. The sensor type is "Kistler 6052C31-piezoelectric crystal" and is mounted on the cylinder number one. The glow plug is removed from the cylinder head and replaced with the pressure sensor adaptor which is created to be same size and same thread size with the glow plug (**Figure 3-7.b**). After that, the pressure sensor was equipped on the adaptor. **Figure 3-8** shows the pressure sensor after installation on tested engine. The in-cylinder pressure data is the most important parameter for the combustion study. The sensor used in this study has the accuracy of ± 0.7 bar.

(a) (b)

Figure 3-7 (a) Pressure sensor and (b) pressure sensor adaptor and glow plug

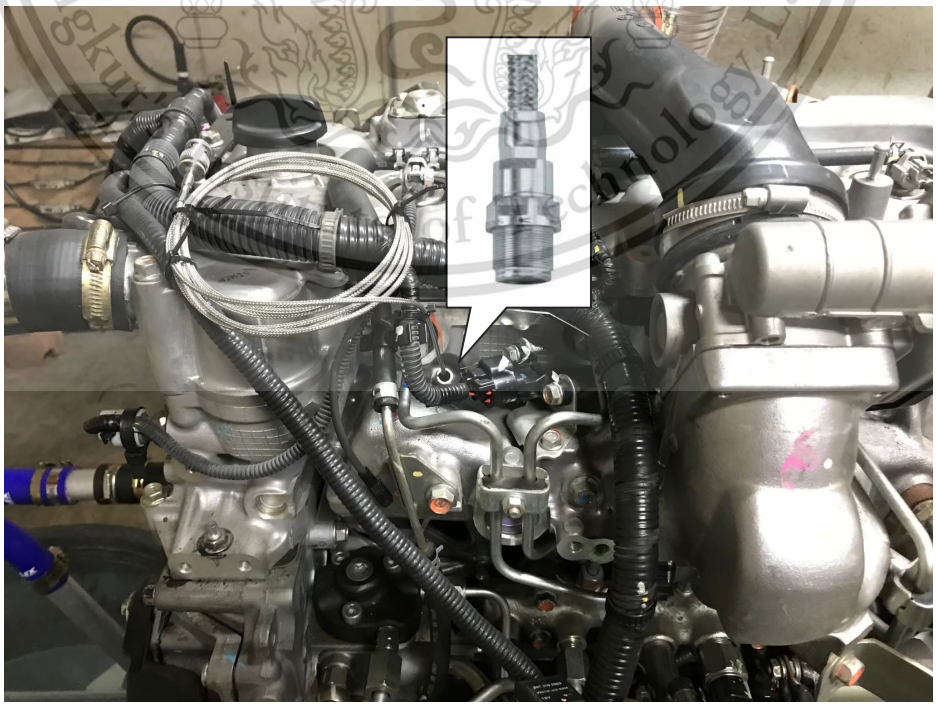

Figure 3-8 Pressure sensor mounted on engine

3.1.5 Crank angle encoder

An angle encoder can measure the rotation of a rotated mechanism in angle degree. The working principle is originated from the transmission light principle: an infrared beam is emitted and received at the sensor unit. A customized marker disk with gaps is fixed on the output shaft of dynamometer. The sensor housing with the U-channel is installed with the stand. Moreover, the marker disk's holes must be in the middle of U-channel. These holes will pass through and block the light between emitter and receiver of sensor house. If the sensor received the light, the receiver transforms the light into a voltage signal.

The encoder model "CA-IRE-720" was applied to measure the real time crank position for the combustion analysis (**Figure 3-9**). The resolution of the encoder is 0.5 degree.

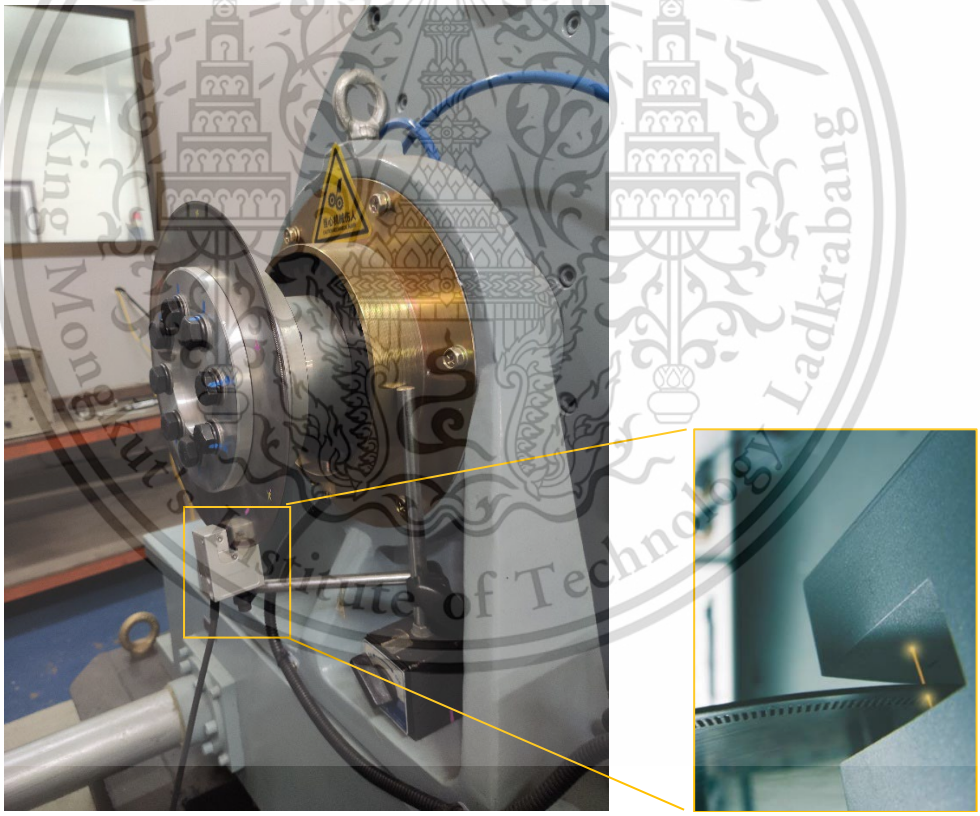

Figure 3-9 Crank angle encoder

3.1.6 Combustion DAQ system

The Dewesoft "SIRIUS-HS" model data acquisition box was applied for the combustion analysis. As the input data, it read and store data from crank angle encoder and pressure sensor and on the other hand, it transfers these data to the computer.

The computer processes the data on the crank angle domain by an integrated Dewesoft software so that the results of pressure versus volume, pressure versus crank angle, and other combustion parameter could be obtained. **Figure 3-10** shows the connection diagram of combustion system between sensors, data acquisition system and computer.

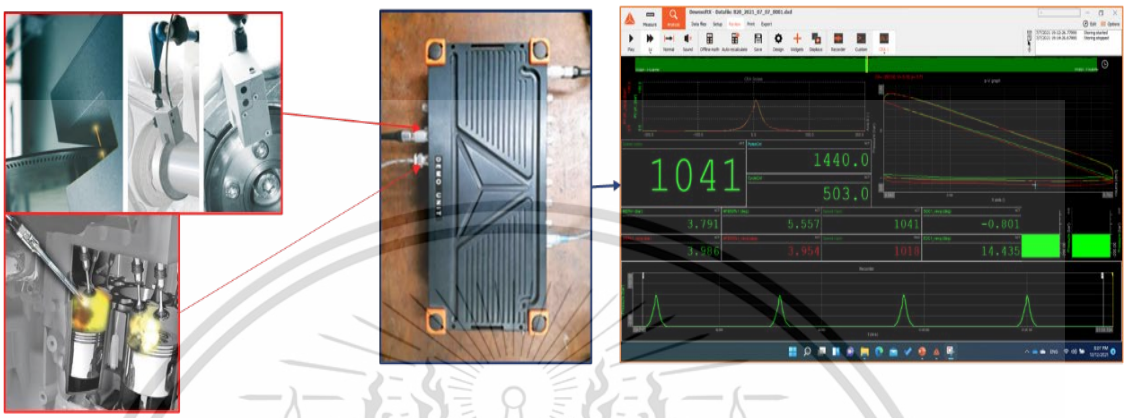

Figure 3-10 Combustion data acquisition system

3.1.7 Exhaust gases analyzer

To measure the amount of engine out gases, an exhaust gases analyzer was connected to the exhaust pipe. The "AVL DITESI GAS 1000" was used. The machine can measure the exhaust gases of carbon monoxide (CO), carbon dioxide (CO_2), hydrocarbon (HC), nitrogen monoxide (NO) and oxygen (O_2). The accuracy and measurement range of AVL exhaust gases analyzer are listed in **Table 3.2.** In addition, Lambda, air -fuel equivalent ratio, is provided as well by calculating back from CO, CO2, HC, O2.

Figure 3-11 AVL exhaust gases analyzer

Table 3.2 Measurement and accuracy of exhaust gases analyzer

Parameter	Measurement limit	Resolution	Accuracy
CO	0~15 %vol	0,01 % vol.	< 10.0 % vol.: ± 0,02% vol., ± 3% o.M. ≥10.0 % vol: ± 5 % o.M.
CO_2	0~20 %vol	0,01 % vol.	< 16.0 % vol.: ± 0, 3 % vol., ± 3 % o.M. ≥ 16.0 % vol: ± 5 % o.M.
HC	0~30,000 ppm vol	≤2.000: 1 ppm vol.	< 2000 ppm vol.: ±4 ppm vol., ±3% o. M. ≥ 5000 ppm vol.: ±5% o. M. ≥10000 ppm vol.: ±10% o. M
O_2	0~25 %vol	0,01 % vol.	± 0,02 % vol. ± 1 % o. M.
NO	0~5,000 ppm vol	1 ppm vol.	± 5 ppm vol. ± 1 % o. M.
Lambda	0~9.999	0,001	Calculated from CO, CO2, HC, O2

3.1.8 Smoke Meter and Filter paper

The emitted engine smoke was collected on the filter paper by using "BOSCH" smoke intensity meter "Okuda DSM-240" model. The machine consists of two main parts as suction pump and reflectometer light. Firstly, the new filter paper was placed under the reflectometer light and calibrated the display value to zero. After that, the particulate matters (PMs) were collected on that filter paper with the help of suction pump. The PMs filtered paper filter was measured under the light again and the display showed the amount of light percent which blocked by collected PMs in percent. These procedures were repeated two time in an engine running condition.


Figure 3-12 BOSCH smoke intensity meter and filter paper

3.2 Tested Fuels

In this research, three types of fuels such as diesel, biodiesel and ethanol were blended in different formula. Moreover, all the fuels come from different resources. Diesel is manufactured from crude oil from the refinery process. On the other hand, in Thailand, biodiesel is produced from palm oil and ethanol is produced from sugarcane, cassava, and molasses.

3.2.1 Blended fuel preparation

The diesel-based fuels of B10 (10 %vol biodiesel and 90 %vol diesel), B20 (20 %vol 133 biodiesel and 80 %vol diesel) and B100 (100% biofuel) were used to mixed with ethanol. The ethanol, used in this study, is 99.95% clear ethanol. Literatures had been pointed out that the major disadvantage of ethanol blended diesel fuel is fuels' phase separation especially at low temperatures ([33], [31], [34]**).** In addition, biodiesel can serve as cosolvent to prevent separation between diesel molecules and ethanol molecules. Therefore, in this research, biodiesel included commercial diesel fuels are chosen as the based fuel to mixed with ethanol.

The ethanol and based fuels (B10, B20, B100) were mixed in weight basic by using the weight scale. The weight scale was calibrated before using it to be higher accuracy. Firstly, the based fuel was put inside the bracket and weight on the weight scale (**Figure 3-13.a).** Then, the weight of ethanol, which needed to be, was calculated by using the **Equation 3.1**. After that, both the ethanol was poured into the based fuel and stirred with the cleaned flat rod around fifteen minutes (**Figure 3-13**).

$$W_{ethanol} = W_{based\ fuel} \times \frac{x}{100\text{-}x} \qquad 3.1$$

Where, x = the percentage of ethanol

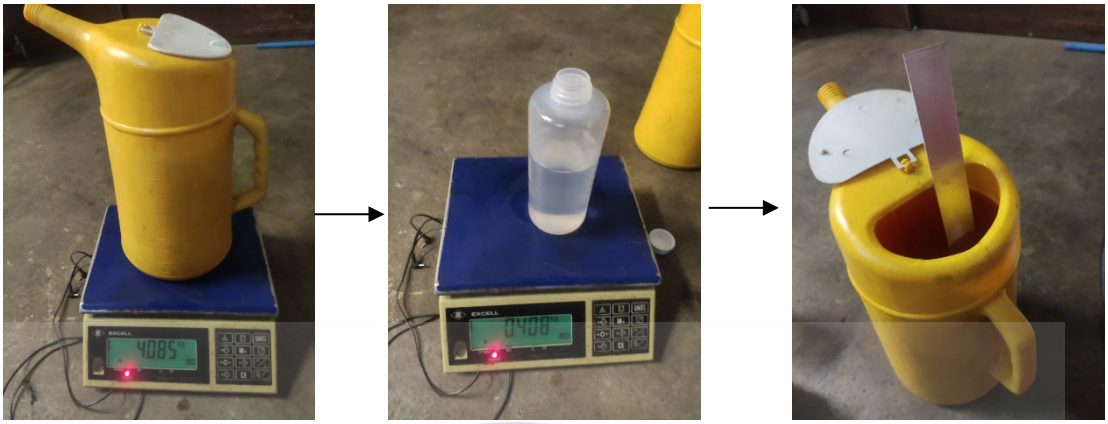

(a) (b) (c)

Figure 3-13 Fuel blending procedures: (a) weighting the based fuel, (b) weighting ethanol, and (c) Mixing two fuels.

In order to study the effect of different proportions of biodiesel and ethanol in diesel-biodiesel-ethanol ternary blended fuel, 10 different fuels are prepared. The major thinking points are the not to have phase separation and fuel calorific value. The identification of fuels and details are listed in **Table 3.3**.

Table 3.3 ID and detail of blended fuel

Fuel ID	Detail			
	Diesel %	Biodiesel %	Ethanol %	Blended by
B10	90	10	0	Volume %
B20	80	20	0	Volume %
B100	100	0	0	-
B10E5	B10 – 95%		5	Weight %
B10E10	B10 – 90%		10	Weight %
B20E5	B20 – 95%		5	Weight %
B20E10	B20 – 90%		10	Weight %
B20E20	B20 – 80%		20	Weight %
B100E5	B100 – 95%		5	Weight %
B100E10	B100 – 90%		10	Weight %

3.2.2 Fuel Properties

Table 3.4 shows the key properties of based fuels (B10, B20, B100 and ethanol). All the properties were tested under the ASTM standard. The properties of blended fuel might address to the properties of based fuels. The pure biodiesel and ethanol contain less carbon and more oxygen than the diesel fuel. Therefore, the carbon content decreased, and oxygen increased with the increasing biofuel amount within the blended fuels. In addition, the lower carbon to hydrogen ratio and the higher oxygen content of biodiesel and 142 ethanol may reduce smoke formation because of pyrolysis combustion process [35]. The density and viscosity of biodiesel are higher than diesel fuel, but on the other hand, the density and viscosity of ethanol are much lower than diesel, around 50%. This could improve ethanol blend atomization and fuel break up while decreasing fuel lubricity. Choosing biodiesel as co-solvent could also recover the fuel lubricity. Biodiesel has a narrower range of distillation temperatures although it starts boiling at 336.2 °C. While ethanol has the lowest distillation temperatures and lowest range. B10 and B20 fuels start their distillation processes at about 180 °C and end at 334.2 °C. **Table 3.5** shows the calorific values of all tested fuels. It is tested with the Leco model AC-500 automatic bomb calorimeter. The calorific values blended fuels decreased with the increasing biodiesel and ethanol percentage because the calorific values of biodiesel and ethanol are lower than that of diesel fuel.

Table 3.4 Basic fuels properties

Fuel Properties	Standard	B10	B20	B100	Ethanol
Carbon (% mass)	ASTM D 5291	84.66	82.61	76.73	52.2
Hydrogen (% mass)	ASTM D 5291	13.56	13.45	12.45	13.0
Oxygen (% mass)	ASTM D 5291	1.79	3.94	10.82	34.8
Calorific value (MJ/kg)	ASTM D 240	45.63	44.95	39.94	28.05
Viscosity @ 40°C (mm^2/s)	ASTM D 445	3.0	3.1	4.5	1.2
Density @ 25°C (kg/m^3)	ASTM D 1298	835	827	875.3	789.0
Distillation (°C)	ASTM D 86-11b				
T10		180	177.4	336.2	77.8
T90		344.2	348.4	352.3	80

Table 3.5 Calorific value of fuel

Fuels	Calorific Values (MJ/kg)	Fuels	Calorific Values (MJ/kg)	Fuels	Calorific Values (MJ/kg)
B10	45.63	B20	44.95	B100	39.94
B10E5	44.38	B20E5	43.95	B100E5	39.31
B10E10	43.65	B20E10	42.72	B100E10	38.07
-	-	B20E20	40.53	-	-

3.3 Research Methods

3.3.1 Experimental setup

The schematic diagram of engine-dynamometer test stand is shown in **Figure 3-14**. A four-cylinder common rail direct injection diesel engine was used for the experiment. The engine's flywheel was connected to the engine flywheel to apply the load on engine. In this experiment, the engine was controlled at four constant loads of 56Nm, 84Nm, 112Nm and 140Nm. Moreover, the engine speed was set at 1000 RPM, 1500 RPM, and 2000 RPM, respectively, by using the accelerator. To measure the fuel consumption, the fuel from fuel tank transfer to the beaker on the weight scale first and the fuel pump suck the fuel from that beaker. During measuring the fuel consumption, the fuel supply to beaker was stopped and refill after the measurement. The computer was connected to the weight scale, allowing for real-time viewing of weight changes. In addition, the ECU was connected to a Carman scan on board diagnosis (OBD) tool to monitor the engine's conditions such as coolant temperature, oil temperature, throttle position, and EGR position.

For the combustion analysis, an in-cylinder pressure was mounted on the first cylinder and a crank angle encoder assembly was installed on the output shaft of dynamometer. These two sensors were connected to the DEWESOFT data acquisition system which is stored and transfer the signal from sensors to the computer. The total of 1000 engine cycles were stored for the offline analysis.

For the emissions analysis, the intensity of emitted smoke was measured via BOSCH smoke intensity meter. The engine out gases like CO, CO_2, and NO were measured with AVL exhaust gases analyzer. The smoke measurement was performed

two times per testing condition and AVL data were recorded one minute per testing condition.

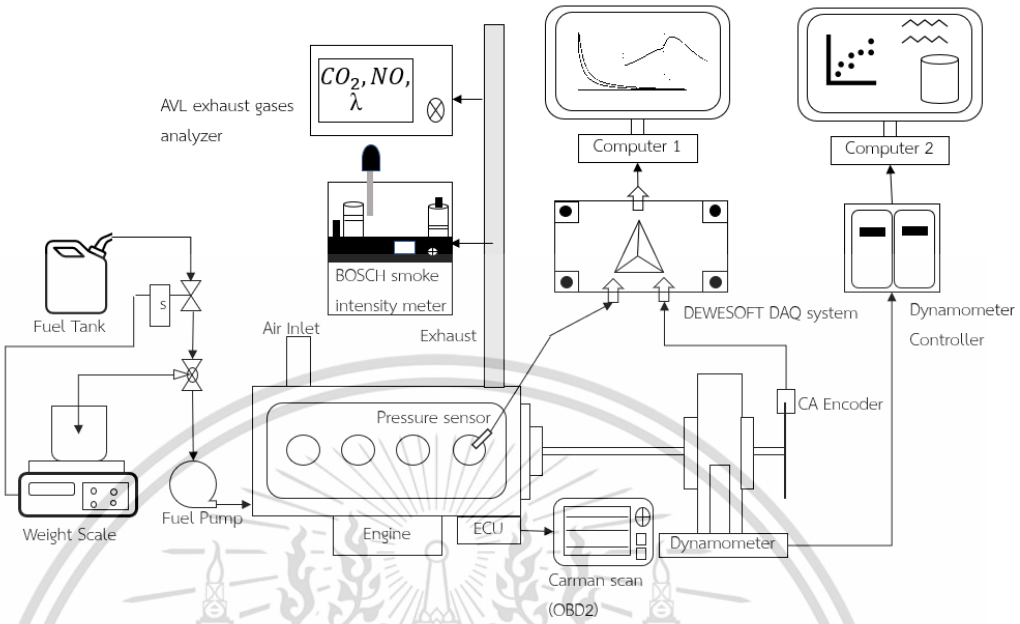

Figure 3-14 Experimental test stand

3.3.2 Combustion analysis

During the experiment, the one thousand engine cycles of in-cylinder pressure data were stored for the advanced combustion analysis.

3.3.2.1 Raw data processing

The data from pressure sensor and crank angle encoder was collected in actual time which means during running the engine. Therefore, the vibration from engine makes a lot of noise on experimental data and it is necessary to filter. The best 200 cycles are filter out first from the 400 cycles. After that, the selected cycles were averaged to one engine cycle of -360degree to 360degree crank angle. Then, third order least square with seven points method **(Equation** 3.2**)** was applied to remove the noise for more accurate results. M.J. Rauckis and W.J. McLean [36] also applied this least square method for raw pressure data smoothing.

$$p_{\theta(\text{smoothed})} = \frac{\left\{-2*\left(p_{\theta-3}+p_{\theta+3}\right)+3*\left(p_{\theta-2}+p_{\theta+2}\right)+6*\left(p_{\theta-1}+p_{\theta+1}\right)+7*p_{\theta}\right\}}{21} \qquad 3.2$$

Where, $p_{\theta(\text{smoothed})}$ is the pressure at crank angle Theda (θ) after smooth and p_{θ} is the pressure at crank angle θ before smooth.

3.3.2.2 Coefficient of variation of IMEP

The indicated mean effective pressure (IMEP) of a cycle is calculated from the raw data of pressure sensor and crank volume at each crank angle. The coefficient of variation of IMEP (COV_{IMEP}) can be calculated by normalizing the standard deviation of IMEP with the average value of IMEP. Cartwright and Fleck [37] derived the equation for COV for any relevant parameter. In this thesis, the equation of COV_{IMEP} (**Equation 3.3**) was followed the equation of Cartwright and Fleck.

$$COV_{IMEP} = \frac{s_{IMEP}}{\overline{IMEP}} \times 100\% \quad 3.3$$

Where, COVIMEP = coefficient of variation of IMEP

SIMEP = standard deviation of IMEP which can be calculated by using Equation 3.4

$\overline{IMEP}$ = average of IMEP

$$s_{IMEP} = \sqrt{\frac{\sum (IMEP - \overline{IMEP})^2}{n-1}} \quad 3.4$$

Where, n = number of samples.

3.3.2.3 Maximum Pressure Rise Rate (MPRR)

The maximum pressure rise rate (MPRR) is the parameter that is directly related to the engine's noise and vibration. MPRR is the maximum value of the first derivative of in-cylinder pressure with the corresponding crank angle.

$$MPRR = \max_{-360<\theta<360} \frac{dp}{d\theta} \quad 3.5$$

3.3.2.4 Net Heat release rate and Cumulative Net Heat Release Rate

The quantitative combustion information can be obtained using the compression and expansion pressure vs crank angle data. For a discussion of combustion phenomena, the heat release profiles are a must. But the difference between gross and net heat release rates is thermal losses. Turbocharged diesel engines experience thermal losses when operating at mid-load and mid-speed. These losses include heat transfer to the cylinder wall, losses from the crevice area, and the use of heat for fuel vaporization. Because of this, in the current work, the impacts of

heat transfer durin-g combustion processes are disregarded, and the net heat release rate (NHRR) was computed using the in-cylinder pressure data and **Equation 3.6**, as per J.B. Heywood. Therefore, to ignore the impacts of heat transfer during the intake stroke and exhaust stroke, the net heat release rate and cumulative net heat release (CNHR) analyses were calculated over the crank angle range of -60° to 60°.

$$\frac{dQ}{d\theta}\ (NHRR)= \left[\frac{k}{k-1}\right] \cdot P \cdot \frac{dV}{d\theta} + \left[\frac{1}{k-1}\right] \cdot V \cdot \frac{dP}{d\theta} \qquad 3.6$$

Where: $\frac{dQ}{d\theta}$ (NHRR)= rate of net heat release (J/deg)

k = ratio of specific heat (c_p / c_v), P = pressure (Pa), V = volume (m^3)

$\frac{dV}{d\theta}$ = change of volume with crank angle (m^3/deg)

$\frac{dP}{d\theta}$ = change of pressure with crank angle (Pa/deg)

3.3.2.5 Combustion duration and Mass Fraction Burnt

As mentioned before, the Dewesoft data acquisition system was used to store and analyze the in-cylinder pressure raw data and crank angle. All the combustion parameters are derived from the in-cylinder pressure automatically, like start of combustion (SOC), end of combustion (EOC), and 5%, 10%, 50%, and 90% mass fraction burnt. The relevant data of selected engine cycles is filtered out and averaged for the one cycle. The combustion duration is the interval between SOC and EOC.

3.3.3 Experimental data analysis

In the results and discussion section of this study, both the brake and indicated sections were covered. Three measurements of fuel usage were conducted using the weight scale and timer for various engine situations. Friction losses and pumping losses are considered in the calculation of lost work as the difference between stated work and brake work. The indicated power was calculated from the indicated work, which was calculated from the in-cylinder pressure, volume, and engine speed. On the other hand, braking power was calculated using engine speed and torque output. The indicated and brake specified fuel consumption was obtained by normalizing the fuel mass flow rate with the corresponding powers. The lower heating value and fuel mass

flow rate were used to determine the input heat energy. **Equations 3.13** and **3.14** were then used to calculate thermal efficiency.

$$W_i = \int_0^{360} P \times dV \tag{3.7}$$

$$\dot{W}_i = 4 \times W_i \times \frac{N}{120} \times 10^{-3} \tag{3.8}$$

$$\dot{W}_b = 2 \times \pi \times T \times \frac{N}{60} \times 10^{-3} \tag{3.9}$$

$$ISFC = \frac{\dot{m}_f}{\dot{W}_i} \times 3600 \tag{3.10}$$

$$BSFC = \frac{\dot{m}_f}{\dot{W}_b} \times 3600 \tag{3.11}$$

$$\dot{Q}_{in} = Q_{LHV} \times \dot{m}_f \tag{3.12}$$

$$ITE = \frac{\dot{W}_i}{\dot{Q}_{in}} \tag{3.13}$$

$$BTE = \frac{\dot{W}_b}{\dot{Q}_{in}} \tag{3.14}$$

Where, the W_i (J/cycle-cylinder) stands for indicated work for one engine cycle and one cylinder and $\dot{W}_i$ (kW) is the indicated power for all four cylinders. $\dot{W}_b$(kW) is the brake power. $\dot{m}_f$ is the mass flow rate of fuel in g/s and Q_{LHV}(MJ/kg) is the lower heating value of fuel which neglecting the heating values of hydrogen included in the fuel molecules. In addition, ITE and BTE are the indicated and brake thermal efficiencies.

3.3.4 Emission Analysis

For the emissions analysis, the comparison of exhaust gases like CO_2, CO, HC, and NO are discussed based on the sensor data of AVL exhaust gases analyzer. In addition, exhaust temperatures were measured with a thermocouple by mounting on the exhaust pipes. As mentioned before, the PMs were collected on the paper filter to measure the smoke intensity. The filter papers were also used to take photograph in microscale under the optical microscope (OM) and scanning electron microscope (SEM). The quantity of PMs fitted on the filter paper can be compared in micro scale as the better visualization. The example images are shown in **Figure 3-15**.

The SEM images was used to evaluate the agglomerate particle size of PMs. The image analysis tool, Image J, was used to measure the size of particles. Firstly, the scale of measurement tool was set equally up with the scale of image. **Figure 3-16** shown the selection of particles from SEM image. The simples were chosen by using rotated rectangle tool and them measured by using measure function (CTRL+M). The image J provide the measurement result by table as shown in **Figure 3-17**. A hundred of samples were accounted for the agglomerate particle analysis. Finally, the agglomerate particle size is the diagonal of RR length and RR width.

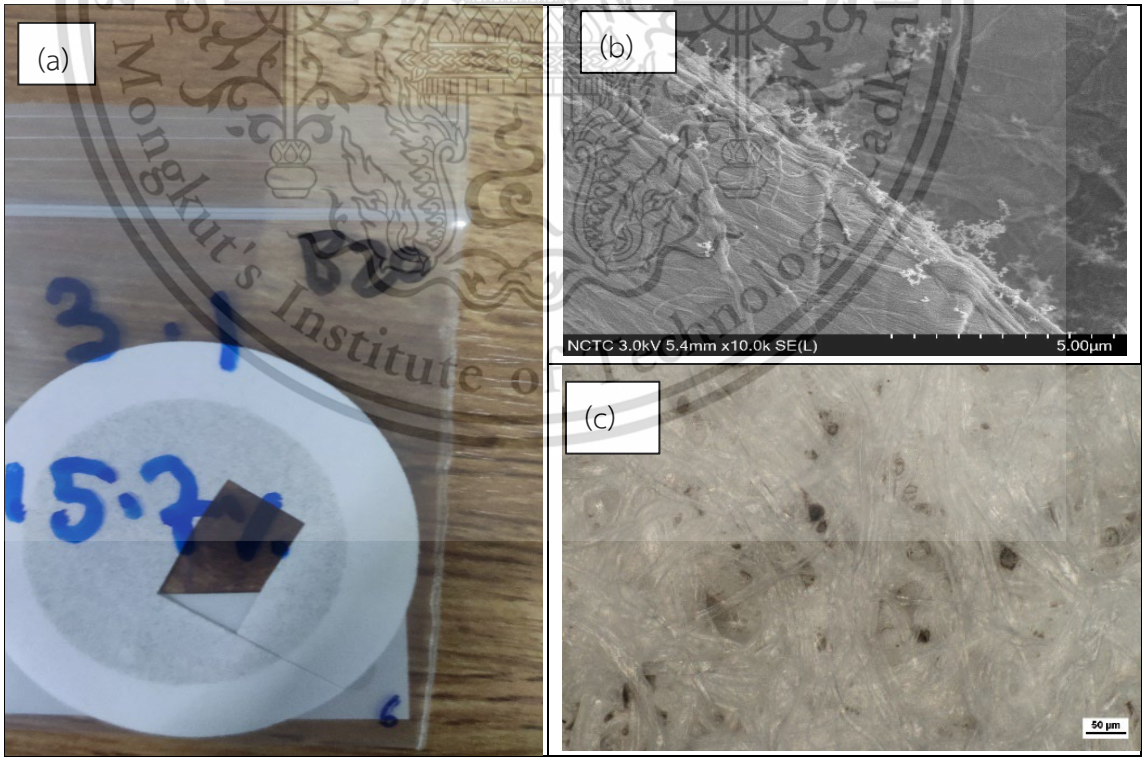

Figure 3-15 (a) camera photograph of filter paper, (b) SEM photograph of filter paper and (c) OM photograph of filter paper

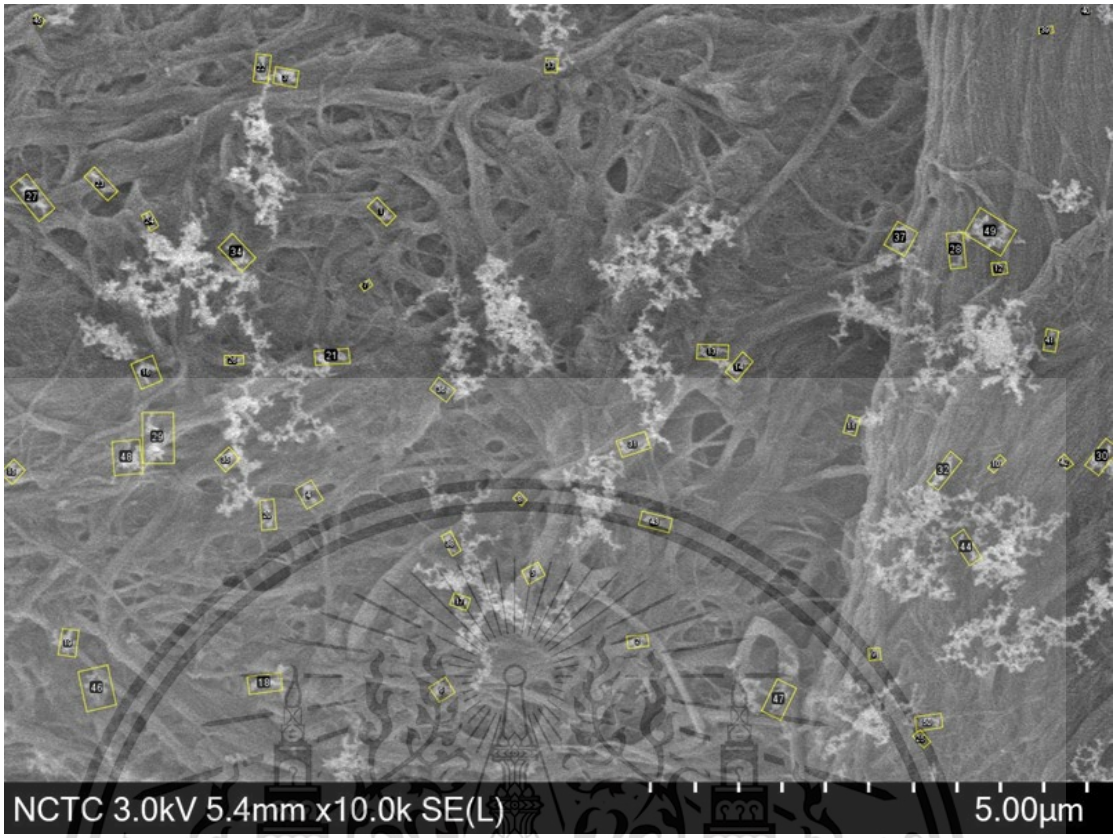

Figure 3-16 Agglomerate particles selection by using image J graphical analysis tool

	A	B	C	D	E	F	G	H	I	J	K
1		Label	Area	Mean	Min	Max	Major	Minor	Angle	RRLength	RRWidth
2	1	20211028_	0.05	120.111	68	201	0.348	0.182	134.997	0.309	0.161
3	2	20211028_	0.033	132.414	67	209	0.271	0.154	6.29	0.24	0.136
4	3	20211028_	0.053	145.461	81	235	0.309	0.219	170.208	0.274	0.194
5	4	20211028_	0.057	122.064	65	200	0.298	0.244	119.235	0.264	0.216
6	5	20211028_	0.037	140.984	78	216	0.242	0.197	28.309	0.215	0.174
7	6	20211028_	0.045	132.507	74	196	0.244	0.235	32.583	0.216	0.209

Figure 3-17 Result example from image analysis tool.

CHAPTER 4

RESULTS AND DISCUSSION

4.1 Engine Performance Parameter

To compare engine performance of different fuels, fuel consumption, indicated specific fuel consumption (ISFC), Brake specific fuel consumption (BSFC), Indicated specific energy consumption (ISEC), Brake specific energy consumption (BSEC), Indicated thermal efficiency (ITE), and Brake thermal efficiency (BTE) were measured and discussed as following.

4.1.1 Fuel Consumption

In this research, the fuel consumption was measured by using weight scale and timer with the thirty seconds duration per time of record. It is measured three times and averaged the results to reduce the uncertainty. And the results are shown in **Figure 4-1**. To produce greater power, an engine's load and speed must be increased, which results in an increase in fuel consumption. On the viewpoint of fuel properties, because biodiesel and ethanol have lower calorific values than diesel fuel, increasing their percentage in blended fuels will result in higher fuel consumption. Among all the tested fuels, B100E10 shows the highest fuel consumption because it possesses the lowest calorific value.

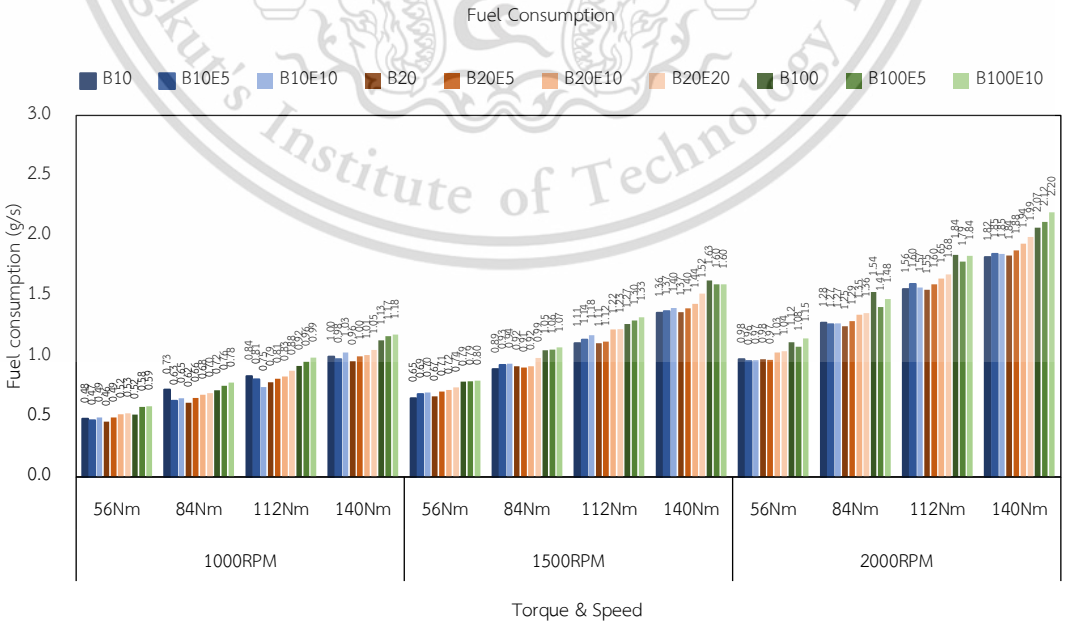

Figure 4-1 Fuel Consumption

4.1.2 Indicated and Brake specific fuel consumption

The ISFC and BSFC are the normalized parameters of fuel consumption by indicated and brake power, respectively. The ISFC and BSFC getting lower with the increasing engine load and speed. The **Figure 4-2** shows the comparison of ISFC of all tested fuel in twelves engine conditions. The indicated power is based on the combustion efficiency of fuel because it is calculated from the in-cylinder pressure and volume. The higher the combustion pressure, the greater the indicated power is. Moreover, it led to lower ISFC. At the lower engine speed and load conditions, the ISFC of low energy content ethanol blends are higher than that of the based fuels because the differences between indicated power of blended fuels and base fuel are not significant. The differences higher with the increasing engine speed and engine load and therefore, the ISFC of ethanol blended fuels lower than that of based fuels at the higher engine speeds and loads.

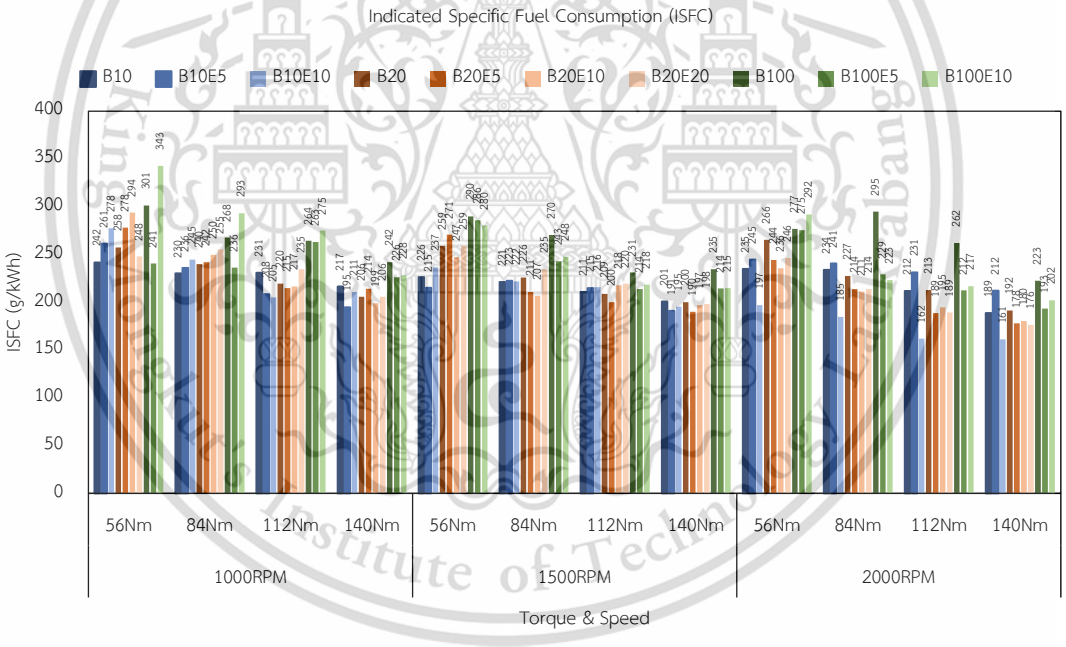

Figure 4-2 Comparison of Indicated Specific Fuel Consumption

Figure 4-3 shows the variation of BSFC according to engine speeds and loads for ten tested fuels. When compared between the tested fuels, similar trends in fuel consumption are described, with a higher BSFC for lower energy content blended fuels. Moreover, at the same engine condition, ISFC is lower than BSFC because indicated power is higher than bake power.

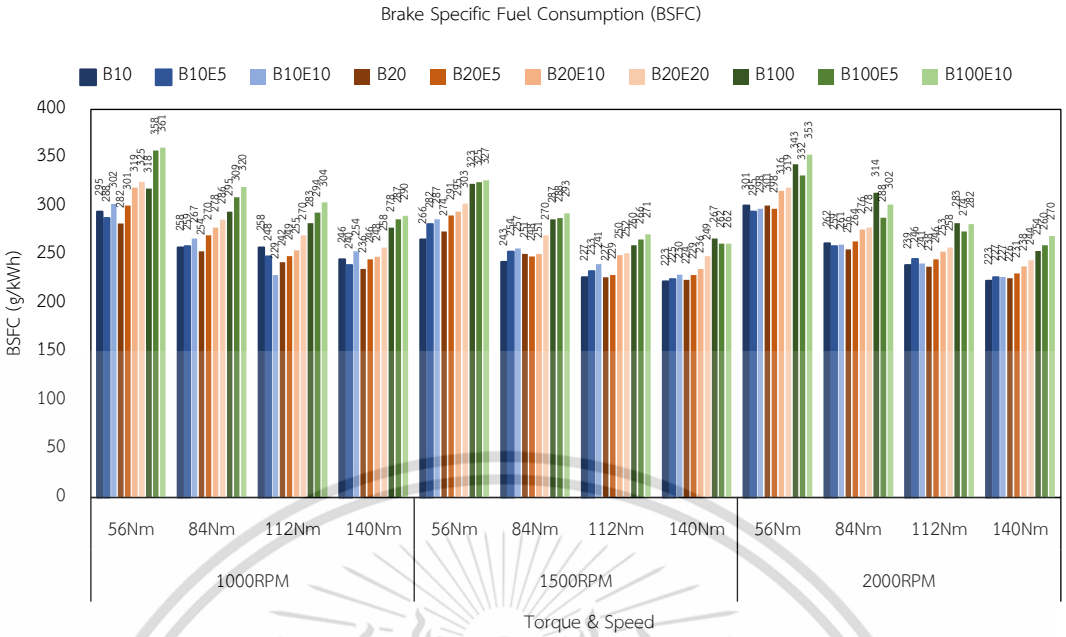

Figure 4-3 Comparison of Brake Specific Fuel Consumption

4.1.3 Indicated and Brake specific energy consumption

Figure 4-4 and **Figure 4-5** show the results of ISEC and BSEC with the unit of kJ/kWh. ISEC and BSEC are the ratios of fuel input energy over the output indicated power and brake power respectively.

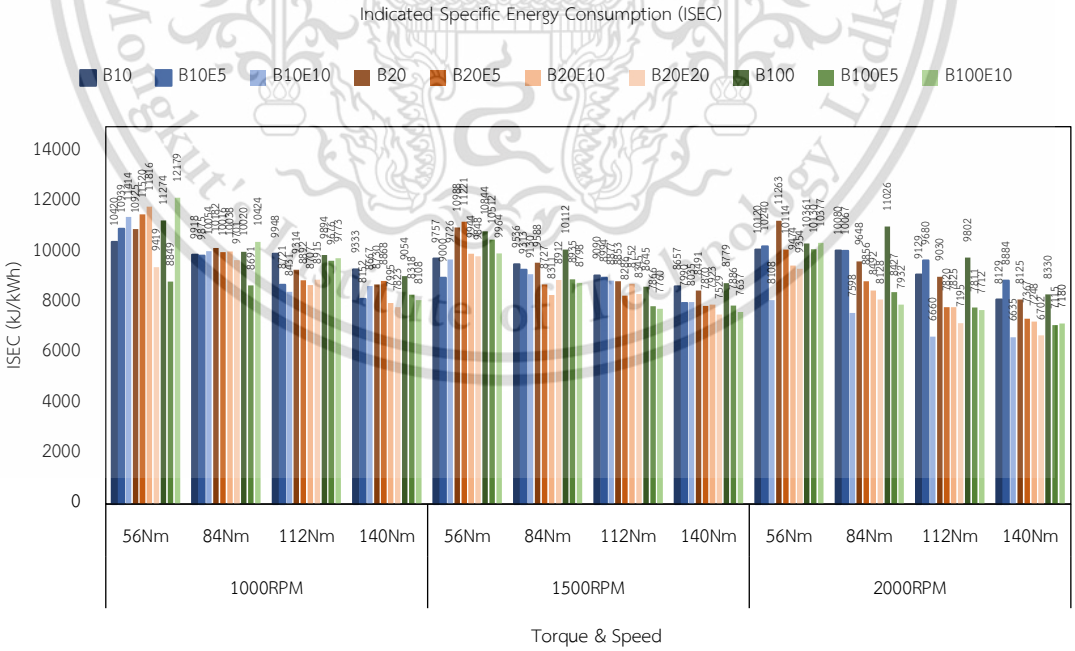

Figure 4-4 Indicated specific energy consumption

Both ISEC and BSEC show the same result trend as it is decreasing with the increasing engine speed and engine load. Moreover, the values of BSEC are higher than

ISEC at the same engine conditions. The ISEC and BSEC is decreasing with the increasing ethanol percent in the blends even more fuel is injected. This is attributed to the less energy content of ethanol blended fuels.

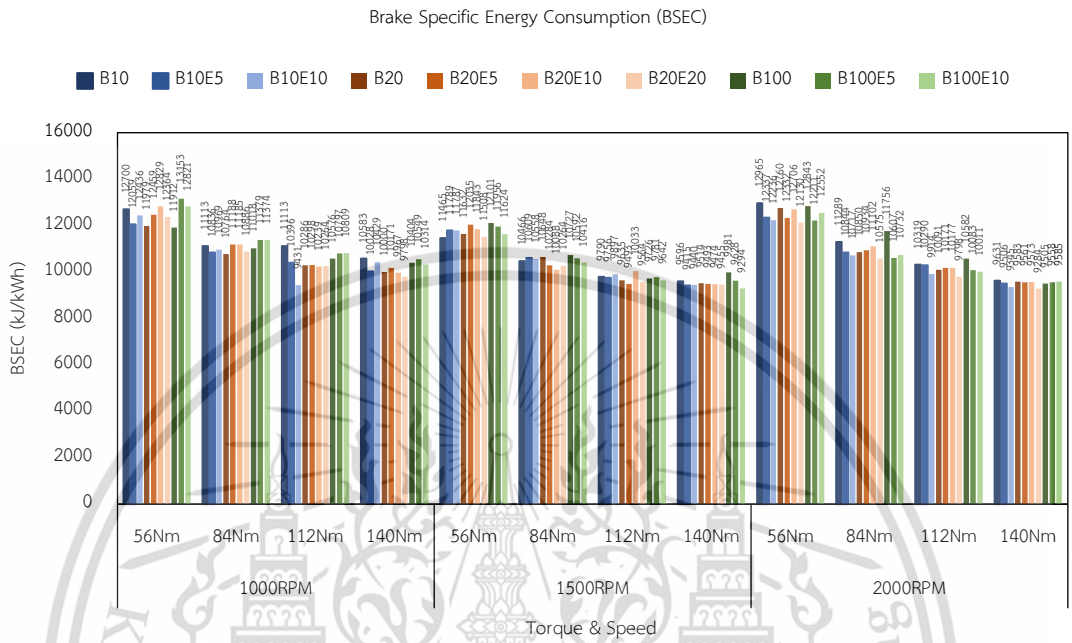

Figure 4-5 Brake specific energy consumption

4.1.4 Indicated and Brake Thermal Efficiency

The engine performance could be mainly compared with thermal efficiency. In this study, both ITE and BTE are analyzed and shown in **Figure 4-6** and **Figure 4-7**. ITE and BTE are higher gradually with the gradually increasing engine loads and speeds.

For ITE analysis, it is the ratio of input heat energy and output indicated power which is directly measured and calculated inside the cylinder chamber. Therefore, mechanical friction losses and thermal losses are disregarded in the case of ITE calculations. Therefore, it is directly proportional with the combustion quality of fuels. Moreover, the combustion behaviors are depending on the various engine parameters and fuel properties, and it will be discussed detail in the next section. Basically, the oxygen content of biodiesel and ethanol could improve the combustion processes, led to higher power output, and resulting to increasing in ITE. The differences between ITE of based diesel-biodiesel blended fuels and ethanol blended fuels are increased with the increasing engine loads and speeds because of more friction losses at higher engine speed.

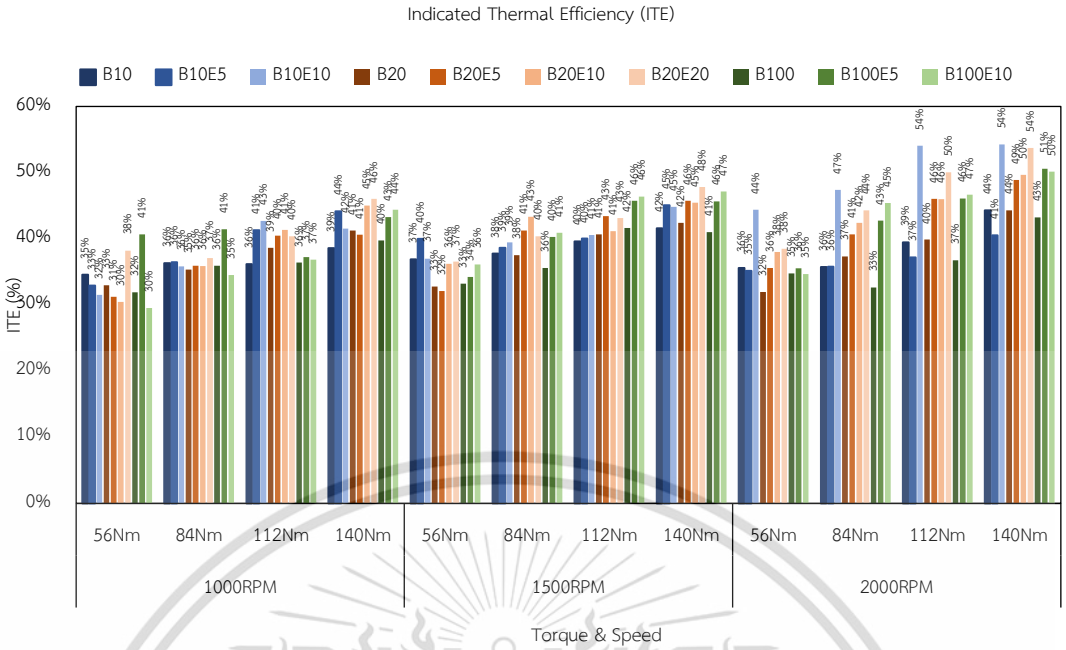

Figure 4-6 Indicated thermal efficiency.

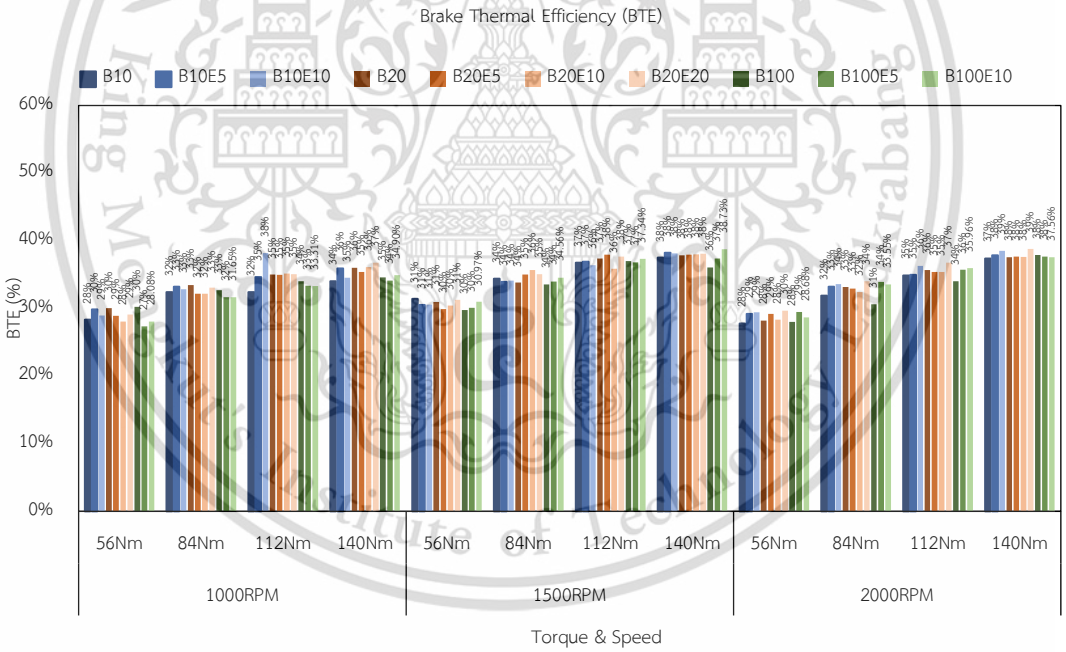

Figure 4-7 Brake thermal efficiency.

For BTE, it is calculated from the ratio of input heat energy and output brake power which is driven from the engine control speed and torque. Losses are accounted for the analysis of BTE. The BTE increased with the increasing engine loads and speed as well. BTE increased with the increasing biodiesel and ethanol content in the blends because of the more oxygen content of blended fuels. In actual, the BTE of B20 is

higher than B10 but it is decreased for B100 because of excessive low calorific value of B100. For all the ethanol blended fuels, BTEs are higher than that of based fuel in almost all the engine conditions.

4.2 Combustion Characteristics

In this study, the combustion characteristics of ten different tested fuels were be discussed based on the in-cylinder pressure, coefficient of variation of IMEP (COV_{IMEP}), maximum pressure rise rate (dP_{max}), Net heat release rate (NHRR), cumulative net heat release (CNHR), combustion duration and mass fraction burnt (MFB). The ten different blended fuels can group into four groups as based biodiesel fuel (B10, B20 and B100), B10 with ethanol (B10, B10E5 and B10E10), B20 with ethanol (B20, B20E5, B20E10 and B20E20), and B100 with ethanol (B100, B100E5, and B100E10).

4.2.1 In-cylinder combustion pressure

The in-cylinder pressure versus crank angle diagrams were plotted as four graphs per condition according to the fuel groups**. Figure 4-8 (a to l)** show the comparison of in-cylinder pressure of all tested fuels at four different engine loads (56Nm, 84Nm, 112Nm, and 140Nm) and three different engine speeds (1000RPM, 1500RPM, and 2000RPM). The analysis results of maximum pressure values and locations are shown in **Figure 4-9** attaching with the data table. As the overall comparison, the results show that the peak of in-cylinder pressure higher when engine loads are higher because more fuel are injected and combust to get higher torque. Regarding engine speed, Fuel air mixing time decreased as engine speed increased due to faster combustion cycles at higher engine speeds. As a result, higher engine revolutions burn less fuel in premixed combustion and a higher percentage of fuel in diffuse combustion when compared to lower engine revolutions. Therefore, the maximum in-cylinder pressure is lower with the faster engine revolution. Moreover, the maximum in-cylinder pressure peaks move father away from the top dead center (TDC) as well with the increasing engine loads and speeds.

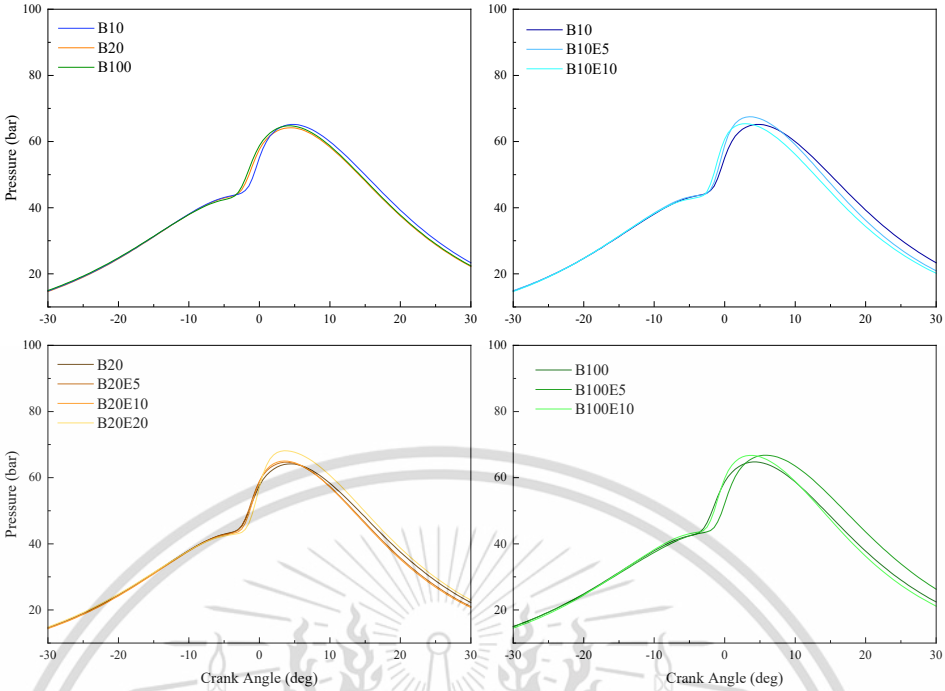

(a) In-cylinder pressure versus crank angle diagrams at 56Nm, 1000 RPM engine condition.

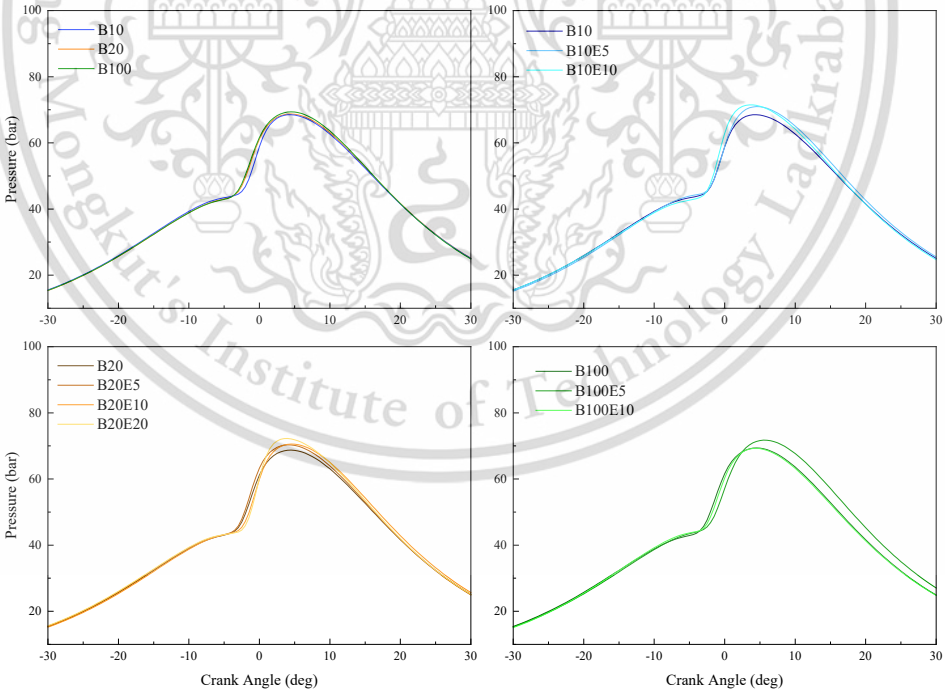

(b) In-cylinder pressure versus crank angle diagrams at 84Nm, 1000 RPM engine condition.

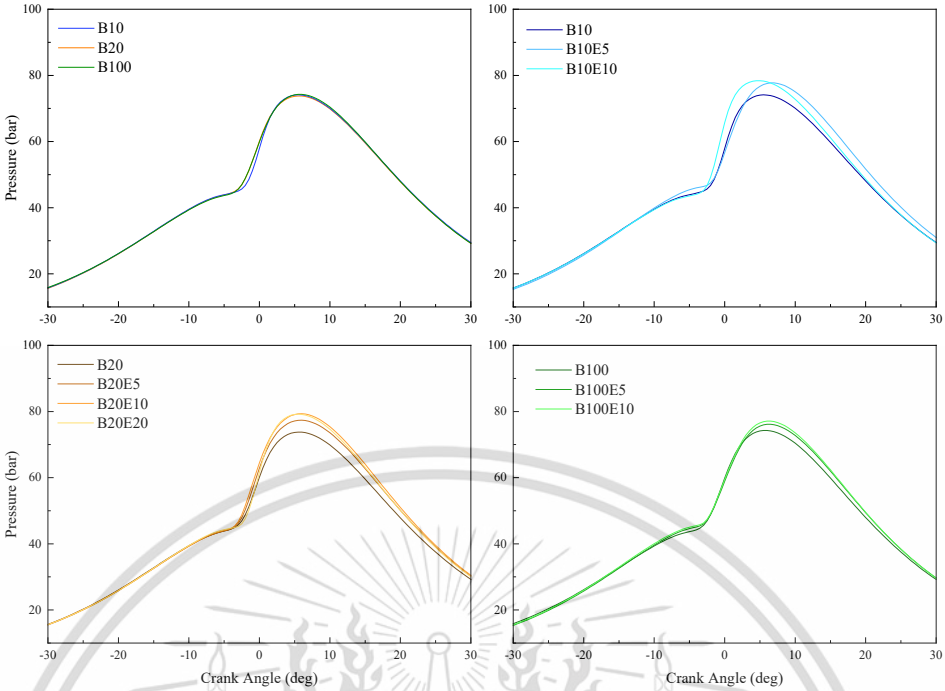

(c) In-cylinder pressure versus crank angle diagrams at 112Nm, 1000 RPM engine condition.

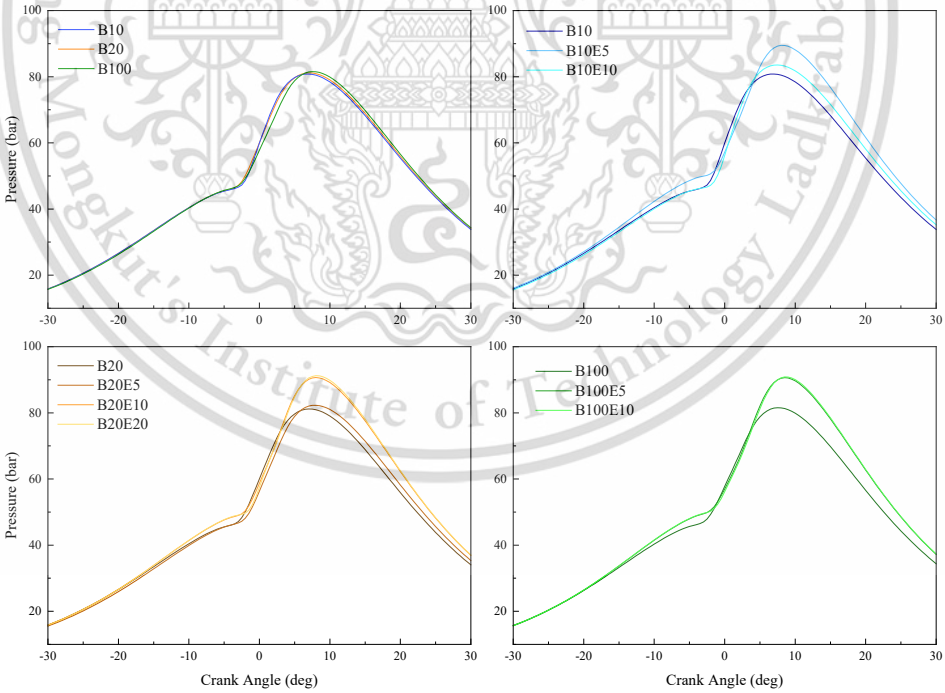

(d) In-cylinder pressure versus crank angle diagrams at 140Nm, 1000 RPM engine condition.

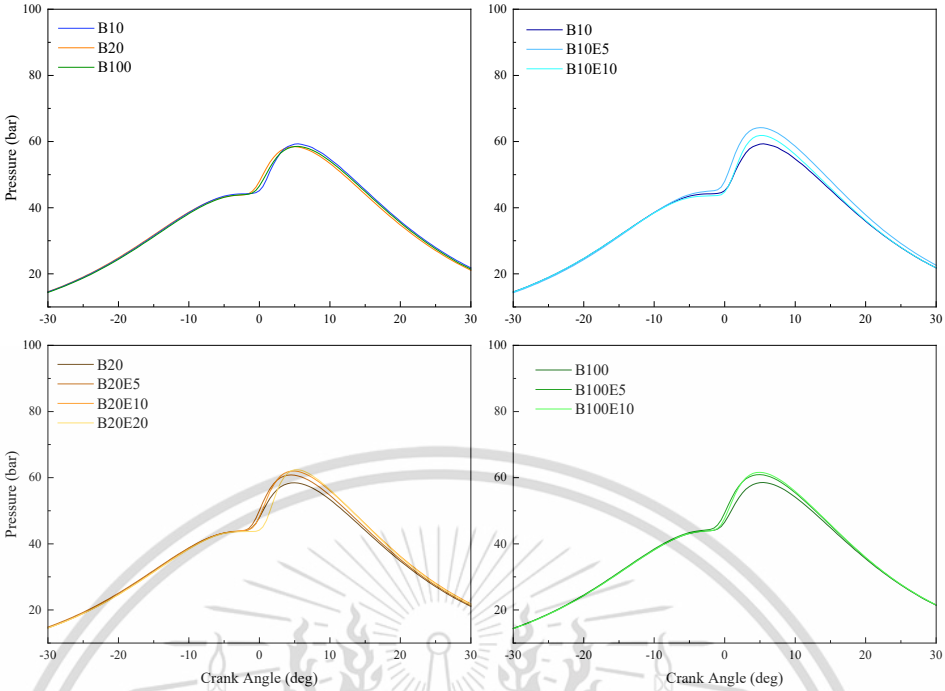

(e) In-cylinder pressure versus crank angle diagrams at 56Nm, 1500 RPM engine condition.

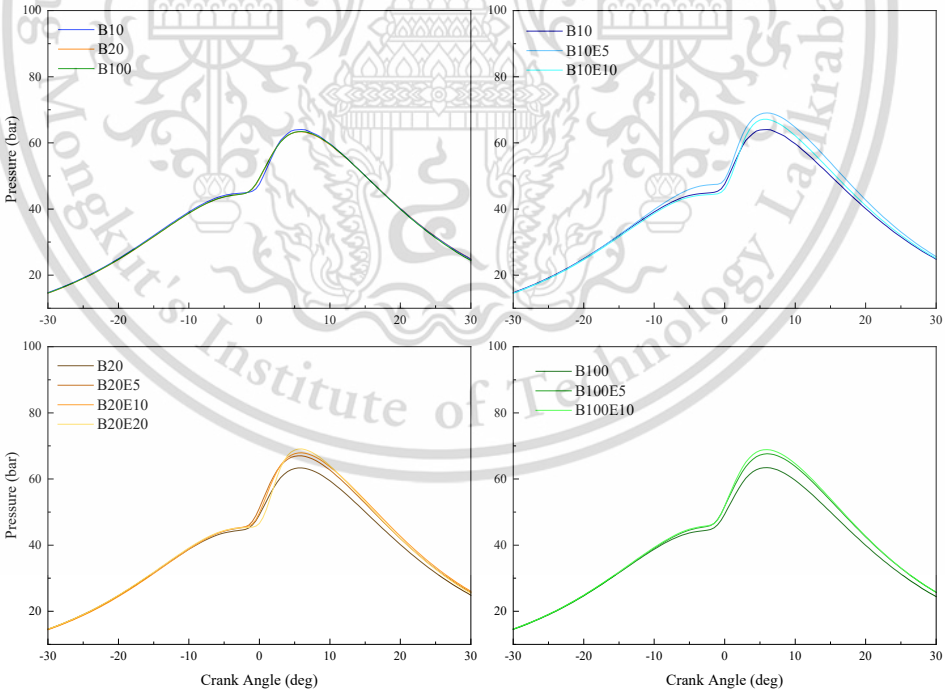

(f) In-cylinder pressure versus crank angle diagrams at 84Nm, 1500 RPM engine condition.

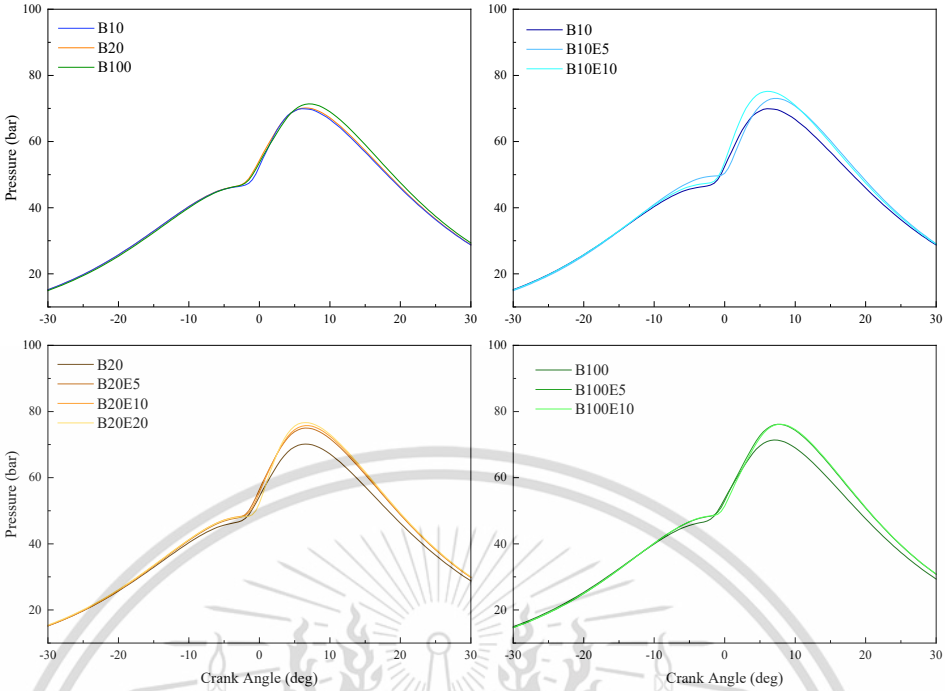

(g) In-cylinder pressure versus crank angle diagrams at 112Nm, 1500 RPM engine condition.

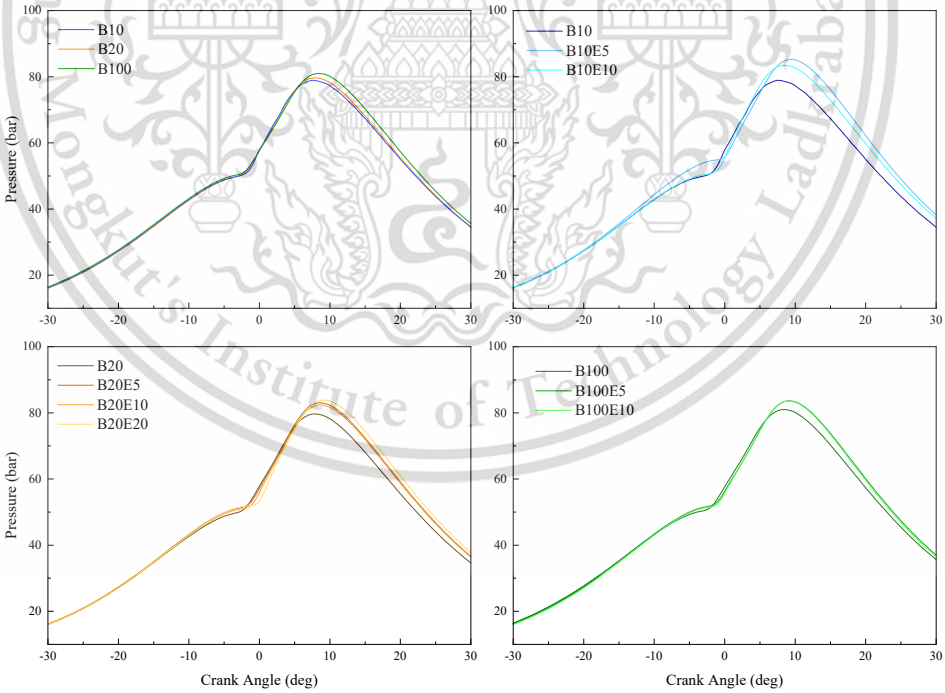

(h) In-cylinder pressure versus crank angle diagrams at 140Nm, 1500 RPM engine condition.

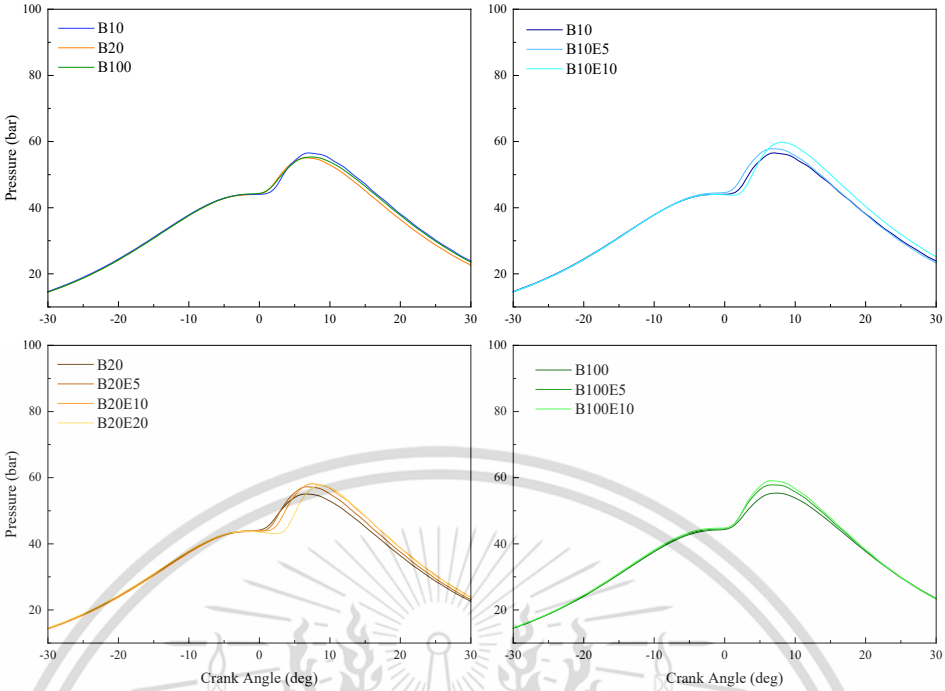

(i) In-cylinder pressure versus crank angle diagrams at 56Nm, 2000 RPM engine condition.

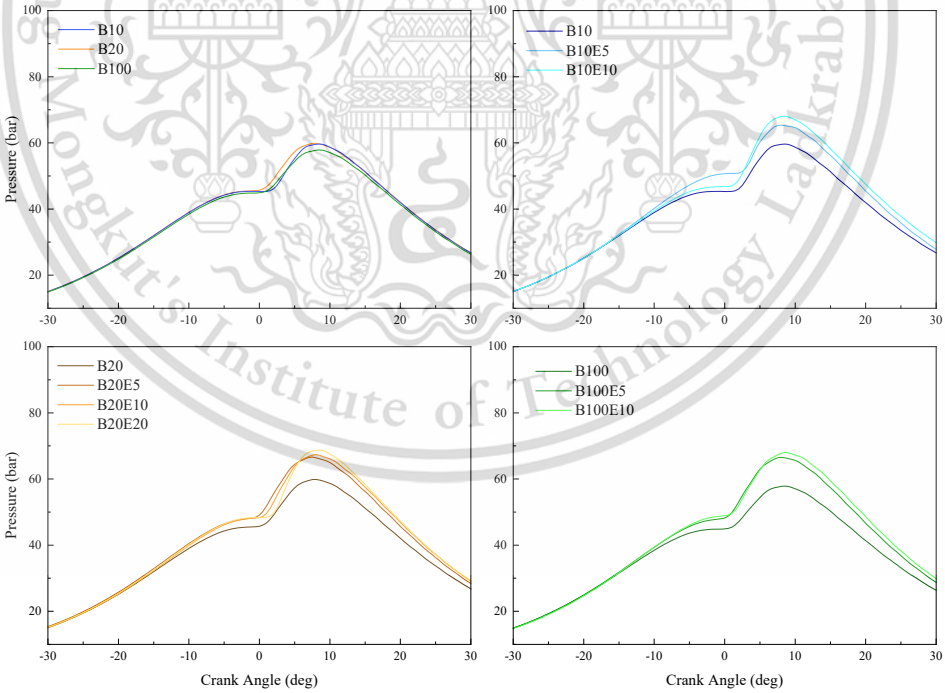

(j) In-cylinder pressure versus crank angle diagrams at 84Nm, 2000 RPM engine condition.

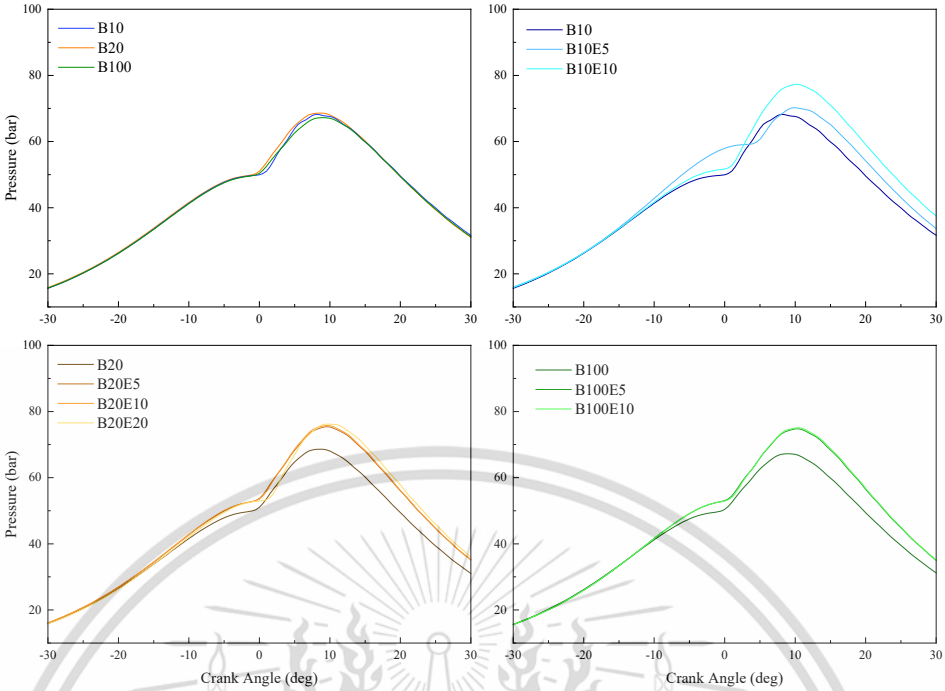

(k) In-cylinder pressure versus crank angle diagrams at 112Nm, 2000 RPM engine condition.

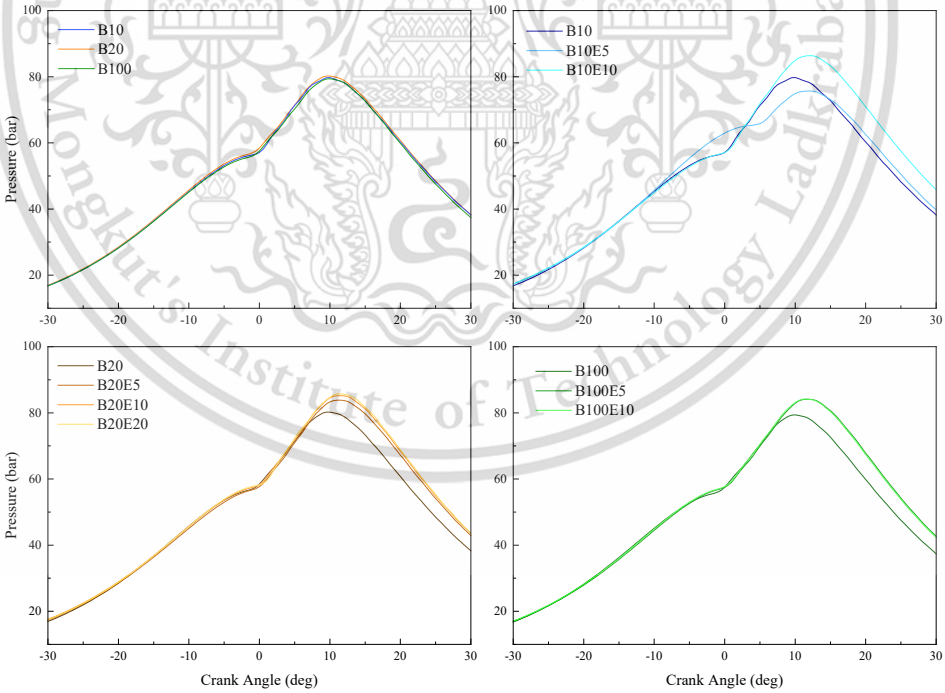

(l) In-cylinder pressure versus crank angle diagrams at 140Nm, 2000 RPM engine condition.

Figure 4-8 In-cylinder pressure versus crank angle diagrams at every tested engine conditions.

When compared between based biodiesel and diesel blended fuels, the differences of locations and values of in-cylinder pressure peaks are not significant. When the ethanol is added, the increasing in in-cylinder pressure is observed. That phenomena will be because of two reasons: higher amount of ethanol blended fuels was burnt in premixed combustion phase and higher oxygen content of ethanol blended fuels promoted the combustion quality.

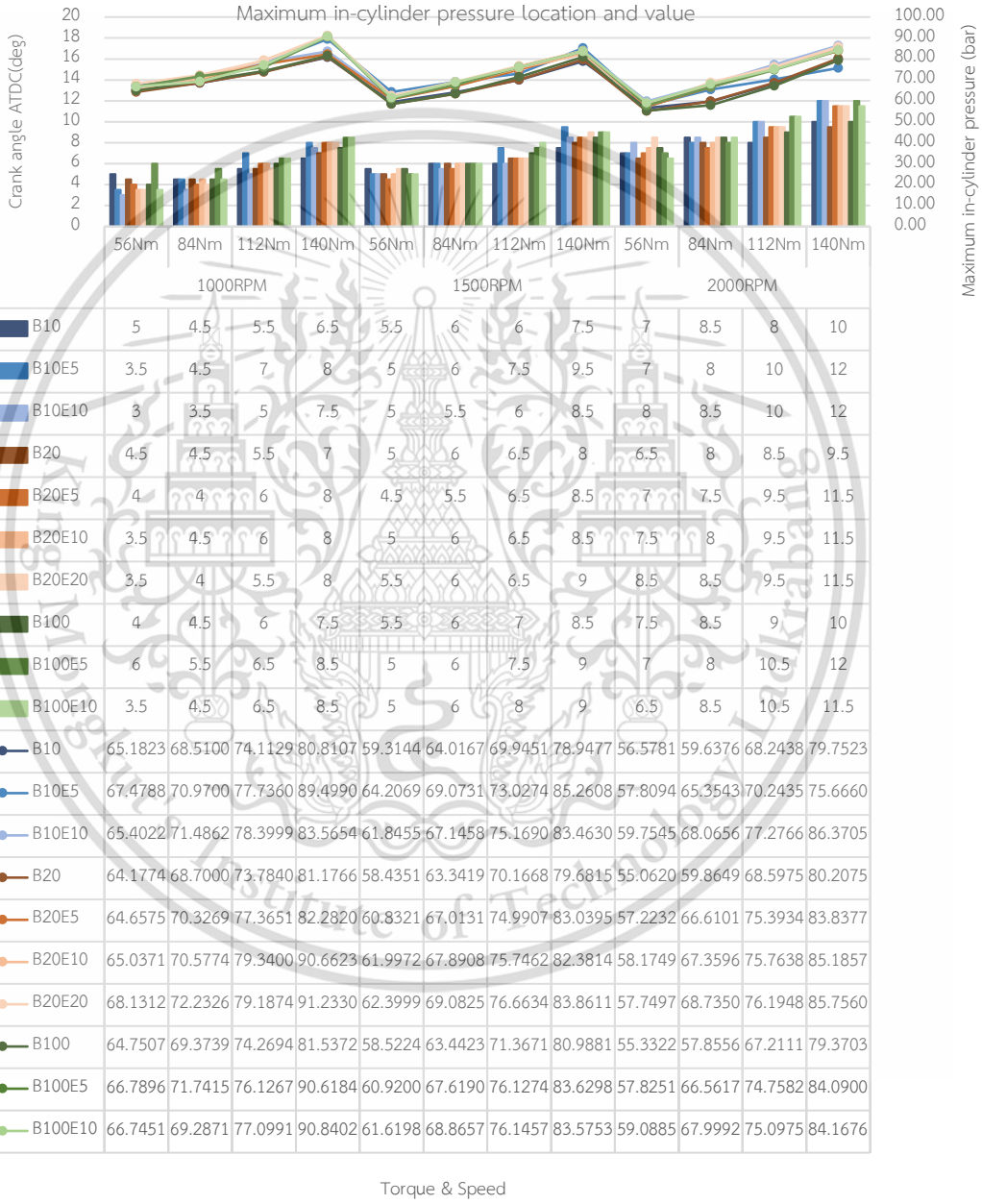

	1000RPM				1500RPM				2000RPM			
	56Nm	84Nm	112Nm	140Nm	56Nm	84Nm	112Nm	140Nm	56Nm	84Nm	112Nm	140Nm
B10	5	4.5	5.5	6.5	5.5	6	6	7.5	7	8.5	8	10
B10E5	3.5	4.5	7	8	5	6	7.5	9.5	7	8	10	12
B10E10	3	3.5	5	7.5	5	5.5	6	8.5	8	8.5	10	12
B20	4.5	4.5	5.5	7	5	6	6.5	8	6.5	8	8.5	9.5
B20E5	4	4	6	8	4.5	5.5	6.5	8.5	7	7.5	9.5	11.5
B20E10	3.5	4.5	6	8	5	6	6.5	8.5	7.5	8	9.5	11.5
B20E20	3.5	4	5.5	8	5.5	6	6.5	9	8.5	8.5	9.5	11.5
B100	4	4.5	6	7.5	5.5	6	7	8.5	7.5	8.5	9	10
B100E5	6	5.5	6.5	8.5	5	6	7.5	9	7	8	10.5	12
B100E10	3.5	4.5	6.5	8.5	5	6	8	9	6.5	8.5	10.5	11.5
B10	65.1823	68.5100	74.1129	80.8107	59.3144	64.0167	69.9451	78.9477	56.5781	59.6376	68.2438	79.7523
B10E5	67.4788	70.9700	77.7360	89.4990	64.2069	69.0731	73.0274	85.2608	57.8094	65.3543	70.2435	75.6660
B10E10	65.4022	71.4862	78.3999	83.5654	61.8455	67.1458	75.1690	83.4630	59.7545	68.0656	77.2766	86.3705
B20	64.1774	68.7000	73.7840	81.1766	58.4351	63.3419	70.1668	79.6815	55.0620	59.8649	68.5975	80.2075
B20E5	64.6575	70.3269	77.3651	82.2820	60.8321	67.0131	74.9907	83.0395	57.2232	66.6101	75.3934	83.8377
B20E10	65.0371	70.5774	79.3400	90.6623	61.9972	67.8908	75.7462	82.3814	58.1749	67.3596	75.7638	85.1857
B20E20	68.1312	72.2326	79.1874	91.2330	62.3999	69.0825	76.6634	83.8611	57.7497	68.7350	76.1948	85.7560
B100	64.7507	69.3739	74.2694	81.5372	58.5224	63.4423	71.3671	80.9881	55.3322	57.8556	67.2111	79.3703
B100E5	66.7896	71.7415	76.1267	90.6184	60.9200	67.6190	76.1274	83.6298	57.8251	66.5617	74.7582	84.0900
B100E10	66.7451	69.2871	77.0991	90.8402	61.6198	68.8657	76.1457	83.5753	59.0885	67.9992	75.0975	84.1676

Torque & Speed

Figure 4-9 The comparison of Maximum in-cylinder pressure values and position ATDC as well as data table.

4.2.2 Coefficient of variation of IMEP (COV_{IMEP})

The COV_{IMEP} is matter in engine analysis to describe the degree of changes in IMEP within the specific engine cycles [38]. **Figure 4-10** presents the coefficient of variation of indicated mean effective pressure for all tested fuels. The graph reveals that the maximum COV_{IMEP} of this study is 8.55%. It is quite high variation, but it is only in few engine conditions. Most of the results are less than 2%. Some conditions show the COV_{IMEP} of around 4 to 5 percent. The limitation of COV_{IMEP} for the diesel engine is 10% for the normal automotive drivetrain system safety [39], [20].

The COV_{IMEP} is high at the low power engine operating condition. In these engine conditions, the accelerator percent is very low and difficult to be stable. Most of the combustion parameters show fluctuations in the low power engine conditions. The COV_{IMEP} decreased with the increasing engine speed and loads. At the low engine conditions, the results show that COV decreased with the increasing biodiesel percentage in the blends because of the higher cetane number of biodiesels [40]. Adopted ethanol-biodiesel-diesel blended fuels result an increase in COV_{IMEP} than the ethanol free tested fuels. This is brought on by the high volatility of the ethanol, which has an impact on how the fuel mixture burns [41].

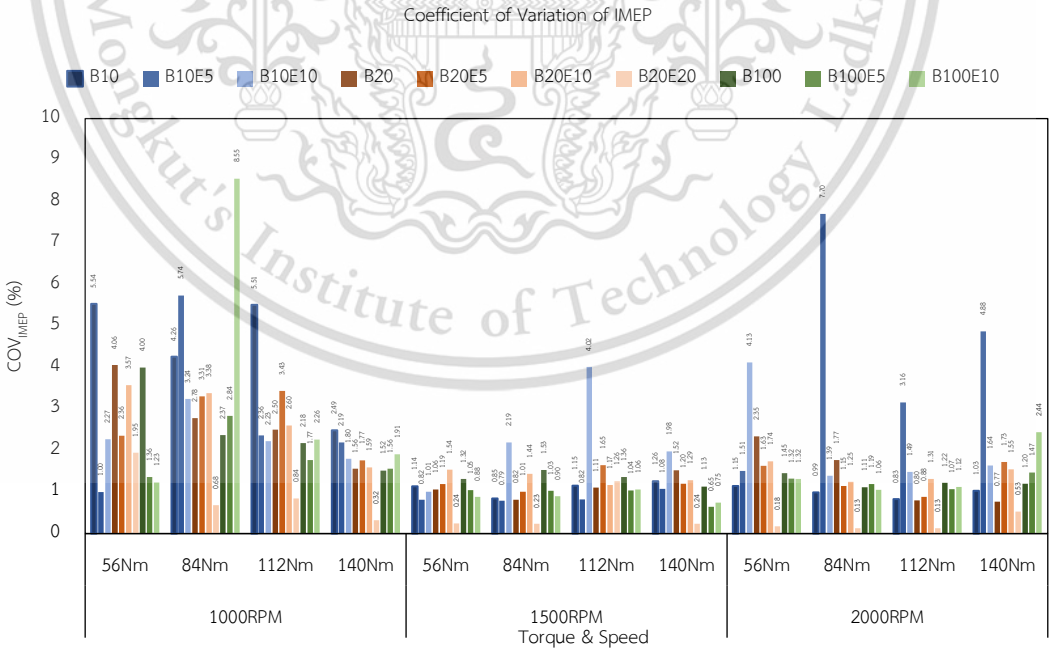

Figure 4-10 Cycle to cycle variation of IMEP (COVIMEP) of tested fuels

4.2.3 Maximum pressure rises rate

Figure 4-11 presents the results of the comparison of maximum pressure rise rate (MPRR) of all tested fuel at all testing engine conditions. If the MPRR is higher, the engine is nosier.

When the engine speeds are increased, the MPRR decreased because of lower premixed combustion ratio. This is attributed to the shorter fuel air mixing duration with the faster engine revolution. This contributes to the less uniform air-fuel mixture before the premixed combustion and therefore, less fuel is burnt in the premixed combustion phase. MPRR is not significantly change with the engine torque even the fuel mixtures are burnt in high temperature and pressure. Because the throttle opens wider at the higher engine load and hence more air enter to the cylinder during the intake stroke. Therefore, the compression pressure is also higher in the compression stroke because more volume of air is compressed. Therefore, the MPRRs are not different at the variable load conditions.

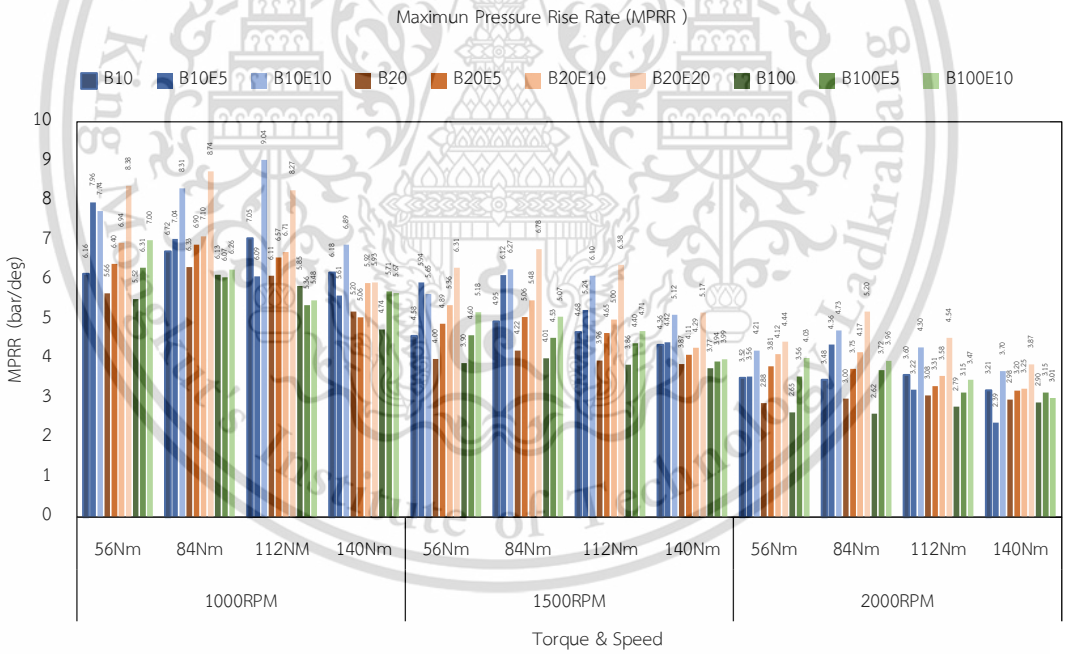

Figure 4-11 Comparison of maximum pressure rise rate (MPRR)

The MPRR decreased with the increasing biodiesel percentage in the blended fuels due to the higher cetane number of biodiesels. The higher cetane number contributes to the shorter the ignition delay period, led to lower premixed combustion ratio and the MPRR decreased. For the ethanol blended fuels, the higher auto ignition temperature and lower cetane number of ethanol prolong the ignition delay and causing the more uniform air fuel mixture. Hence, the premixed combustion ratio

higher with the increasing ethanol percentage in the blends. Additionally, the higher MPRR is presented [42].

4.2.4 Net heat release rate and Cumulative net heat release rate

The net heat release rate (NHRR) and cumulative net heat release (CNHR), averaged over 200 engine cycles, for the different tested fuels, are compared in **Figure 4-12** and **Figure 4-13.** The four groups of tested fuels are plotted as four graphs per engine condition. The plotted crank angle interval for NHRR graphs is -30 to 30 and for CNHR graphs is -60 to 60 crank angle degree to get the better visualization. All the investigated fuels have the NHRR trend: premixed combustion followed by diffuse combustion. Moreover, the negative heat release values were observed before the top dead center (TDC) after the start of the injection of fuel to evaporate the fuel droplets.

Due to the previously mentioned reduction in mixing time, the percentage of premixed combustion phase narrows as engine speeds increase. This contributes to lower peak NHRR in the premixed combustion phase for the higher engine speed. On the other hand, the heat release during the diffuse combustion phase increased with the engine speed. And the total cumulative net heat release (CNHR) increased as well. Furthermore, the maximum NHRR is discovered to be 84Nm for 1000 RPM and 1500 RPM engine speeds, but 140Nm for 2000 RPM engine speeds. This outcome is consistent with those of L. Zhu [43]. The lines of CNHR rise corresponding to the engine speed and engine load. This is as a result of the higher power output requiring more fuel to be used.

On the common rail direct injection diesel engine, the methyl ester biodiesel will begin the combustion sooner when compared to petroleum diesel fuel due to its higher bulk modulus [44]. Moreover, because of thermal cracking, injected biodiesel droplets may produce low molecular weight molecules inside engine cylinders [45]. These gaseous molecules were easily ignitable. Because of the upper reasons, blended fuels consisting of higher biodiesel percent start the combustion earlier. Therefore, B10 possesses the longest ignition delay among the based fuels, resulting in a higher NHRR than other biodiesel blends, especially at low engine torque of 56Nm and 84Nm. Nevertheless, NHRR of B10 is lower than the B20 and B100 at 140Nm engine load of 1500RPM and 2000RPM. The CNHR graphs reveal that the CNHR of B10 is highest in

lowest tested load 56Nm, but it is lowest in 140Nm engine load for every tested engine speed.

Unlike biodiesel and diesel fuel, the oxygen content of ethanol is incredibly high, and ethanol occupies higher autoignition temperature, higher heat of vaporization as well as lower cetane number. Due to these fuel properties, the ignition duration is more longer according to the ethanol contamination in the blended fuels [46]. This contributes to have finer uniform air-fuel mixture and lead to higher premixed combustion ratio. The result is a higher peak of NHRR, in-cylinder pressure, and MPRR than the free ethanol blends. The NHRR of ethanol blended fuels are higher than the based fuels during the diffuse combustion phase and the combustion end earlier as well because of the enrich oxygen content of ethanol blended fuels. The start and end of combustion as well as MFB will be briefly discussed in the next section. In the results of CNHR, the CNHR boosted by adding ethanol to the based fuels although the heating values of ethanol blends are lower. This is to be expected as both premixed combustion and diffused combustion phases had improved combustion quality due to the oxygen concentration of ethanol blended fuels.

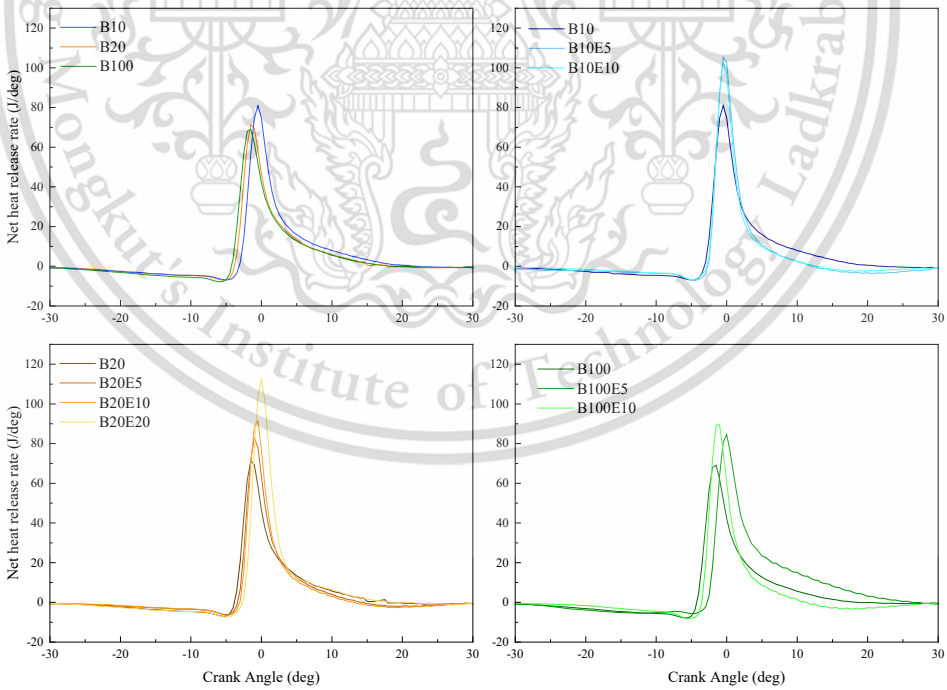

(a) Net heat release rate versus crank angle diagrams at 56Nm, 1000RPM engine condition.

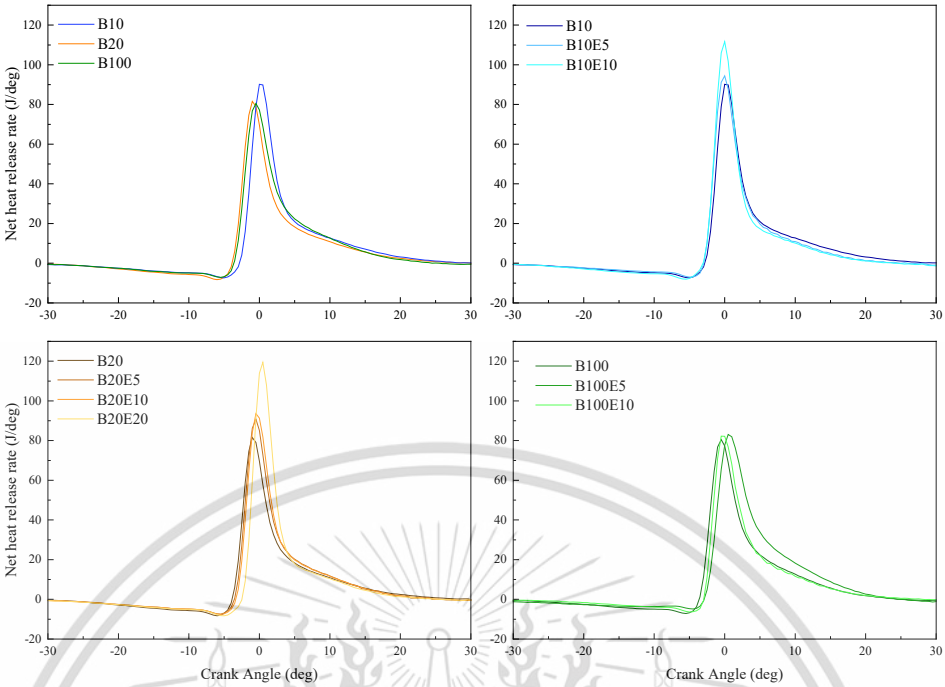

(b) Net heat release rate versus crank angle diagrams at 84Nm, 1000RPM engine condition.

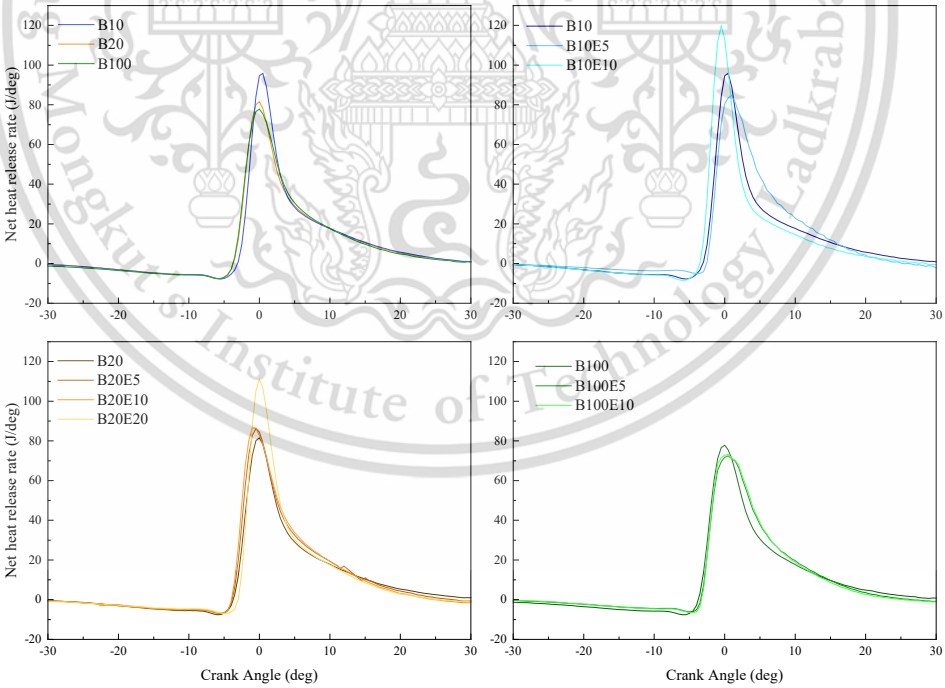

(c) Net heat release rate versus crank angle diagrams at 112Nm, 1000RPM engine condition.

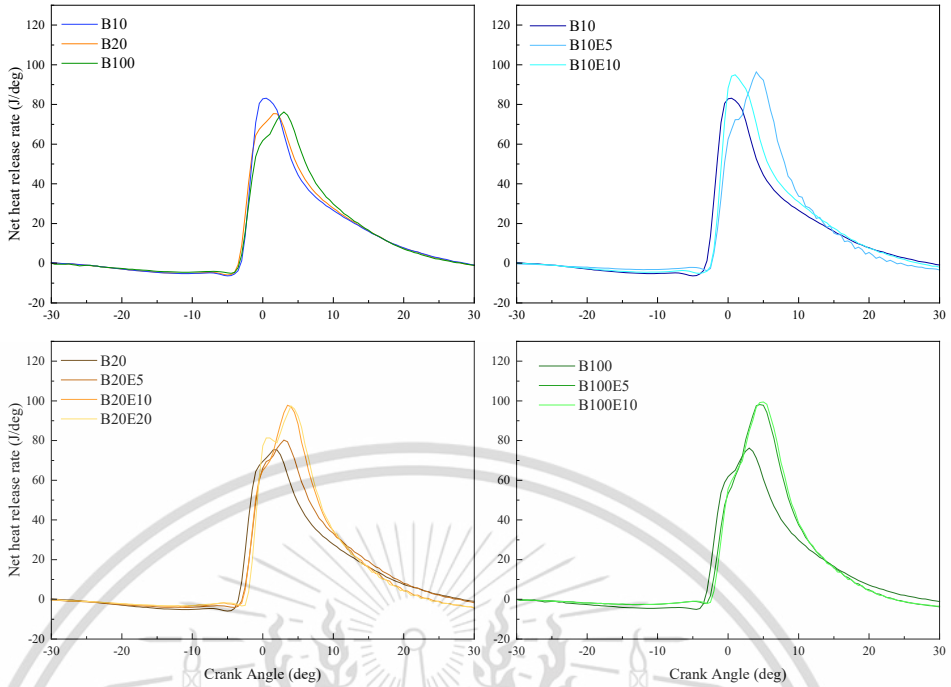

(d) Net heat release rate versus crank angle diagrams at 140Nm, 1000RPM engine condition.

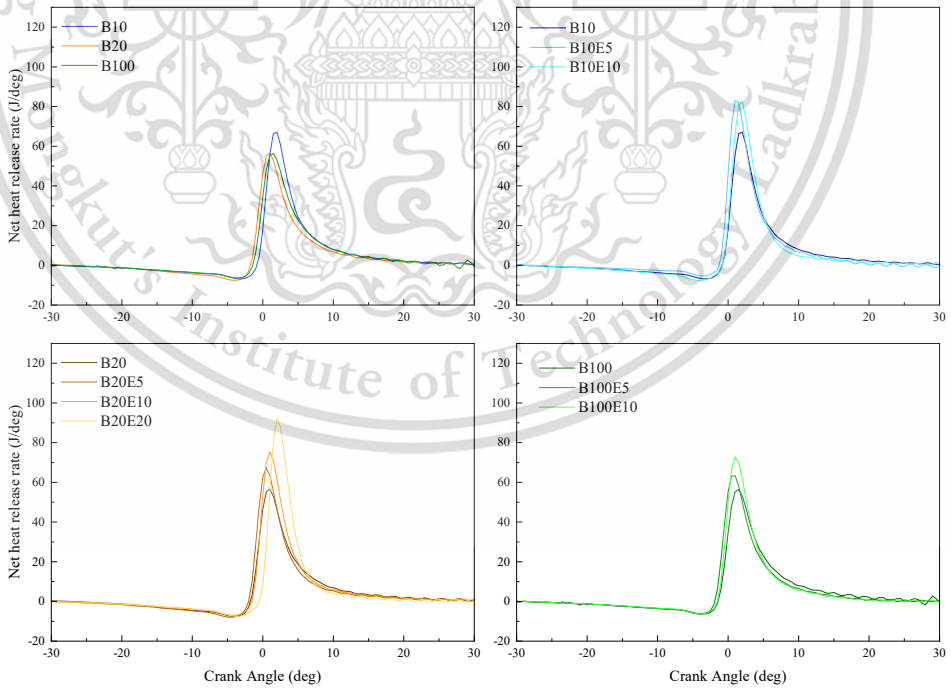

(e) Net heat release rate versus crank angle diagrams at 56Nm, 1500RPM engine condition.

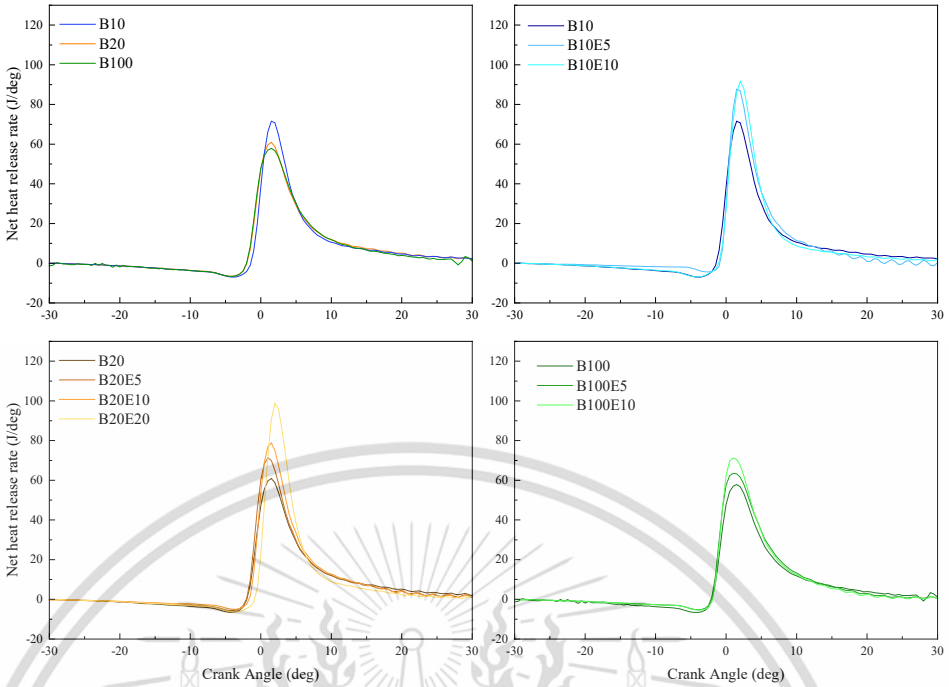

(f) Net heat release rate versus crank angle diagrams at 84Nm, 1500RPM engine condition.

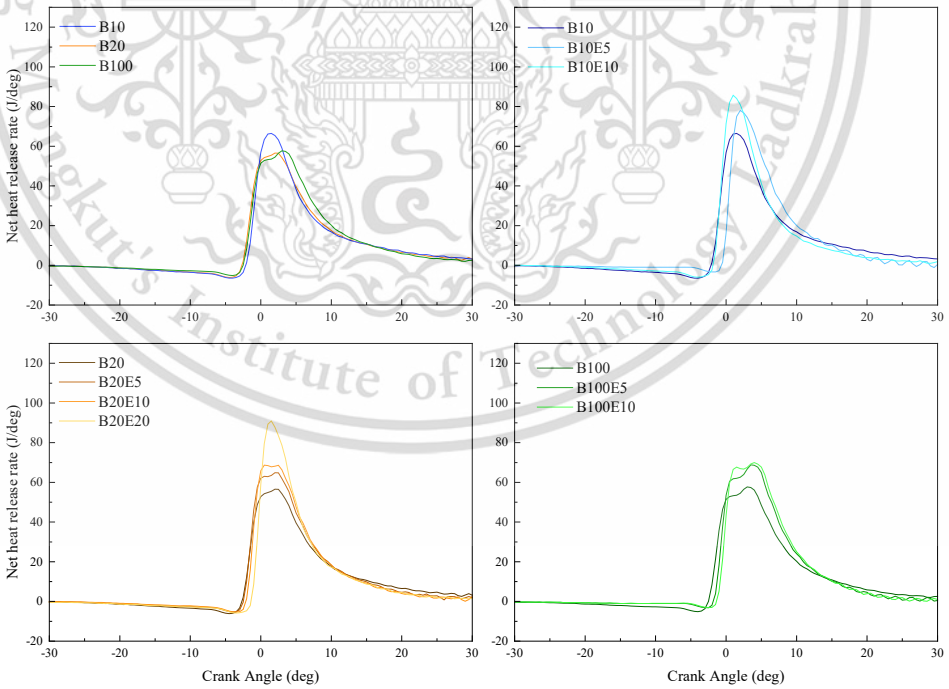

(g) Net heat release rate versus crank angle diagrams at 112Nm, 1500RPM engine condition.

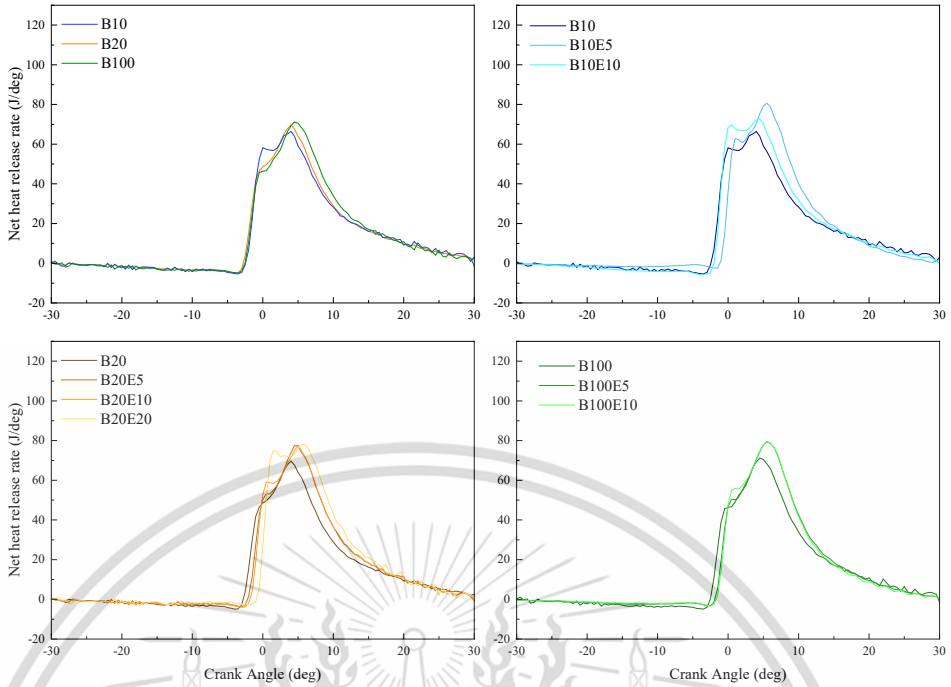

(h) Net heat release rate versus crank angle diagrams at 140Nm, 1500RPM engine condition.

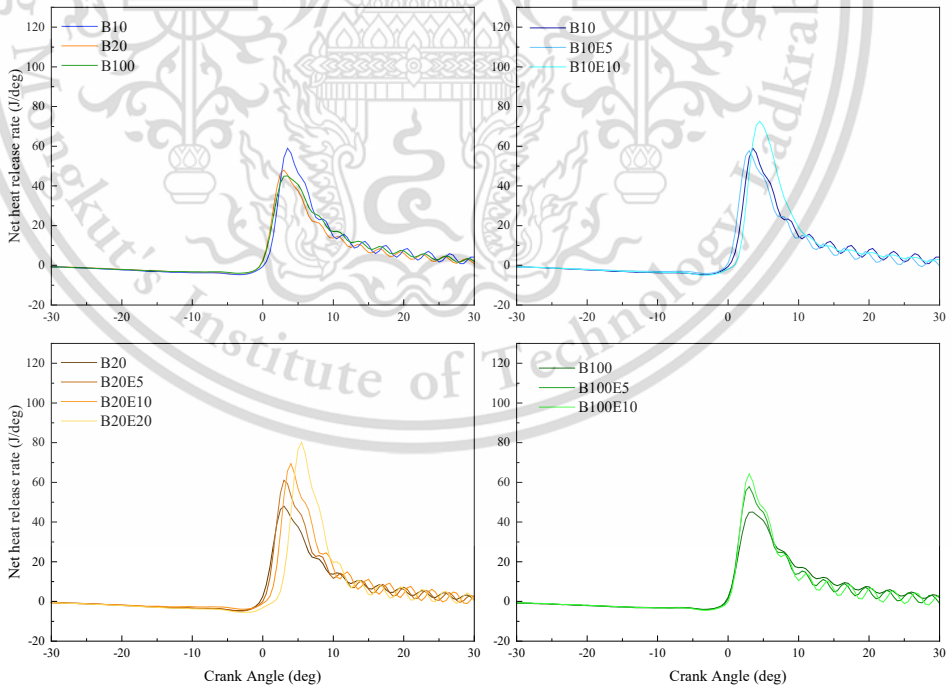

(i) Net heat release rate versus crank angle diagrams at 56Nm, 2000RPM engine condition.

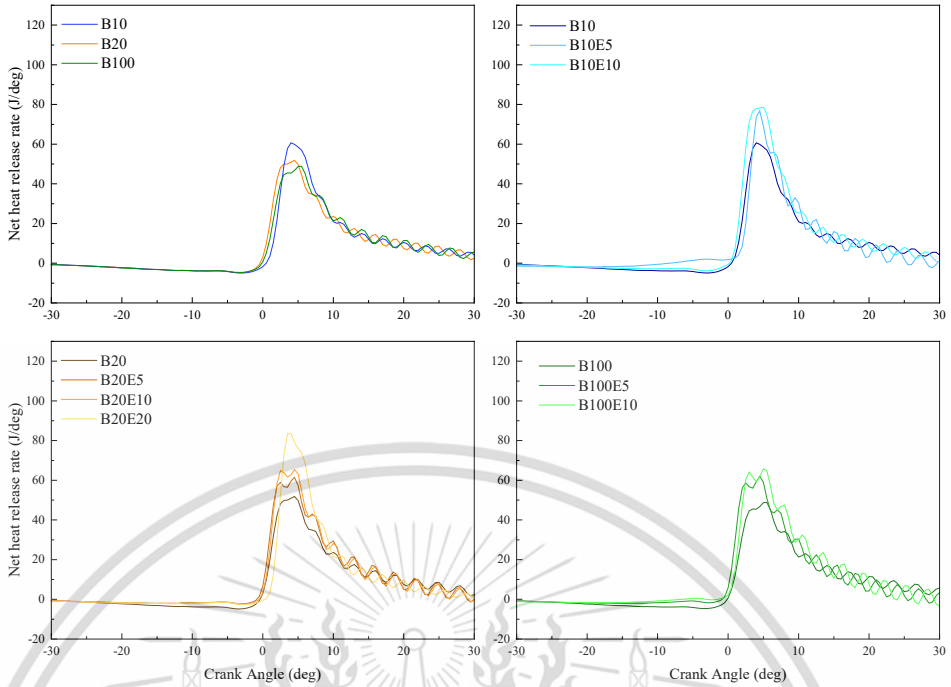

(j) Net heat release rate versus crank angle diagrams at 84Nm, 2000RPM engine condition.

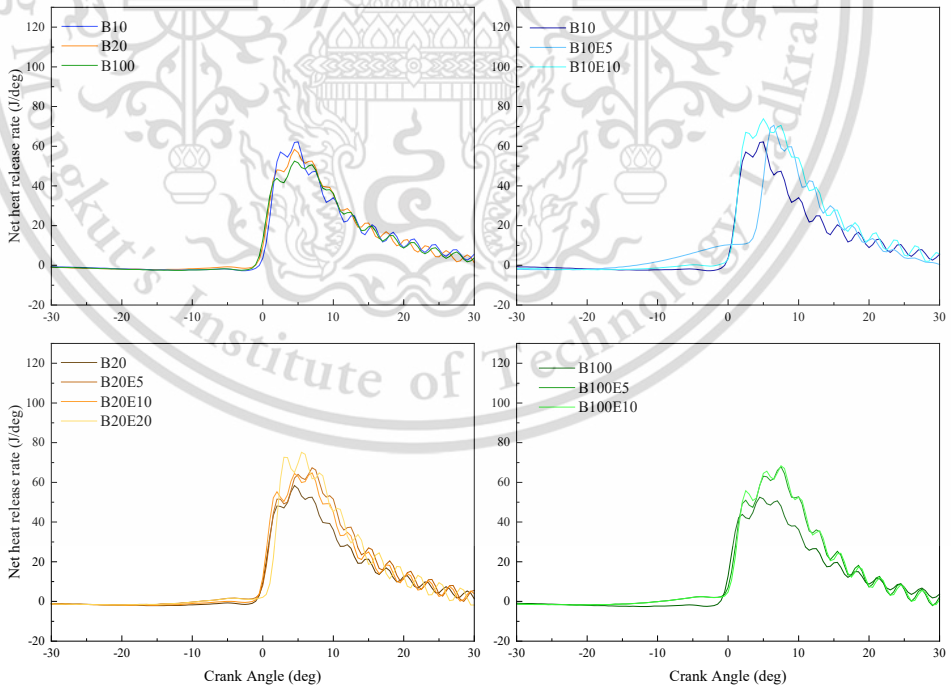

(k) Net heat release rate versus crank angle diagrams at 112Nm, 2000RPM engine condition.

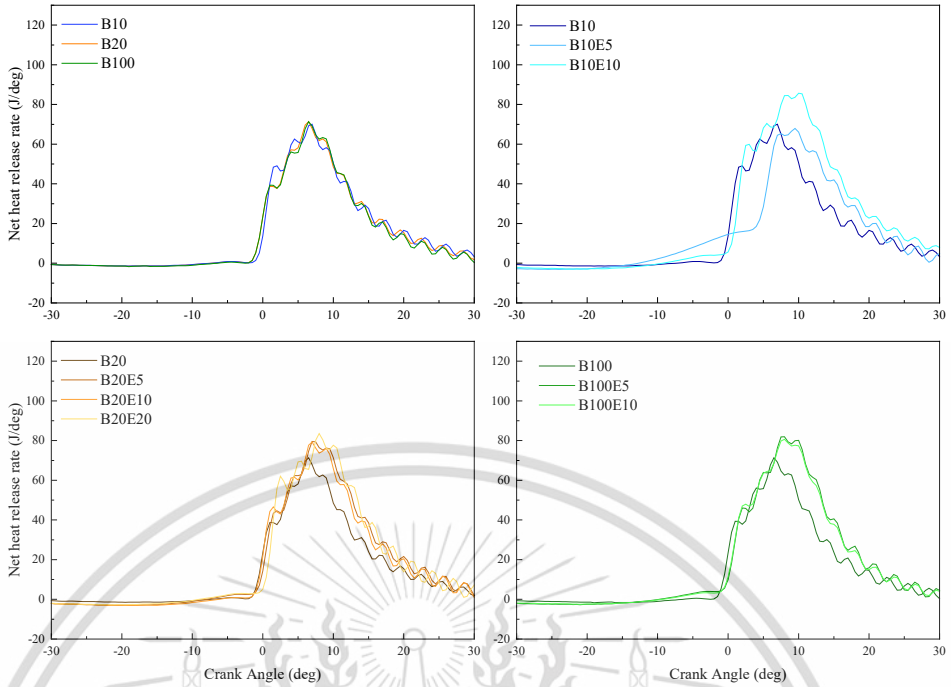

(l) Net heat release rate versus crank angle diagrams at 140Nm, 2000RPM engine condition.

Figure 4-12 Net heat release rate versus crank angle diagrams at every engine conditions.

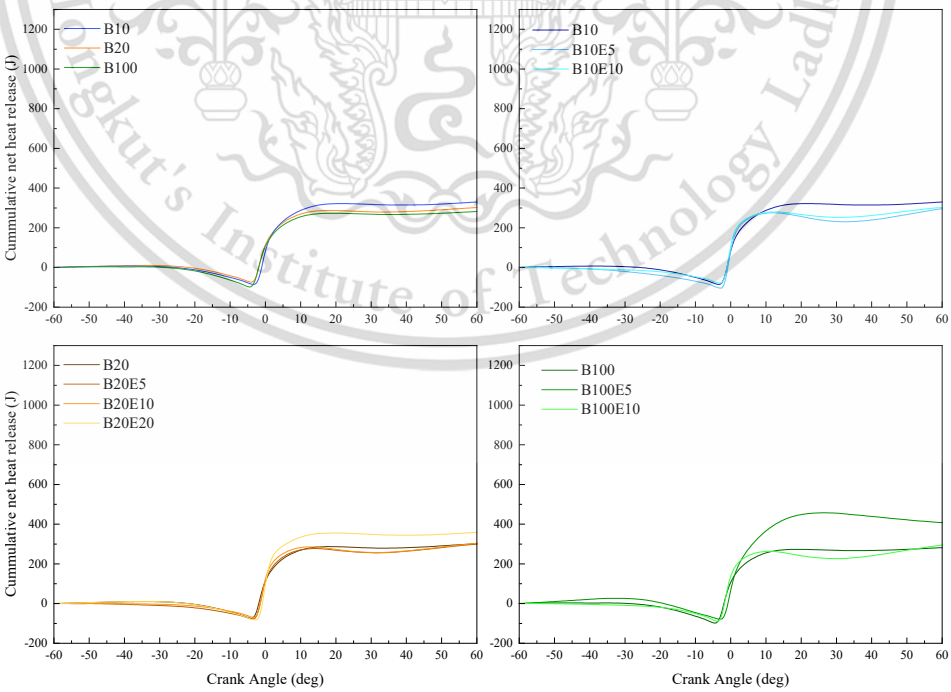

(a) Cumulative net heat release versus crank angle diagrams at 56Nm, 1000RPM engine conditions.

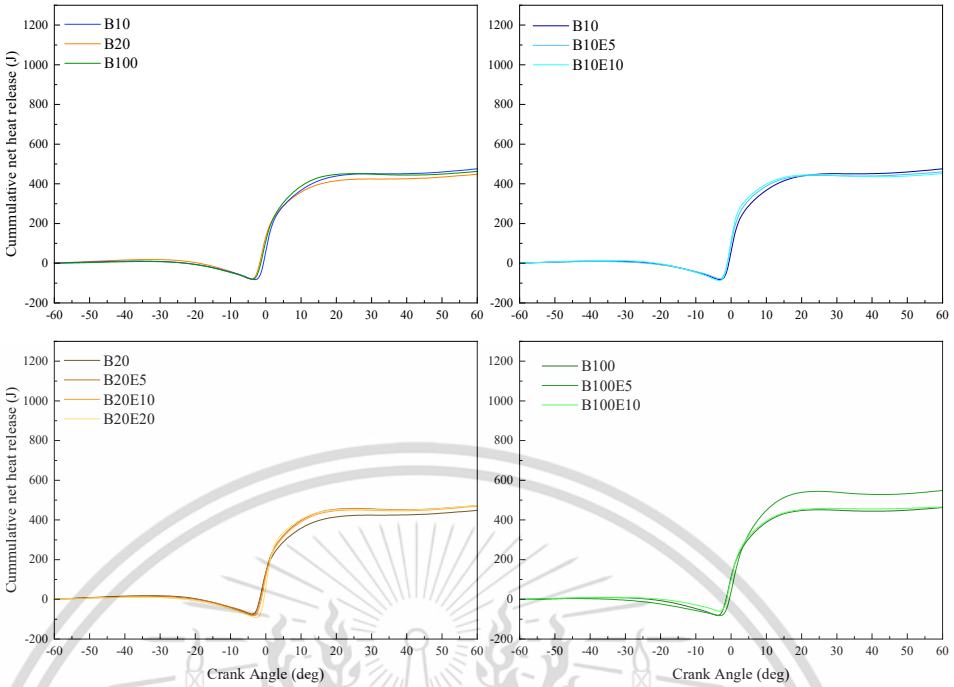

(b) Cumulative net heat release versus crank angle diagrams at 84Nm, 1000RPM engine conditions.

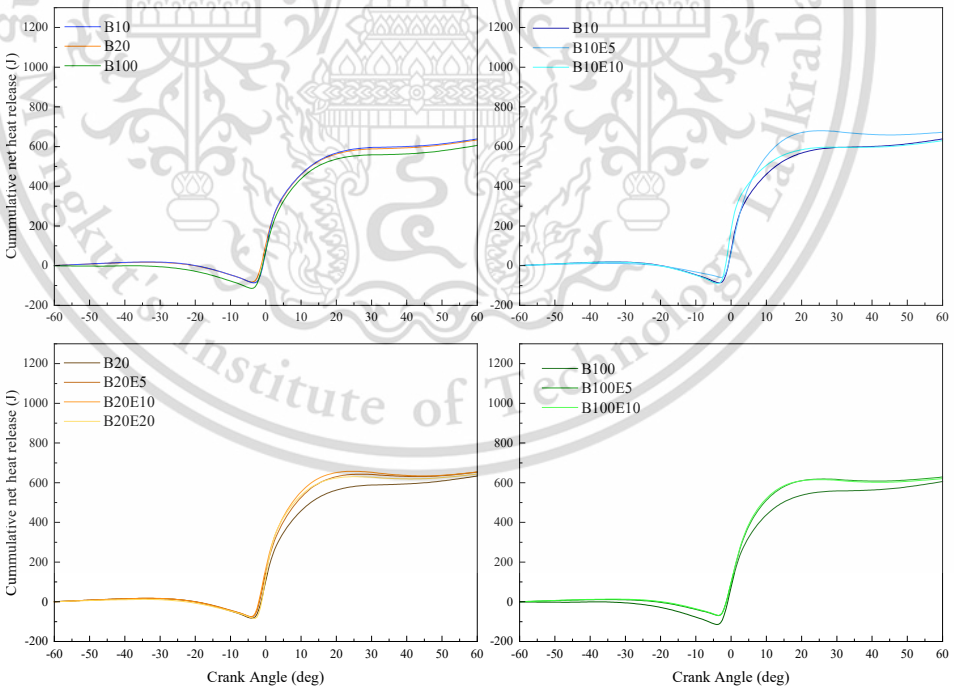

(c) Cumulative net heat release versus crank angle diagrams at 112Nm, 1000RPM engine conditions.

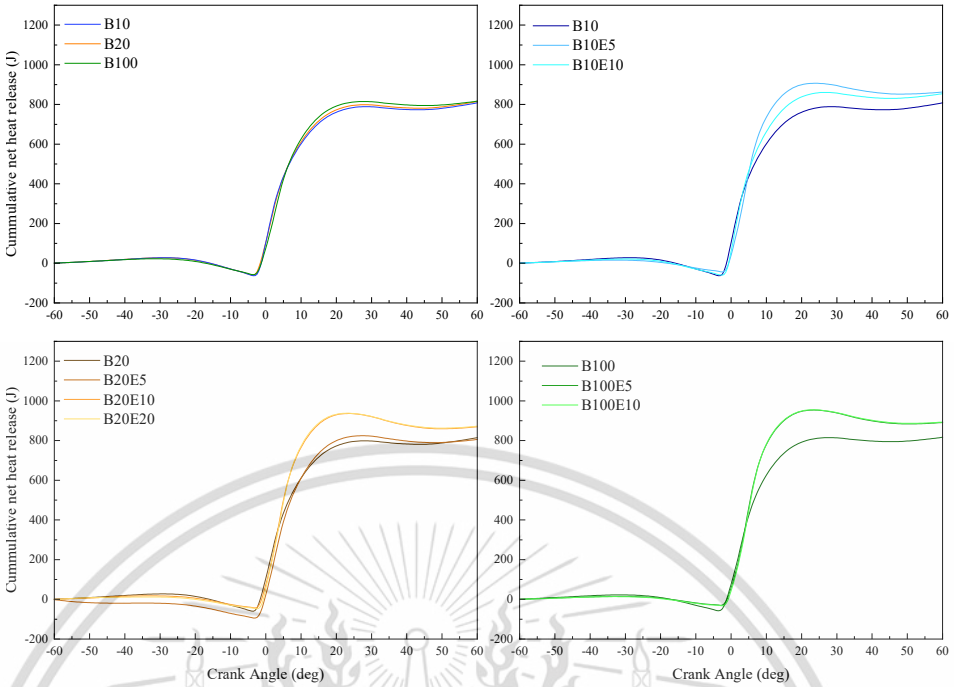

(d) Cumulative net heat release versus crank angle diagrams at 140Nm, 1000RPM engine conditions.

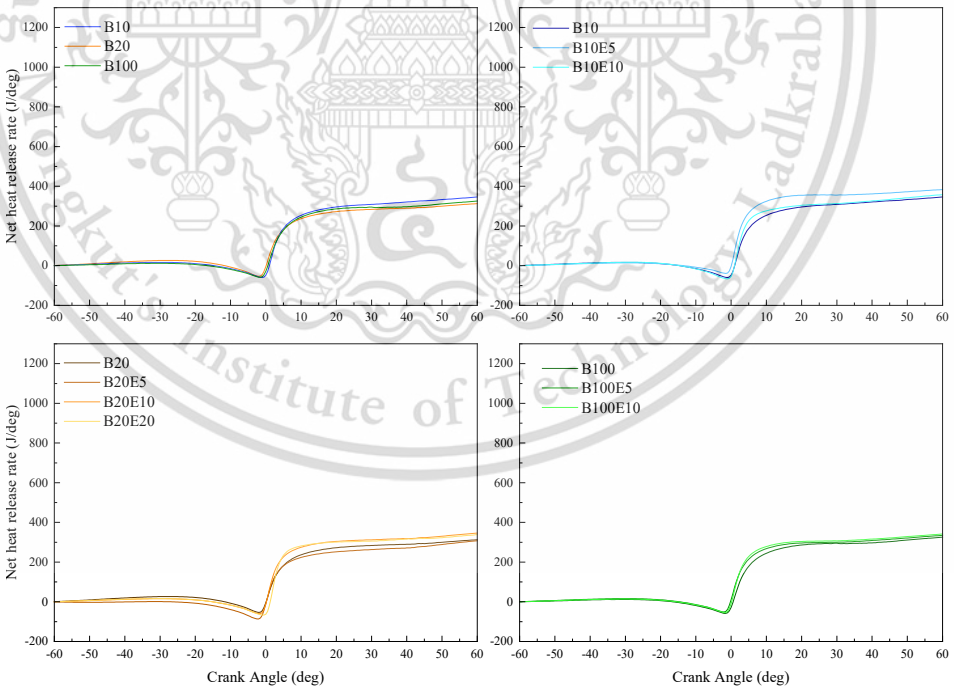

(e) Cumulative net heat release versus crank angle diagrams at 56Nm, 1500RPM engine conditions.

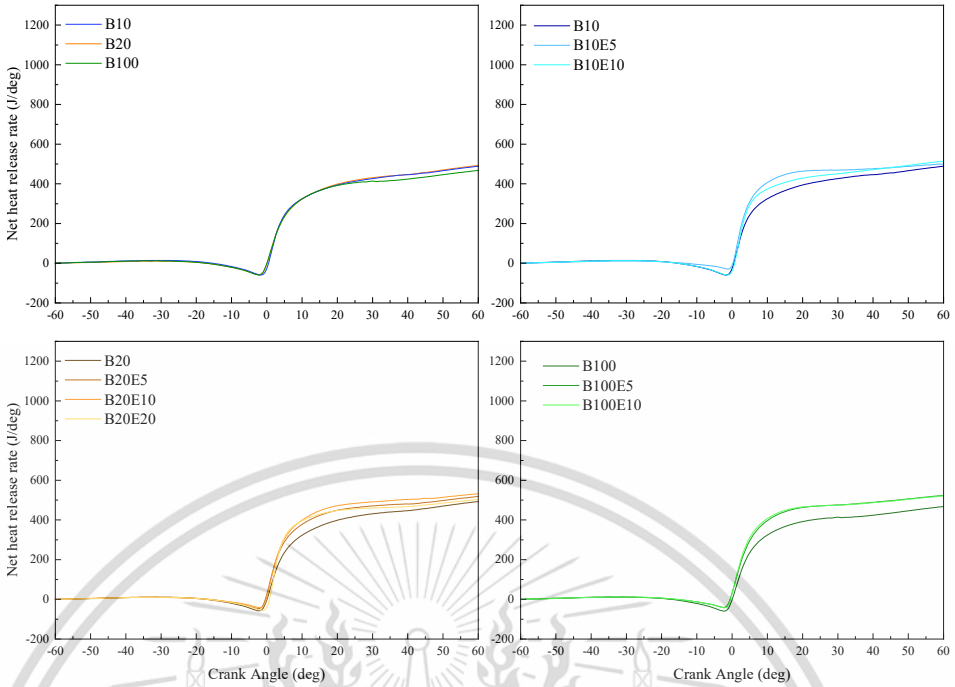

(f) Cumulative net heat release versus crank angle diagrams at 84Nm, 1500RPM engine conditions.

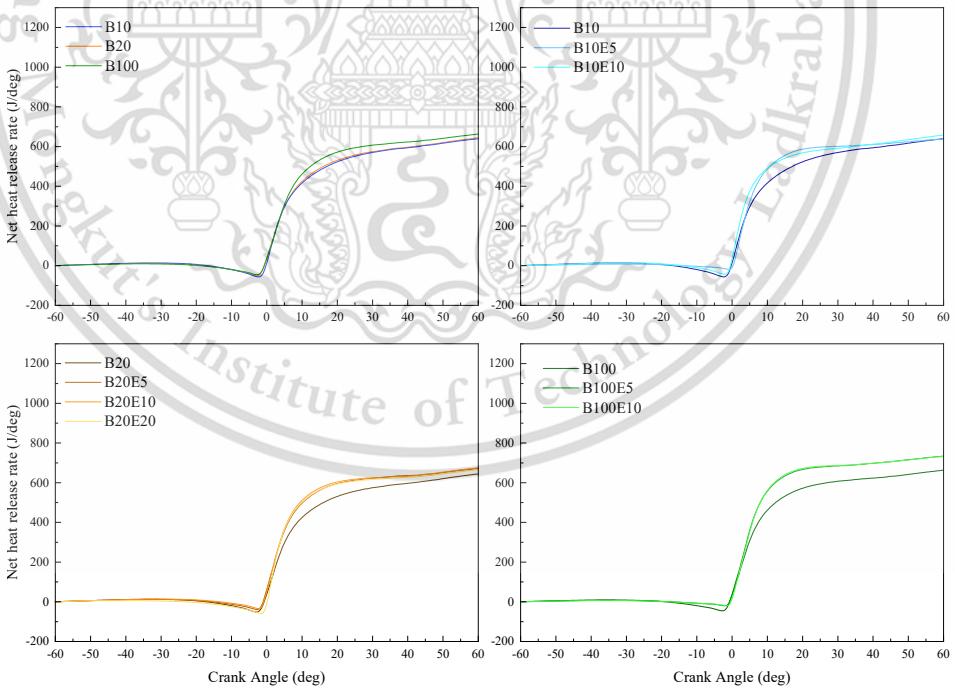

(g) Cumulative net heat release versus crank angle diagrams at 112Nm, 1500RPM engine conditions.

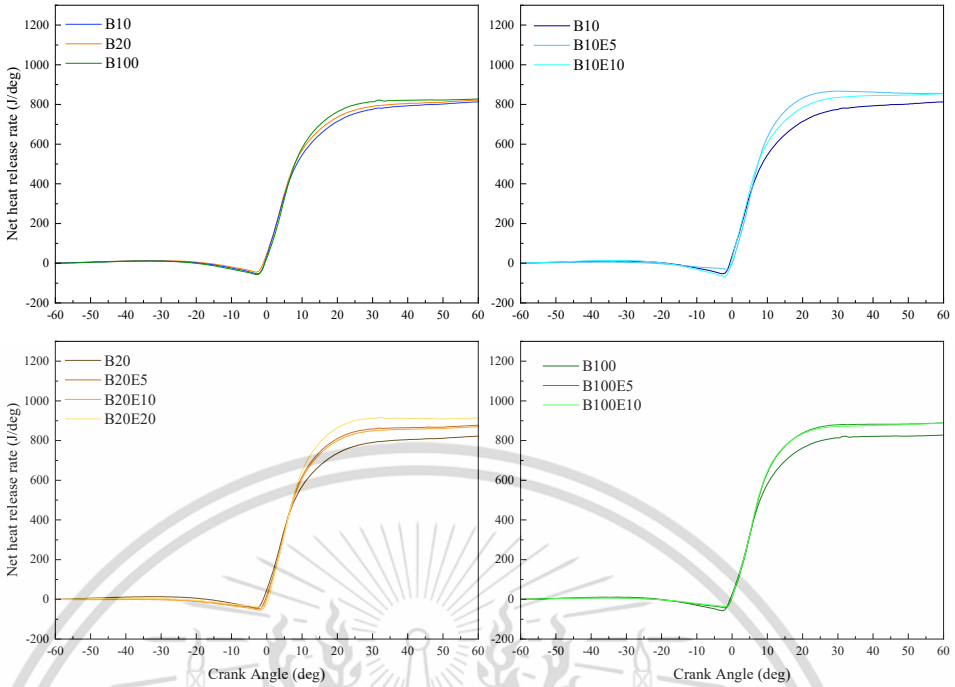

(h) Cumulative net heat release versus crank angle diagrams at 140Nm, 1500RPM engine conditions.

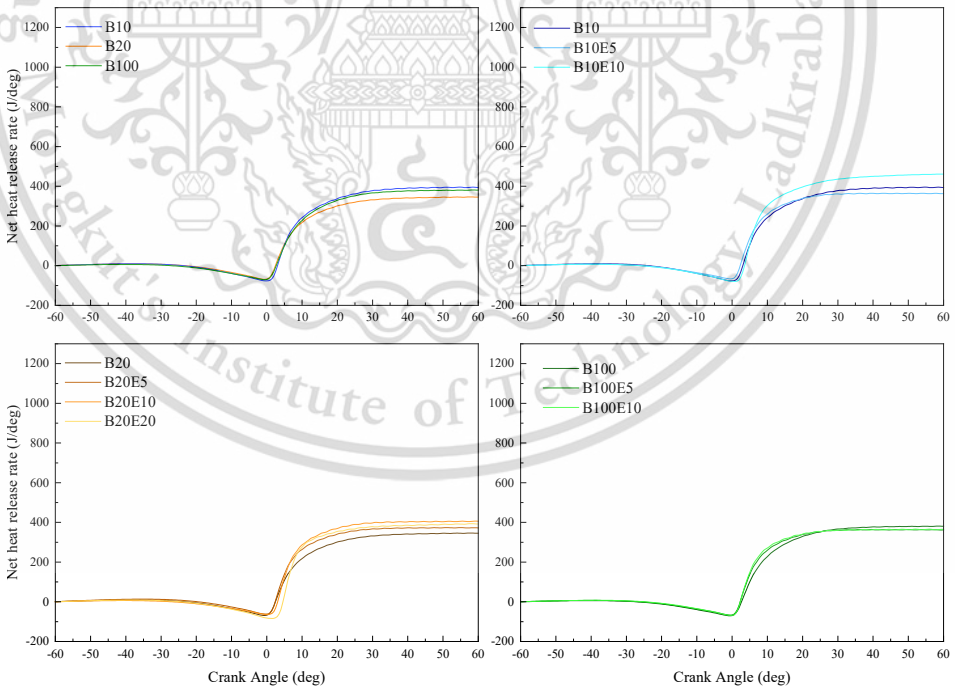

(i) Cumulative net heat release versus crank angle diagrams at 56Nm, 2000RPM engine conditions.

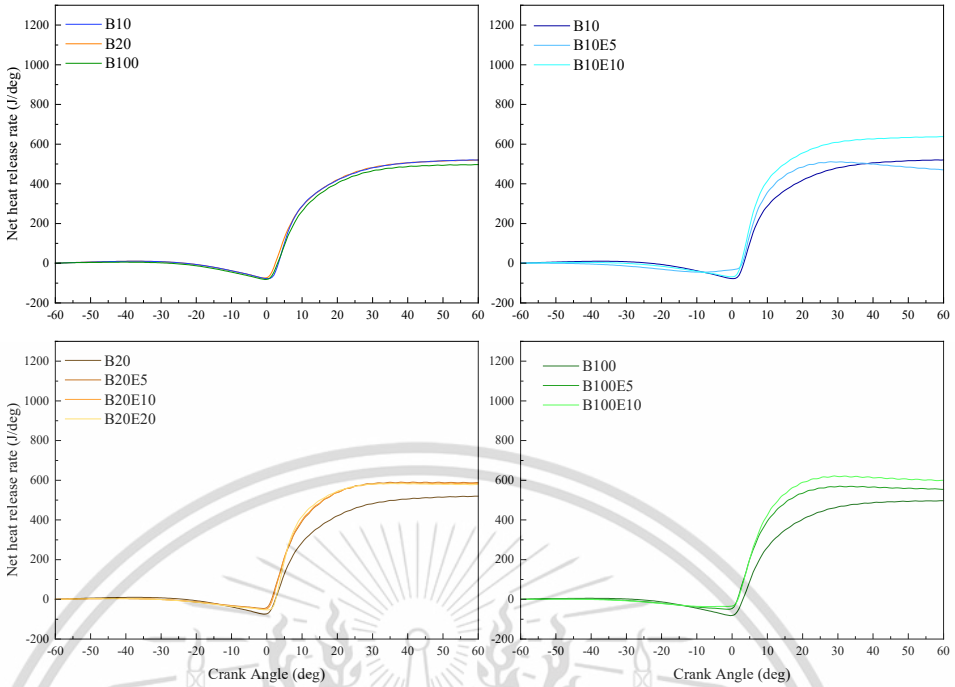

(j) Cumulative net heat release versus crank angle diagrams at 84Nm, 2000RPM engine conditions.

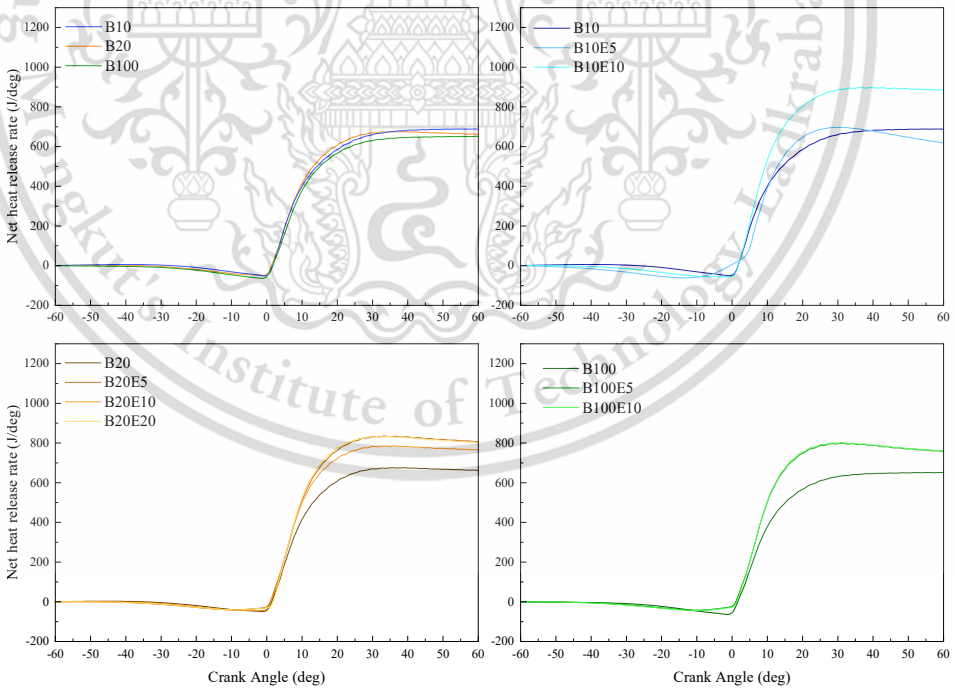

(k) Cumulative net heat release versus crank angle diagrams at 112Nm, 2000RPM engine conditions.

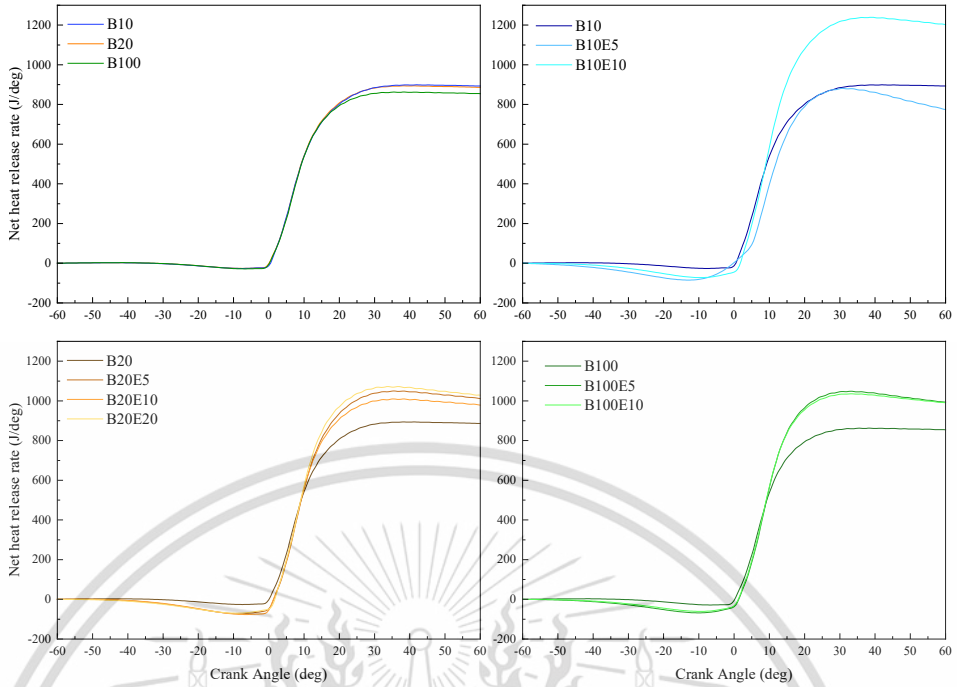

(l) Cumulative net heat release versus crank angle diagrams at 140Nm, 2000RPM engine conditions.

Figure 4-13 Cumulative net heat release (CNHR) versus crank angle diagrams at every engine conditions

4.2.5 Combustion Duration

Figure 4-14 describes the difference of combustion duration of all tested fuel at every engine testing conditions. It is the period between the start of combustion and end of combustion. More fuel is needed to supply to get higher power. Therefore, the combustion time is longer with the increasing engine speed and loads.

The **Figure 4-14** declared that the combustion duration is shorter with the increasing biodiesel and ethanol in the blend. According to this finding, the oxygenated biofuels, both biodiesel and ethanol, could boost the oxidation, hence resulting the shorter combustion duration. This consequence could be approved by literatures. R.J Donahue and D.E Foster also pointed out that Higher oxygen content while burning from oxygenated fuel or intake air diminishes pyrolysis and boosts oxidation [47]. Due to the longer ignition delay of ethanol blended fuels in comparison to other biodiesel blends, more fuel is ready for atomization, perfectly mixed and gets accumulated into the cylinder, which leads to a shorter combustion time. The shorter combustion

duration might increase the thermal efficiency because of the reduction of thermal losses to the cylinder wall [48].

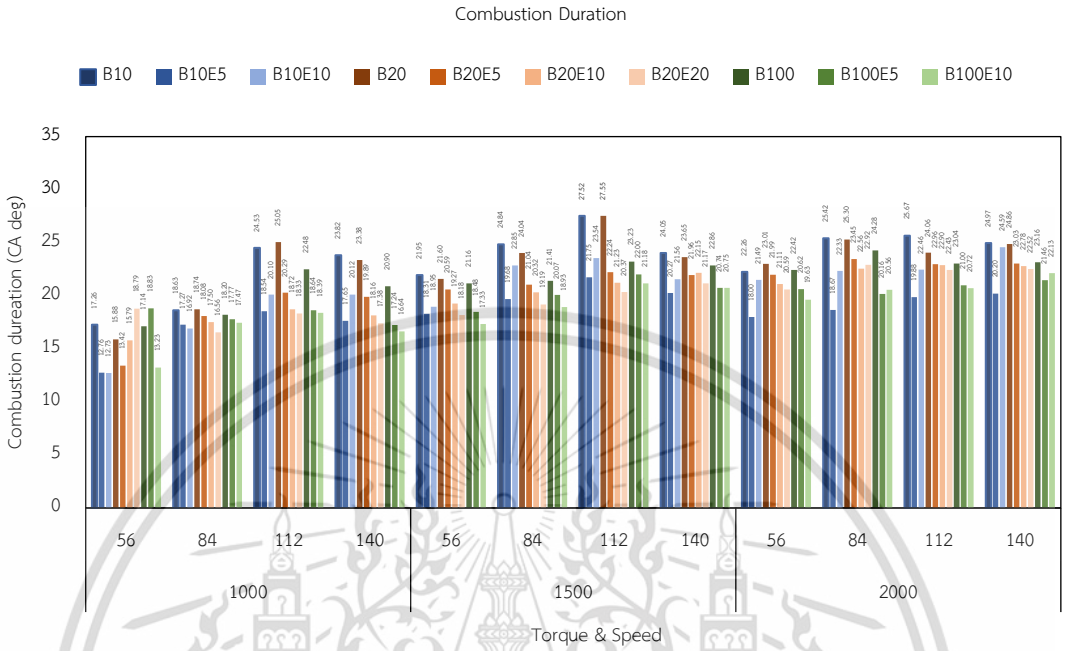

Figure 4-14 Comparison of combustion duration of every tested fuel at every engine conditions

4.2.6 Mass fraction burnt

For the better understanding of diesel-biodiesel-ethanol ternary blended fuel combustion, the mass fraction burned (MFB) analysis was added to this study. **Figure 4-15** shows the effect of different engine conditions and different fuel blends on the crank angle corresponding to 5%, 10% and 90% MFB. The 5% MFB could be estimated as start of combustion and the 90%MFB could be estimated as end of combustion. The maximum heat release rate was observed at 50% MFB crank angle.

As seen in the figures, combustion shifted to right and longer as the engine speed and load are grown. This is due to the increased amount of injected fuel requiring more time to evaporate and burn. The 5% MFB results prove the former statement that the more biodiesel content fuels start the combustion earlier as well as the more ethanol content fuels start the combustion later. On the other hand, the 50% MFB gives information about thermal efficiency. The more the 50% MFB is near the TDC, the greater the power output is and the higher the thermal efficiency. The figures reveal that although ethanol blends started the combustion recently, they finished the combustion early.

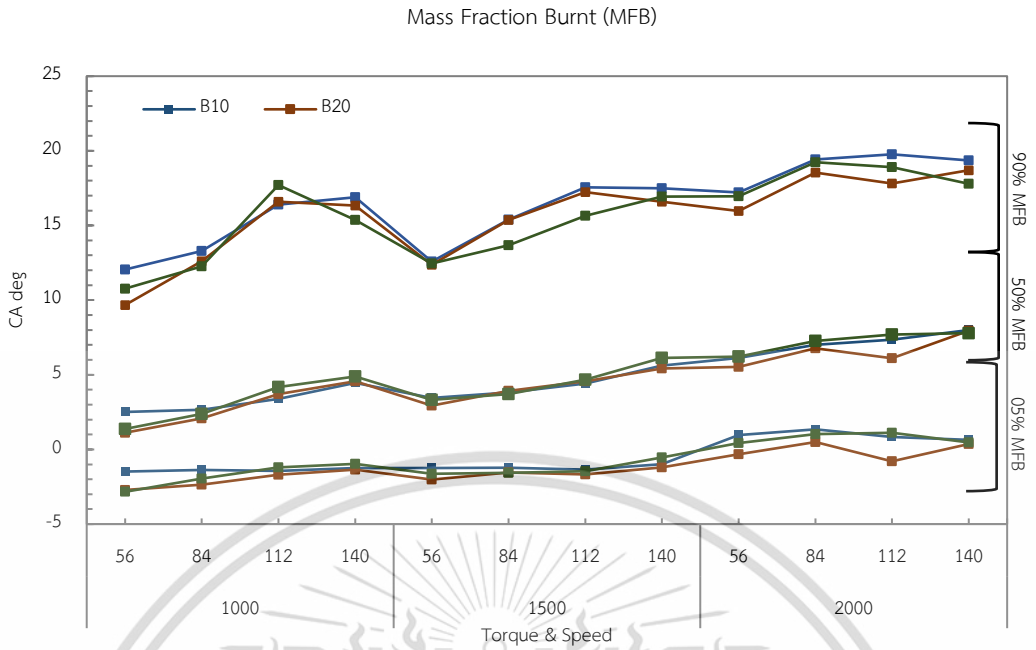

(a) B10, B20, and B100

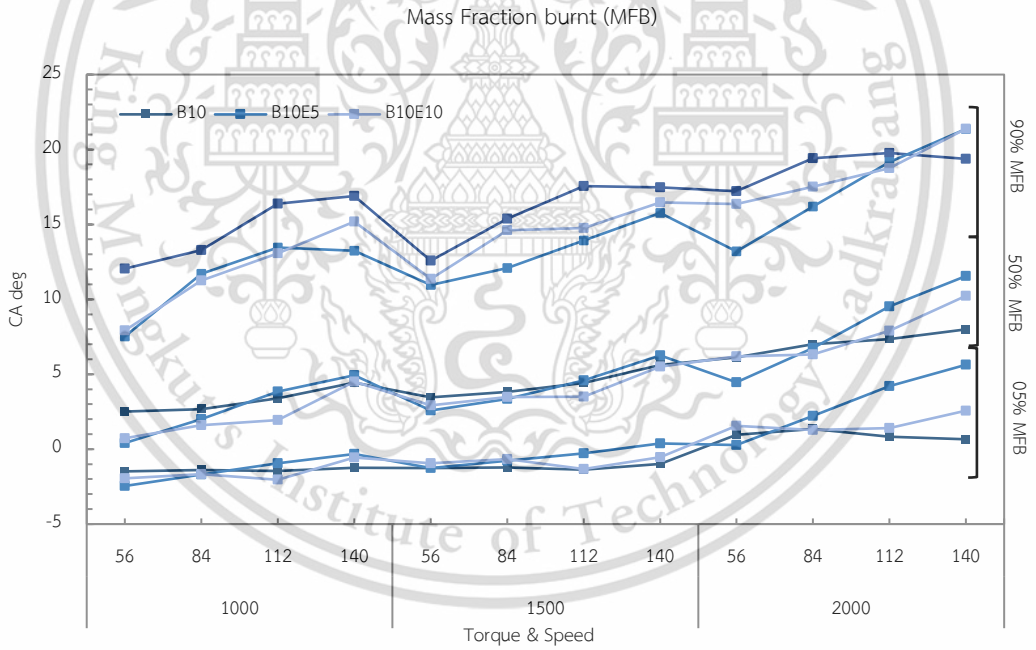

(b) B10, B10E5, and B10E10

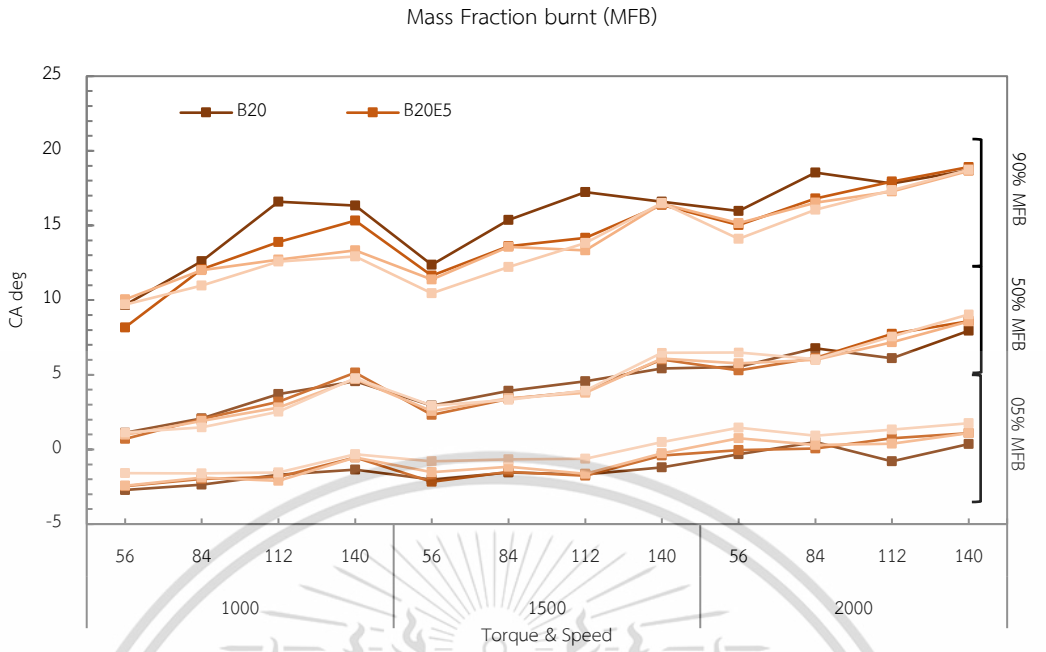

(c) B20, B20E5, B20E10, and B20E20

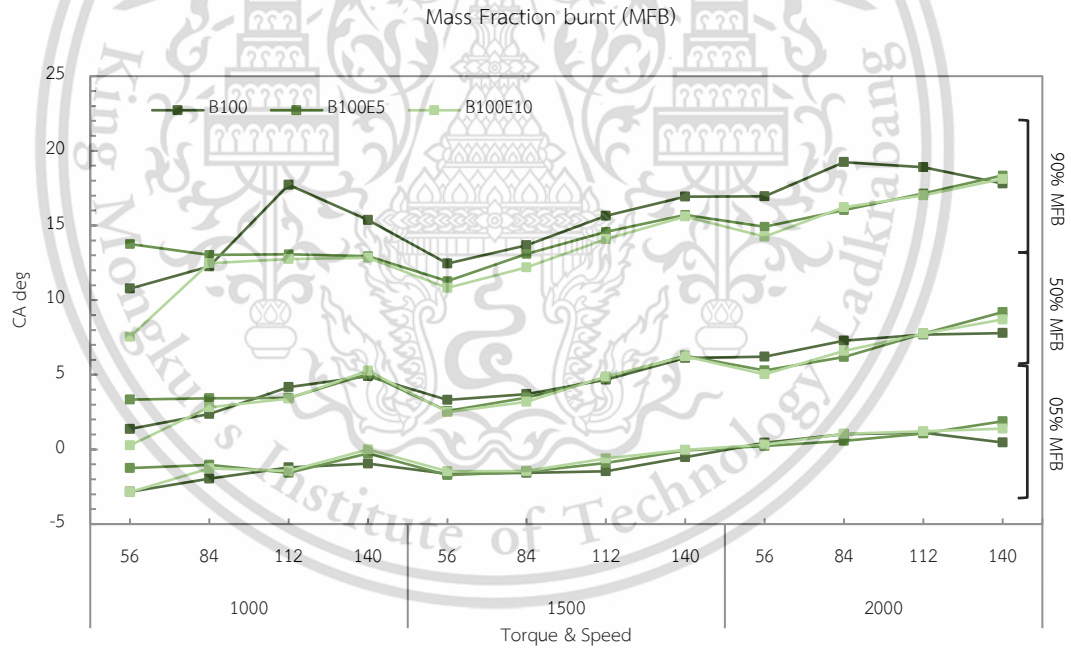

(d) B100, B100E5 and B100E10

Figure 4-15 Comparison of crank angle degree position of 5% MFB, 50% MFB and 90% MFB of (a) B10, B20 and B100, (b) B10, B10E5, and B10E10, (c) B20, B20E5, B20E10, and B20E20 and (d) B100, B100E5, and B100E10.

4.3 Emissions Characteristics

4.3.1 Fuel-air equivalent ratio

In this study, the mass of air flow was not measured at the air inlet, although the mass of air-fuel ratio can be estimated by equivalencing the exhaust gases of HC, CO, CO2 and O2. **Figure 4-16** presents what is the impact of engine conditions and fuel properties on the fuel-air equivalent ratio. The fuel-air equivalent ratio significantly changes because of the engine speed than because of the engine load. The graph illustrates that the fuel-air equivalent ratio increased gradually with the increased engine because more fuel is injected into the cylinder. However, it is decreased at the higher engine speed because of higher turbocharger boost pressure. At the higher engine speed, the faster movement of cylinders push out the exhaust gases with higher flow rate and the turbocharger is driven by that exhaust gases flow. Therefore, the turbo pressure increased at the higher engine speed. This contributes to suck more air to the cylinder and decreased fuel-air equivalent ratio at the higher engine speed.

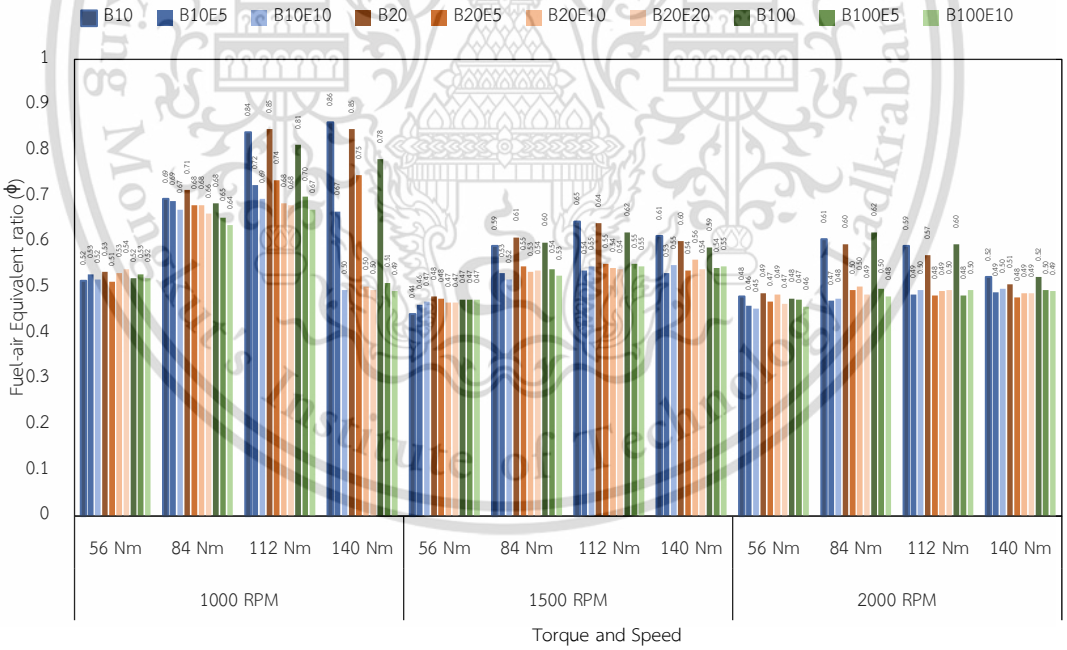

Figure 4-16 Fuel-air equivalent ratio

As mentioned before, the estimation of the fuel-air equivalent ratio is derived from the emissions of exhaust gases and hence the effects of fuel oxygen on the fuel-air equivalent ratio, leading to a lower number. This means that the fuel-air ratio

decreases with the increasing biofuel and ethanol portion in the blends because of the higher oxygen content of biofuels.

4.3.2 Emissions of smoke

The smoke intensity was measured by using the BOSCH smoke intensity meter and shown in **Figure 4-17**. Moreover, the smoke intensity was normalized by engine brake power and described in **Figure 4-18.** The smoke intensity decreased at the optimum engine conditions of 1500 RPM and 2000 RPM according to engine performance than the idle engine speed of 1000 RPM. At the optimum power output conditions, the smoke emission reduces as well. In the 1000 RPM engine speed, the smoke intensity grows with the engine loads because more fuel is used to produce higher load [49]. The smoke emissions, at 112Nm and 140Nm of 1000 RPM engine speed, are incredibly higher than other engine conditions because of torque and speed unbalance. In these engine conditions, huge amounts of fuel are injected into the combustion chamber to get the high torque although the turbocharger boost pressure is lower than the higher engine speed and led to higher fuel-air ratio. Therefore, a lot of fuel droplets are unburned and exhausted as black smoke. At the same situation, the more biodiesel and ethanol percentage blended fuel emit less smoke because fuel oxygen content could be led to local lean combustion.

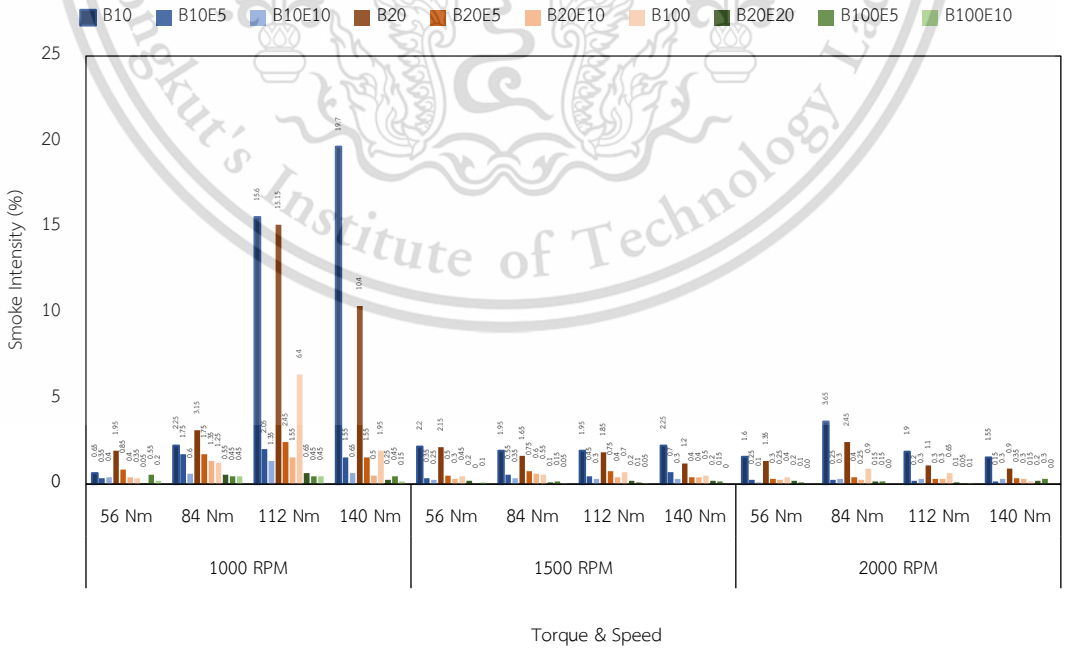

Figure 4-17 Smoke intensity

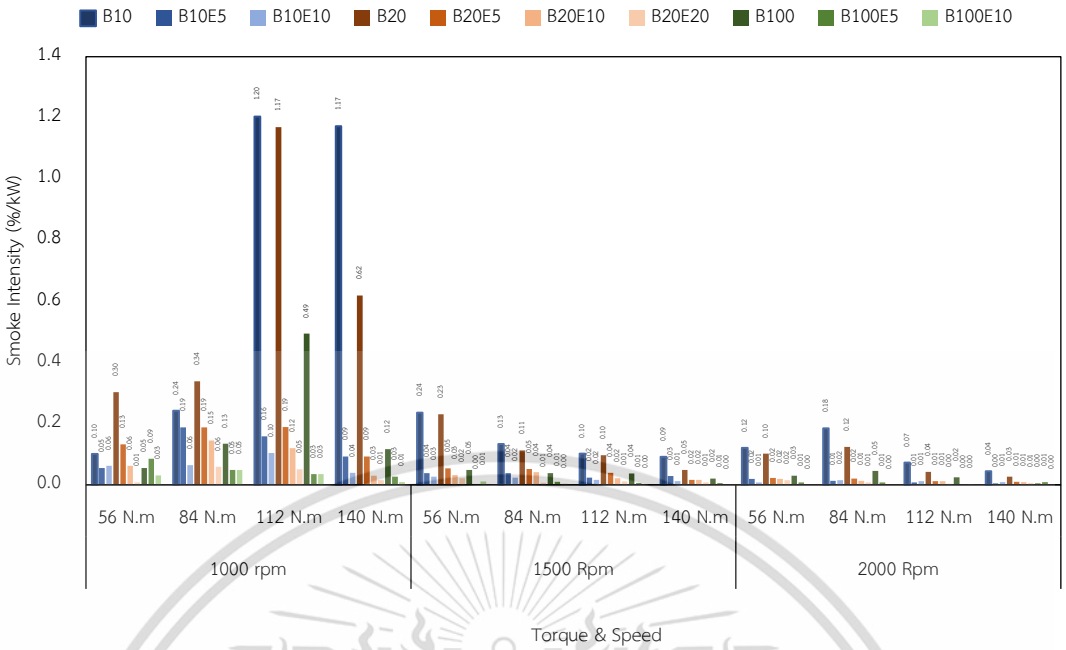

Figure 4-18 Normalized smoke intensity

The application of ethanol-biodiesel-diesel blended fuels reduced smoke intensities by an average of almost 75%, as shown in **Figure 4-17 and Figure 4-18**. This results from ethanol's interaction with atomic oxygen molecules, which exerts positive chemical control over the soot generation process [49], [50], [51]. Moreover, premixed combustion has a very high local air fuel ratio, therefore less soot is produced. However, diffuse combustion, which involves fuel-rich burning, produces more soot [52]. Therefore, ethanol blended fuels have lower soot formation in both the premixed and diffuse combustion phases due to their higher premixed combustion percentage and more fuel oxygen molecules.

4.3.3 Emission of Nitrogen Monoxide (NO)

Among the pollutants from diesel engines, nitrogen oxide is the most problematic. **Figure 4-19 and Figure 4-20** show the emission results of nitrogen monoxide of different tested fuels at every tested engine conditions. The NO_x emissions of an internal combustion engine depend on the combustion temperature, participation of oxygen in combustion, reaction time and fuel-air equivalent ratio [26].

The exhaust temperature was measured at the exist of exhaust manifold and described in **Figure 4-24**. It is increasing with the engine speed and engine load. This mean that the combustion is higher when engine speed and engine load increased. Therefore, the NO emissions higher as well. Moreover, all the nitrogen molecules are

addressed from the inlet air. At the higher engine revolutions, the turbocharger pressure is increased and let more air enter the combustion chamber when compared to low engine speed. Hence, NO emissions grow with the engine speed.

When compared between the B10, B20 and B100, the NO emissions show the increasing trends with the increasing biodiesel content in the fuel. It is advanced when ethanol is added to these based fuels. This is due to the higher combustion temperature of blending oxygenated fuel. For lack of ethanol biodiesel and diesel blended fuels, the higher bulk modulus biodiesel oxidizes faster and advances the start of combustion as well as shows higher in-cylinder pressure and heat release rate. This result is consistent with the results of Szybist (2003) [53]. On the other side, the addition of ethanol fuel to fossil fuel reduces cetane number, increasing ignition delay and raising NOx emissions [54]. The engine condition of 140 Nm-1000 rpm yields the unexpected result. B10E10, B20E10, B20E20, B100E5, and B100E10 NOx emissions have extremely high levels, reaching up to over 2000 ppm. That was reasonable given that the EGR was shut off under these settings to attain 140 Nm of engine load. EGR was shut down for these fuels due to their lower energy content. The decreasing EGR rate resulting in lower smoke emissions and higher NO emissions.

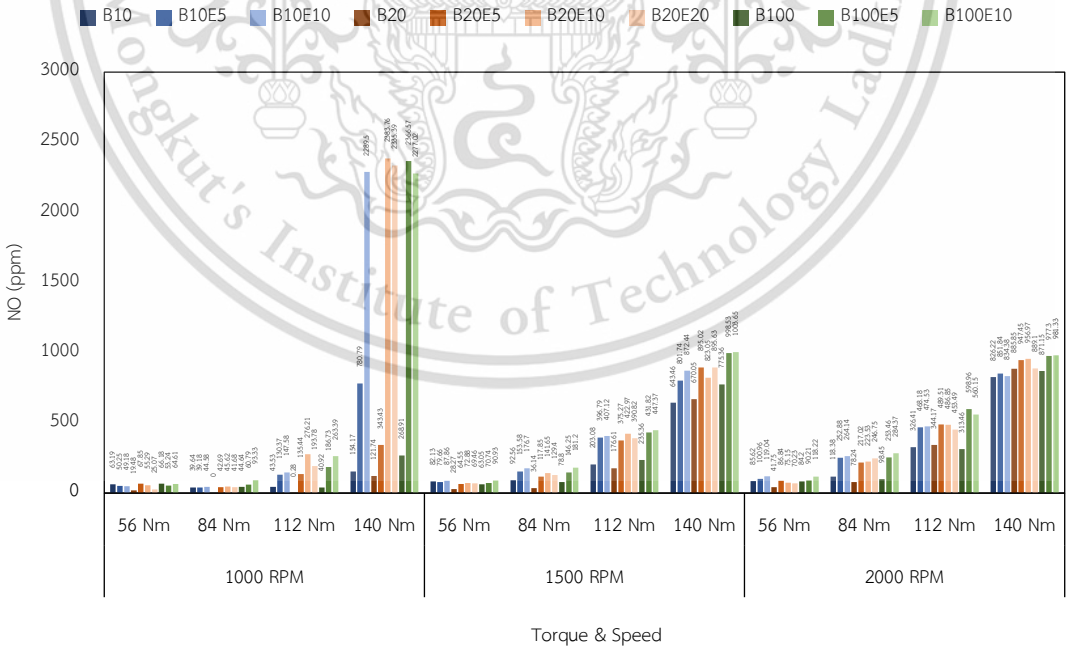

Figure 4-19 Emission of Nitrogen oxide

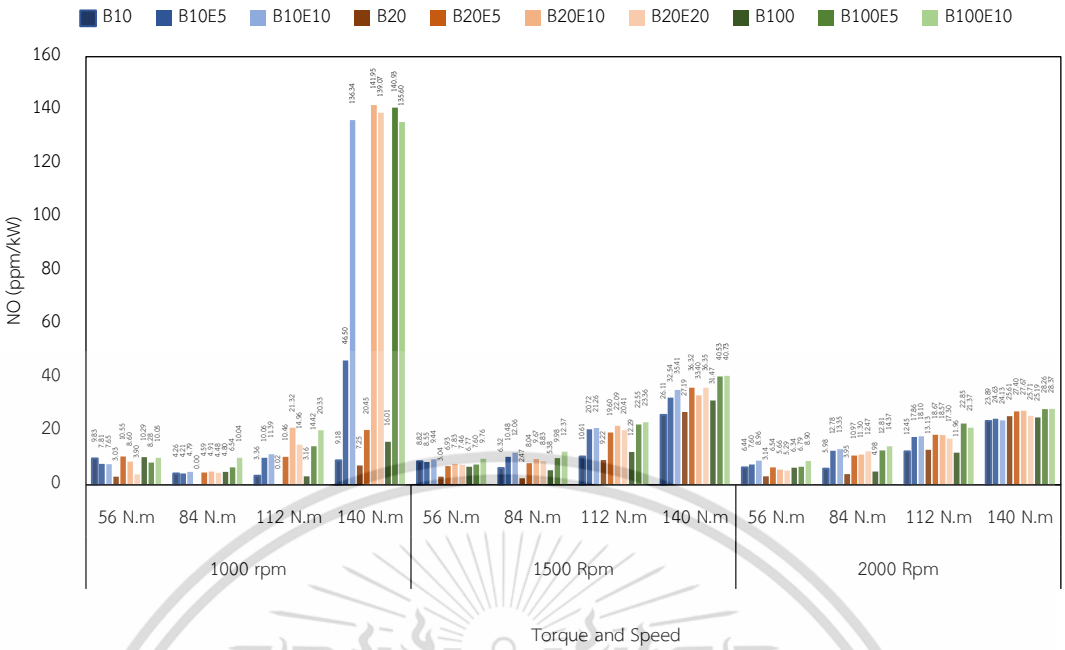

Figure 4-20 Normalized emission of nitrogen oxide

4.3.4 Carbon monoxide (CO) and carbon dioxide (CO2) emissions

The impact of fuel properties and engine conditions on the carbon monoxide emissions are presented in **Figure 4-21.** It is mostly generated from the incomplete fuel rich combustion. The emissions of CO from the tested engine are very low. All the measured values show less than 0.1% vol expect from 112Nm and 140Nm engine torque of 1000 RPM. These are the unbalance engine conditions because the engine is not tuned for such engine conditions. The CO emissions decreased with the loads at constant engine speed because, with the increasing engine load, the combustion temperature was higher, the exhaust gas temperature was also higher, resulting in a higher oxidation rate of CO to CO2. It is decreased as well with the engine speed at the constant load conditions because of lower fuel-air equivalent ratio. The results of CO_2 and O_2, demonstrated in **Figure 4-22** and **Figure 4-24**, are the prove of oxidation of CO to CO_2 at the higher load. The CO_2 emissions increased with the engine loads and the O_2 emissions decreased with the engine load at the constant engine speed. The CO emissions problem could be solved by partial adding oxygenated biofuels to the petroleum fuel. The oxygen molecules in the fuel contribute to a higher oxygen to fuel ratio, which lowers CO emissions [55], [56]. The normalized emission of carbon

dioxide is shown in **Figure 4-23**. The graph reveals that the emissions of CO_2 decreased with the engine power.

The most frequent byproducts of burning hydrocarbon fuel are carbon dioxide (CO2) and water. **Figure 4-22** compare the emission of carbon dioxide (CO_2) at the different engine loads and engine speed for all blended fuels. When the engine load increased, the CO_2 emissions increased because more fuel and air are burnt. Although, the turbo charger boost pressure which help to took part more air during the combustion at the higher engine speed. As a result, the more oxygen is available at higher engine speeds (see **Figure 4-24**), which contributes to lower CO_2 emissions. The variations in biodiesel concentration have no discernible impact on CO2 emissions. Although, adding ethanol to diesel-biodiesel blend reduce the CO_2 emissions, in addition to lower the CO emissions as well which is significant at the engine conditions of 112Nm and 140Nm engine loads of 1000 RPM. This is due to the lower carbon content of ethanol and biodiesel than the petroleum diesel.

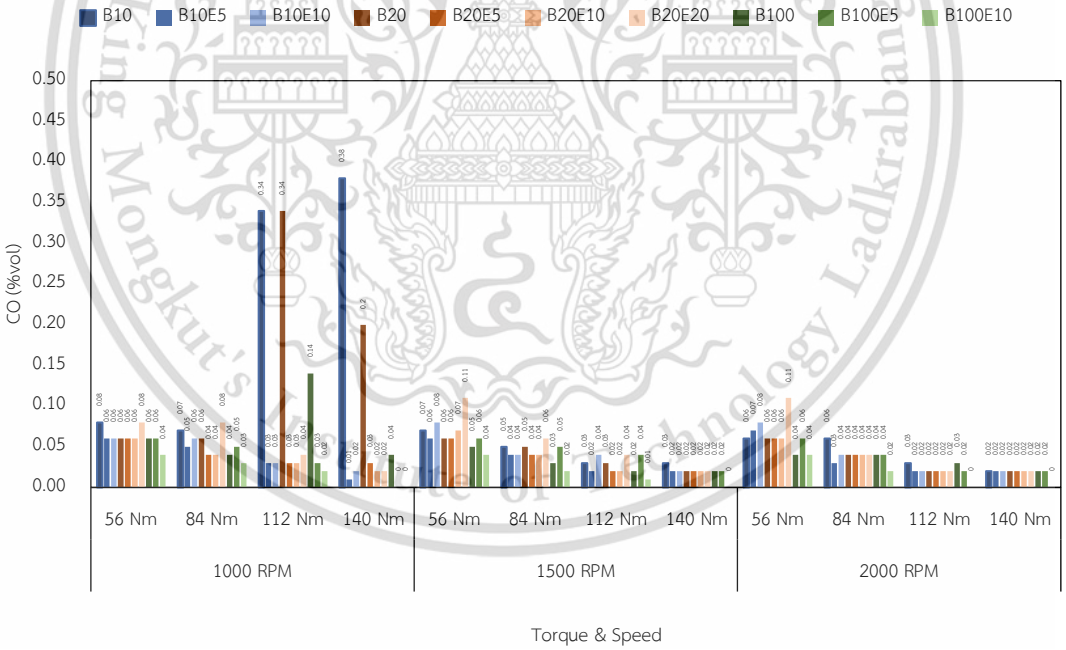

Figure 4-21 Emission of carbon monoxide

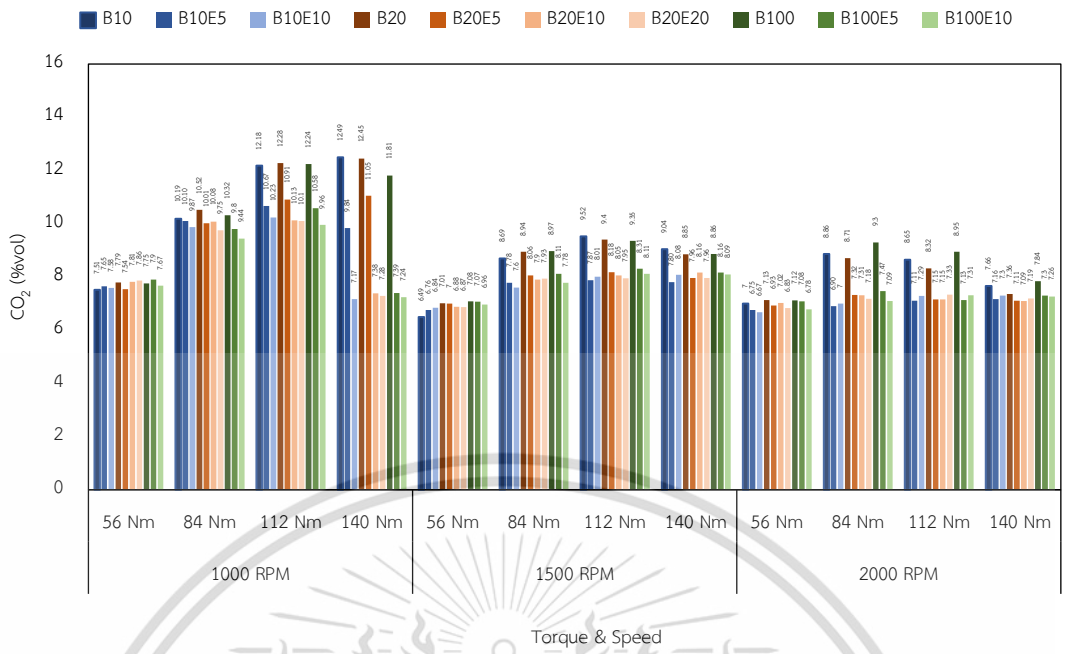

Figure 4-22 Emission of carbon dioxide

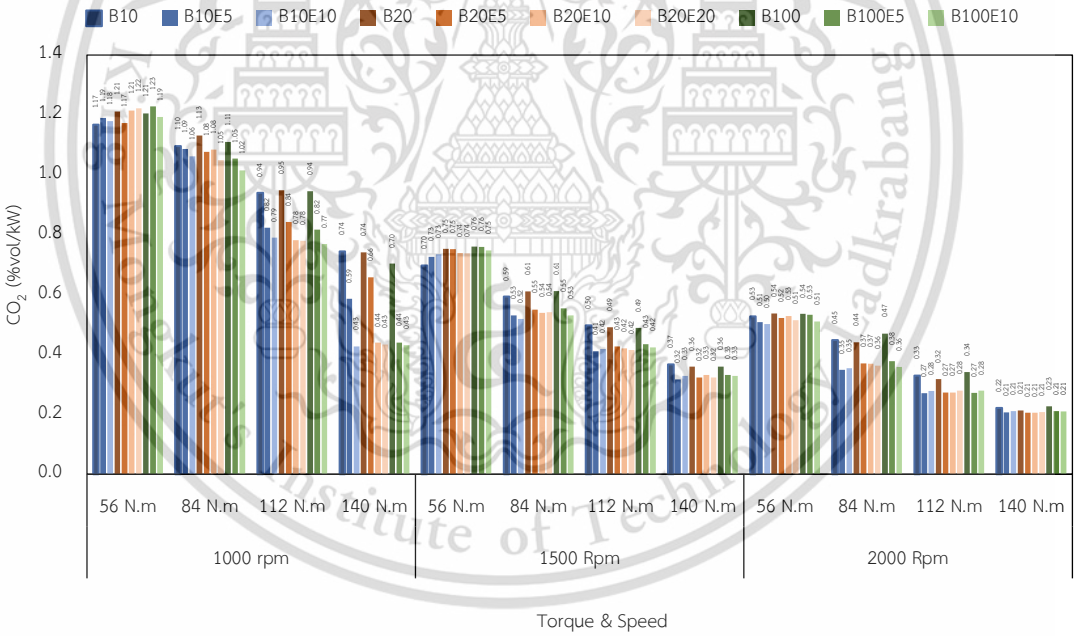

Figure 4-23 Normalized emission of carbon dioxide

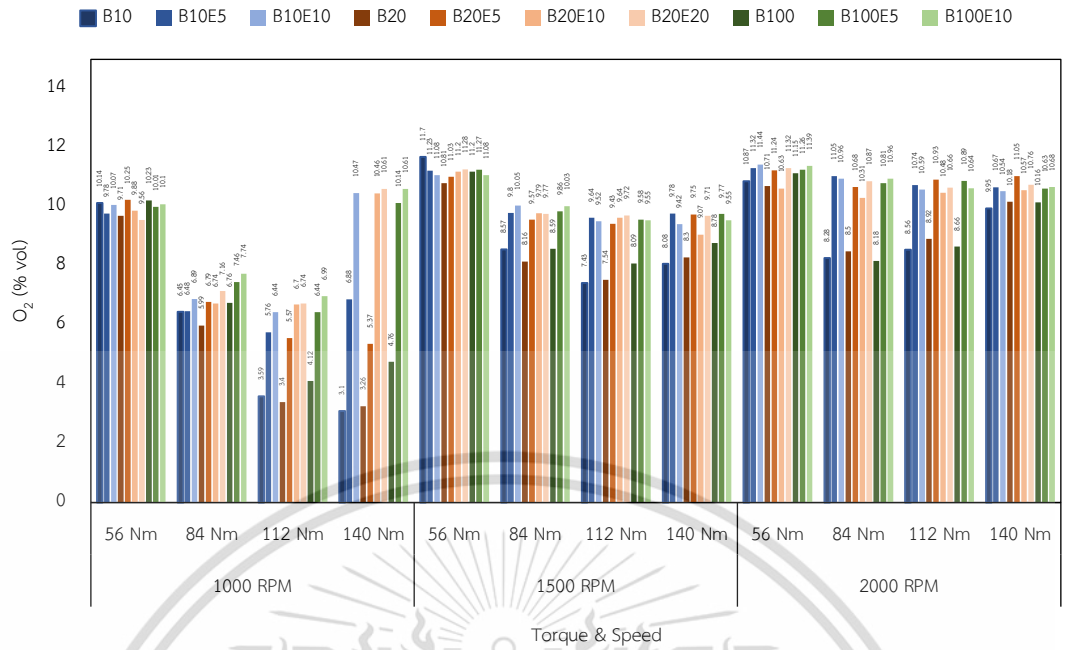

Figure 4-24 Exceed oxygen.

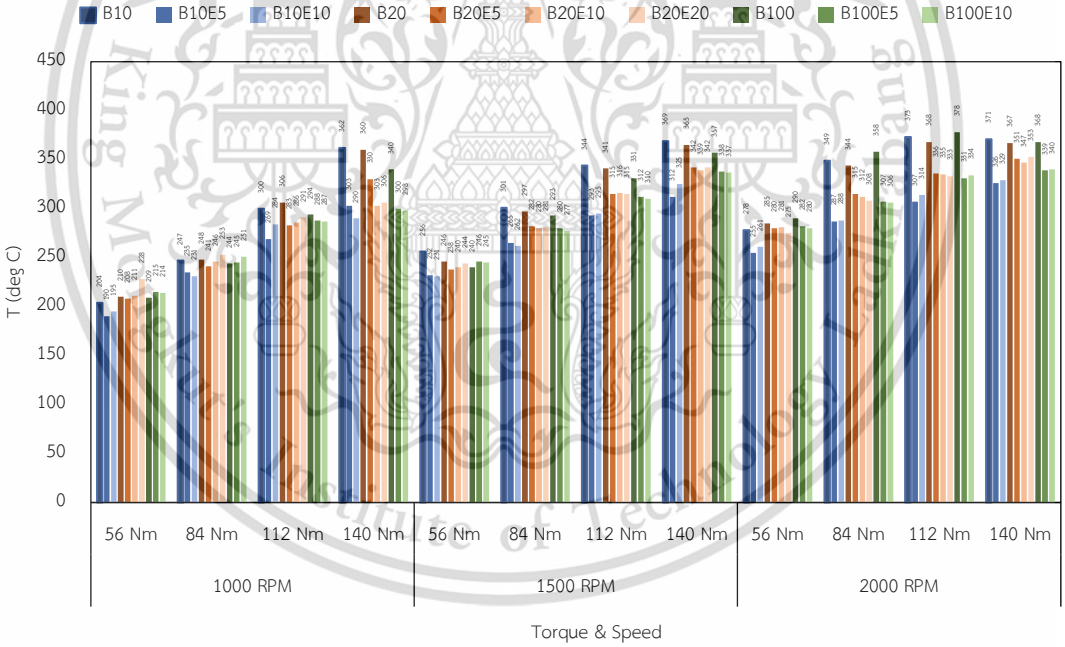

Figure 4-25 Exhaust Temperature

4.3.5 Soot Morphology

This section discusses the morphology of particulate matter (PMs) utilizing excellent microscopic images obtained using an optical microscope (OM) and a

scanning electron microscope (SEM). The OM and SEM images of ten blended fuels are listed on **Table 4-1.**

The OM images are taken at a micro scale of 200 micrometers. The PMs adhered to the filter are easily visible at that scale as the black drops are the PMs and others are the fibers of filter paper. According to the visual judgement of OM images, the partial replacement of biodiesel and ethanol diminishes the quantity of PMs emitted from diesel engines with respect to the percentage of oxygen in the blends. The burning processes were retarded by blending with the low cetane number ethanol, which led to higher premixed to diffuse combustion ratios and reduced the PM emissions. The reduction of PMs can be seen in the SEM images as well with the 5 micrometers scale. The PMs are attaching on the fibers of filter paper.

For the better understanding the effect of biofuels on the soot morphology, the particle size analysis was performed by using image analysis tool (Image J). A hundred agglomerate particles were measured in this study to reduce the bias. After that, the frequency of size distribution is described in **Figure 4-26** and in addition, the average agglomerate particle sizes are revealed in **Figure 4-27.** Among three different biodiesels, the B20 shows the biggest particle diameter. On the other hand, when compared B10 and B100, the B100 shows the smaller particle size. This could prove that the oxidation of PMs with the fuel oxygen molecules. When the ethanol is added, the size of PMs gets smaller with the ethanol percentage of the blended fuels.

As the summary of soot analysis, the quantity of PMs decreased, and the size is smaller as well with the increasing biodiesel and ethanol percent in the blends. In addition, all the emitted particle from the tested engine is smaller than 1 micrometer but bigger than 0.1 micrometer. Therefore, all the tested fuels emit $PM_{2.5}$ (PMs which are smaller in size of 2.5 micrometer). Anyhow, the smaller the emitted PM size, the faster to oxidize inside the exhaust after treatment system.

Table 4-1 Visual Comparison of particulate matter emission based on optical microscope images and scanning electron microscope images.

Fuels	Optical Microscope Image (200 μm scale)	Scanning Electron Microscope Image (5 μm scale)

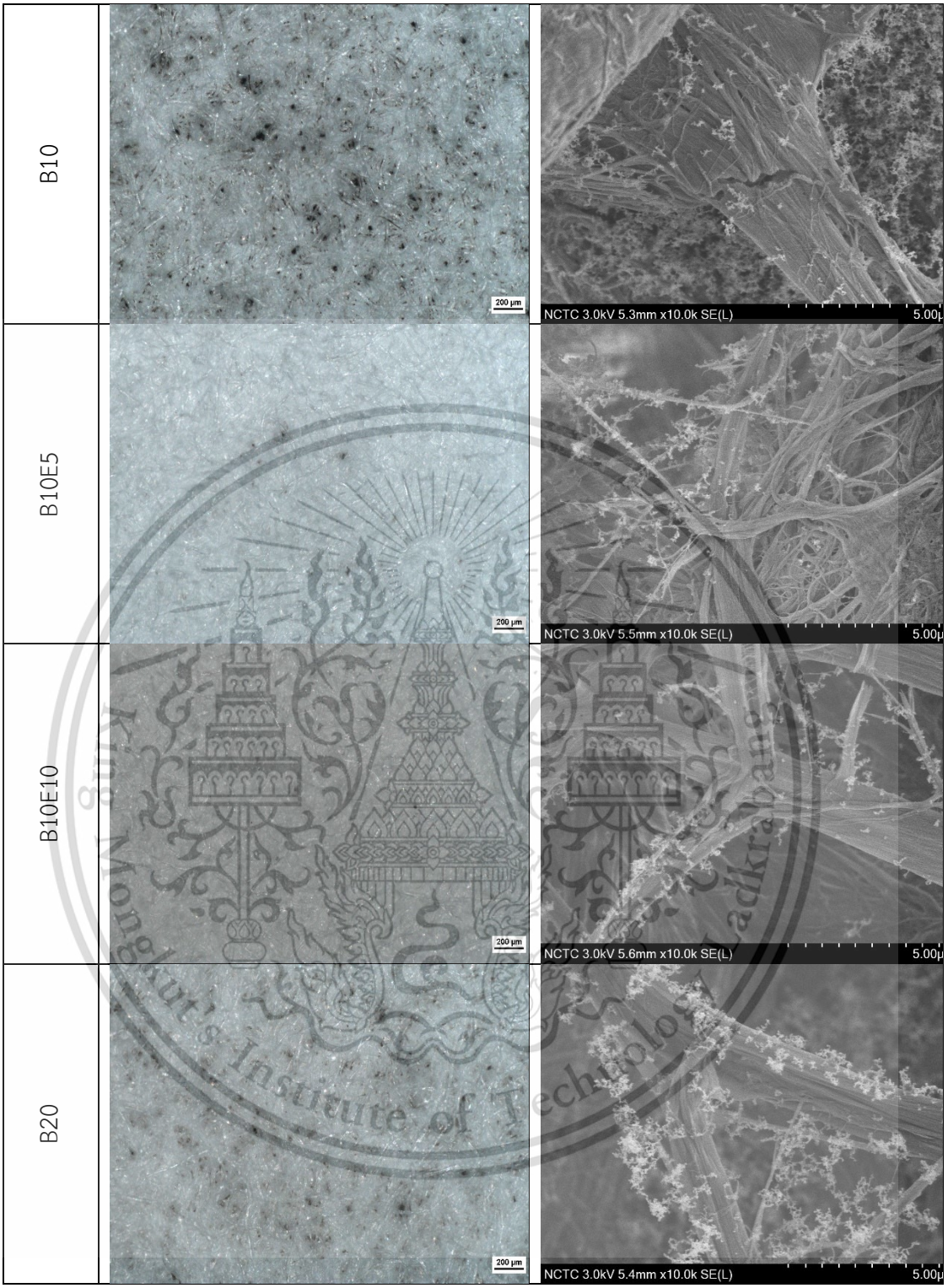

B20E5		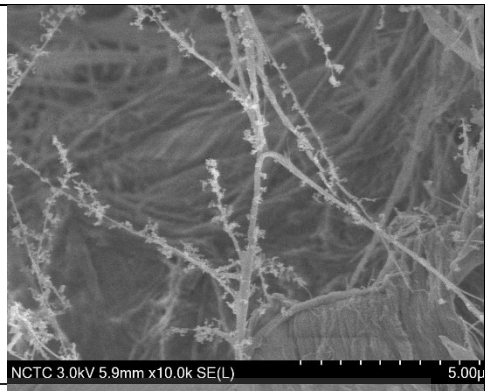
B20E10	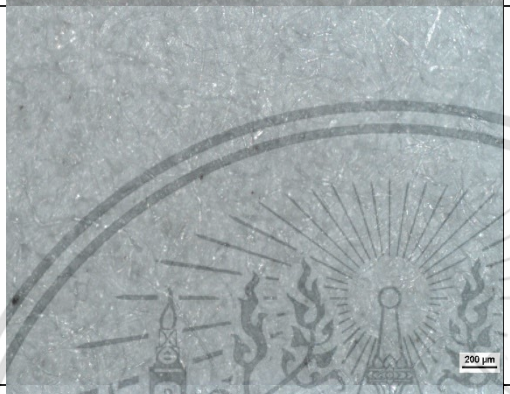	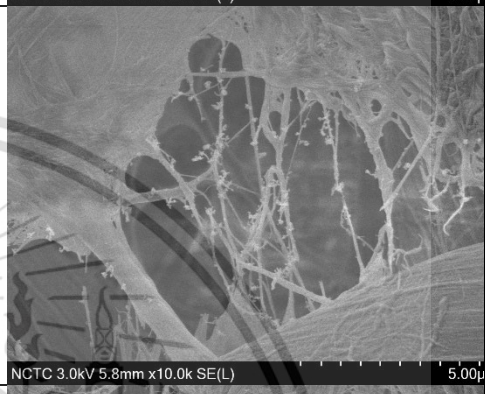
B20E20		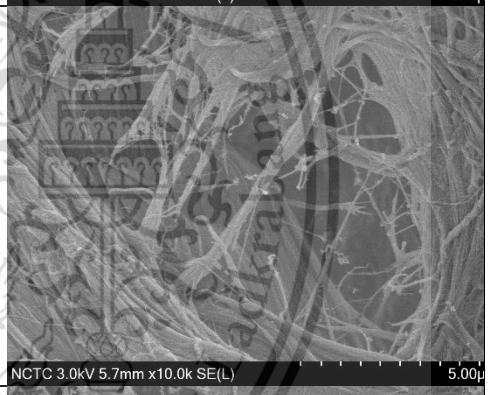
B100		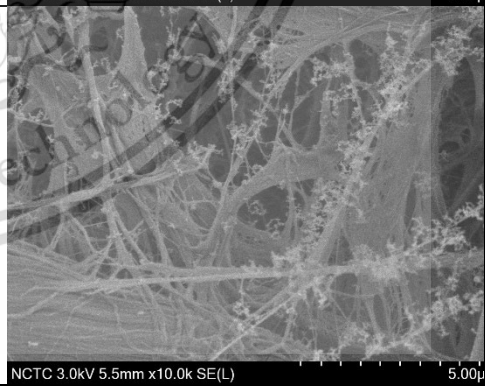

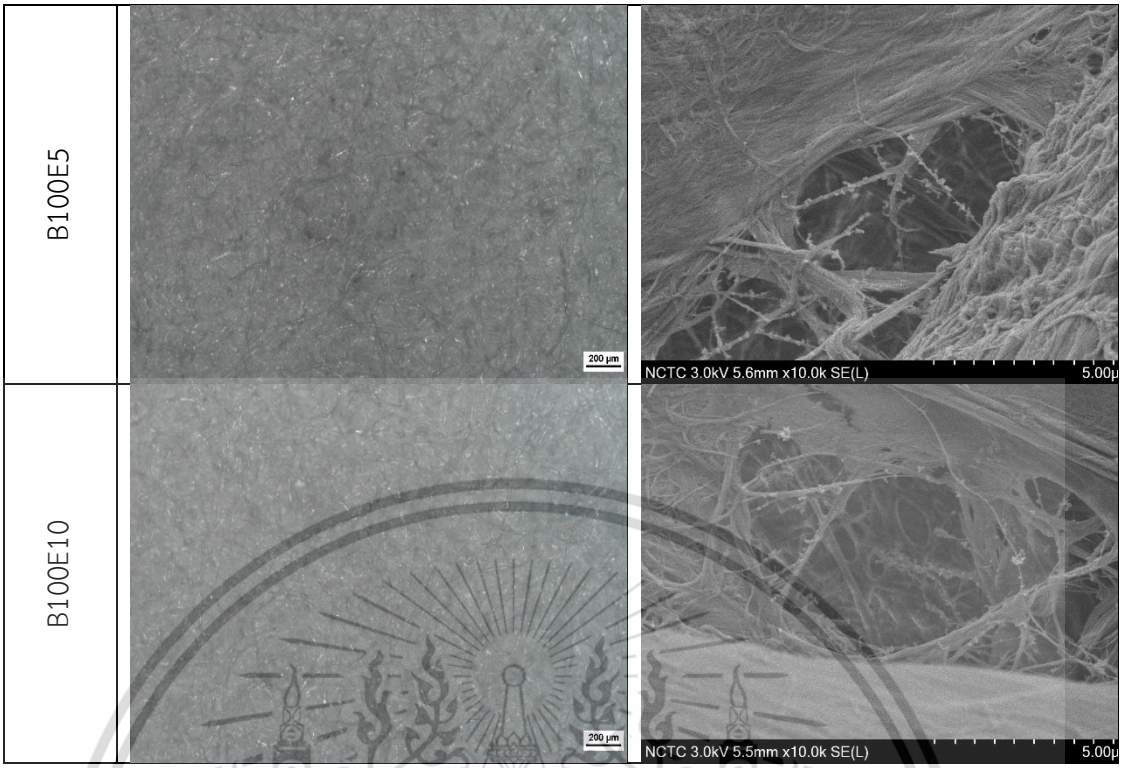

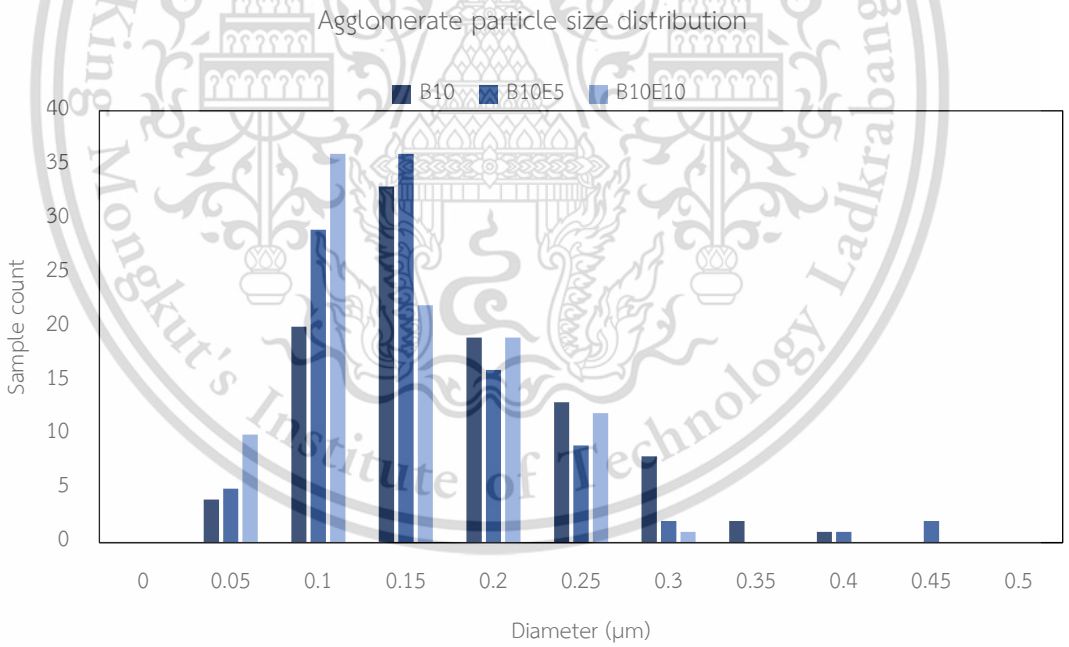

(a)

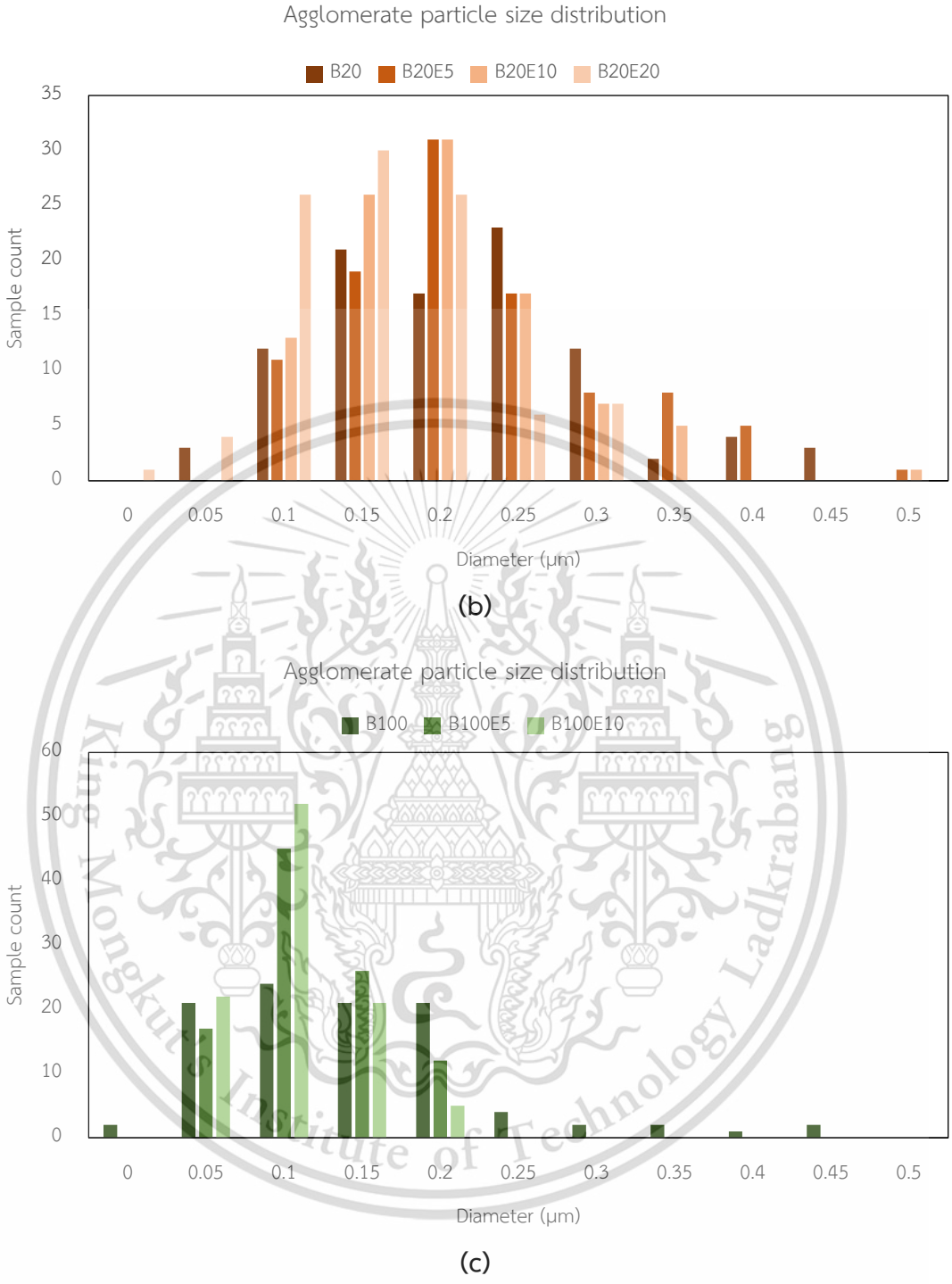

Figure 4-26 Agglomerate particle size distribution of (a) B10 and B10 with ethanol, (b) B20 and B20 with ethanol, and (c) B100 and B100 with ethanol

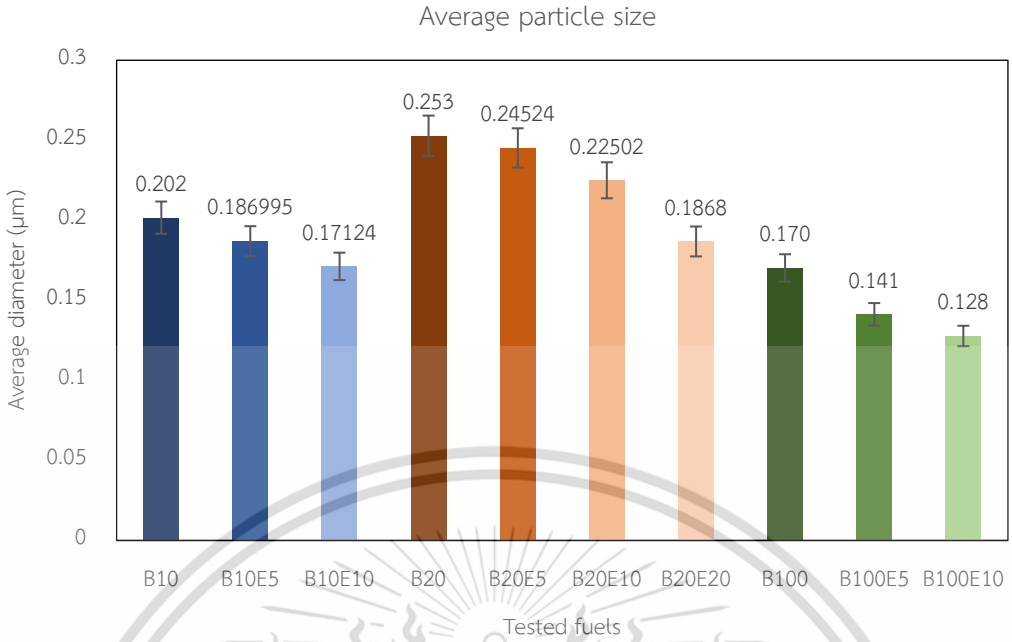

Figure 4-27 Average agglomerate particle size of ten tested fuels

CHAPTER 5

CONCLUSIONS AND RECOMMENDATIONS

In this research, ethanol-biodiesel-diesel blended fuels' combustion behavior and emission characteristics were tested on a three-liter, four-cylinder common rail diesel engine with an eddy current dynamometer testbed. The experiment was performed at four engine loads of 56 Nm, 84 Nm, 112 Nm, and 140 Nm at the corresponding three engine speed of 1000 rpm, 1500 rpm, and 2000 rpm. The maximum pressure and heat release rate is lower with engine speed, but they are higher with engine loads. The cumulative heat release and combustion duration are increased as the engine speed and loads increased. The fuel consumption increased with the engine speed and loads while specific fuel consumption decreased. The highest thermal efficiencies were observed at 1500 rpm engine speed.

In the viewpoint of difference biodiesel portion, the combustion starts earlier as the biodiesel percent increased. B10 shows the highest peak of pressure, peak of heat release rate and highest cumulative heat release at 56 Nm engine load of every engine speed because longer ignition delay time advanced the local air fuel mixing. However, at higher engine load, B100 shows the highest pressure, heat release rate and cumulative heat release values. The combustion duration is shorter with the increasing biodiesel content in fuels because the oxygenated fuel speeds up the combustion processes. The fuel consumption increased with the increasing biodiesel percent because of the lower calorific values of biodiesel. Although, it does not significantly impact on engine performance by using biofuels because the energy was recovered from the better combustion of oxygen-rich fuel. The smoke reduction could be clearly observed at 140 Nm – 1000 rpm engine condition. It is decreased by around 50% for B20 and around 90% for B100 than B10 fuel. The formation of nitrogen oxide increased with the biodiesel percent higher while carbon dioxide emissions are similar.

When ethanol is added, because of higher autoignition temperature, lower cetane number and higher heat of vaporization of ethanol, ethanol-biodiesel-diesel blended fuels need more time for fuel evaporation and led to longer ignition delay. Therefore, higher maximum pressures and maximum heat release rates were observed

in every engine condition. The cumulative heat release also increased, and the combustion duration is shorter because there are more oxygen molecules in ethanol mixed fuel. The calorific values lower and hence fuel consumption is higher for ethanol blended fuels. Thermal efficiency was increased by blending ethanol because the oxygen content of fuel advanced the combustion processes. Moreover, for emission, the smoke emission decreased by around 50% compared to fuels without ethanol. Nitrogen oxides emissions increased for ethanol blended fuels because of higher combustion temperature and more oxygen molecules are available in exhaust gas.

In this study, morphology of soot is also studied by collecting soot on the filter paper and took photographs under the scanning electron microscope and optical microscope. The less soot emissions with the increasing biodiesel and ethanol percentages were occurred visually from the optical microscopic images and scanning electron microscopic images. The particle size analysis was performed by using Image J tool. The results show that the particle sizes of agglomerate particulate matters are smaller with the increasing ethanol percentage in the blends because the more oxygen availability in the exhaust stream oxidize the soot partially.

As recommendation, more percentage of ethanol in diesel-ethanol blend will require more biodiesel as additive to compensate the negative effects of ethanol and ethanol with neat biodiesel blends should not use in DI engine without modified the engine injection system because of its low heating values might need to supply massive amount of fuel. In addition, adding ethanol will degrade the fuel lubricity.

References

[1] J. Hill, "Environmental Costs and Benefits of Transportation Biofuel Production from Food-and Lignocellulose-Based Energy Crops: A Review," in *Sustainable Agriculture*, Springer Netherlands, 2009, p. 125–139.

[2] M. Grahn, C. Azar and K. Lindgren, "The role of biofuels for transportation in CO2 emission reduction scenarios with global versus regional carbon caps," *Biomass and Bioenergy,* vol. 33, p. 360–371, March 2009.

[3] L. Gustavsson, P. Börjesson, B. Johansson and P. Svenningsson, "Reducing CO2 emissions by substituting biomass for fossil fuels," *Energy,* vol. 20, p. 1097–1113, January 1995.

[4] H. Kopetz, "Build a biomass energy market," *Nature,* vol. 494, p. 29–31, February 2013.

[5] M. Balat and M. Balat, "Political, economic and environmental impacts of biomass-based hydrogen," *International Journal of Hydrogen Energy,* vol. 34, p. 3589–3603, May 2009.

[6] J. C. Tyndall, E. J. Berg and J. P. Colletti, "Corn stover as a biofuel feedstock in Iowa's bio-economy: An Iowa farmer survey," *Biomass and Bioenergy,* vol. 35, p. 1485–1495, April 2011.

[7] A. K. Azad, M. G. Rasul, M. M. K. Khan, S. C. Sharma and M. A. Hazrat, "Prospect of biofuels as an alternative transport fuel in Australia," *Renewable and Sustainable Energy Reviews,* vol. 43, p. 331–351, March 2015.

[8] C. Jin, M. Yao, H. Liu, C.-f. F. Lee and J. Ji, "Progress in the production and application of n-butanol as a biofuel," *Renewable and Sustainable Energy Reviews,* vol. 15, p. 4080–4106, October 2011.

[9] S. K. Bhatia, S.-H. Kim, J.-J. Yoon and Y.-H. Yang, "Current status and strategies for second generation biofuel production using microbial systems," *Energy Conversion and Management,* vol. 148, p. 1142–1156, September 2017.

[10] S. N. Naik, V. V. Goud, P. K. Rout and A. K. Dalai, "Production of first and second generation biofuels: A comprehensive review," *Renewable and Sustainable Energy Reviews,* vol. 14, p. 578–597, February 2010.

[11] S. H. I. ALLEN ZIHAO, K. O. H. LIAN PIN and T. A. N. HUGH T. W., "The biofuel potential of municipal solid waste," *GCB Bioenergy,* vol. 1, p. 317–320, October 2009.

[12] M. P. Dorado, F. Cruz, J. M. Palomar and F. J. López, "An approach to the economics of two vegetable oil-based biofuels in Spain," *Renewable Energy,* vol. 31, p. 1231–1237, July 2006.

[13] J. Yang, M. Xu, X. Zhang, Q. Hu, M. Sommerfeld and Y. Chen, "Life-cycle analysis on biodiesel production from microalgae: Water footprint and nutrients balance," *Bioresource Technology,* vol. 102, p. 159–165, January 2011.

[14] A. Callegari, S. Bolognesi, D. Cecconet and A. G. Capodaglio, "Production technologies, current role, and future prospects of biofuels feedstocks: A state-of-the-art review," *Critical Reviews in Environmental Science and Technology,* vol. 50, p. 384–436, June 2019.

[15] I. M. Atadashi, M. K. Aroua and A. A. Aziz, "High quality biodiesel and its diesel engine application: A review," *Renewable and Sustainable Energy Reviews,* vol. 14, p. 1999–2008, September 2010.

[16] W. G. Wang, D. W. Lyons, N. N. Clark, M. Gautam and P. M. Norton, "Emissions from Nine Heavy Trucks Fueled by Diesel and Biodiesel Blend without Engine Modification," *Environmental Science {\&}amp$\mathsemicolon$ Technology,* vol. 34, p. 933–939, February 2000.

[17] P. Karin, A. Tripatara, P. Wai, B.-S. Oh, C. Charoenphonphanich, N. Chollacoop and H. Kosaka, "Influence of ethanol-biodiesel blends on diesel engines combustion behavior and particulate matter physicochemical characteristics," *Case Studies in Chemical and Environmental Engineering,* vol. 6, p. 100249, December 2022.

[18] M. Vohra, J. Manwar, R. Manmode, S. Padgilwar and S. Patil, "Bioethanol production: Feedstock and current technologies," *Journal of Environmental Chemical Engineering,* vol. 2, p. 573–584, March 2014.

[19] A. Demirbas, "Producing and Using Bioethanol as an Automotive Fuel," *Energy Sources, Part B: Economics, Planning, and Policy,* vol. 2, p. 391–401, October 2007.

[20] J. Heywood, Internal Combustion Engine Fundamentals 2E, McGraw Hill Professional, 2018.

[21] X. &. S. Seykens and R. L.M.T. & Baert, "Modeling of common rail fuel injection system and influence of fluid properties on injection process," *Proceedings of VAFSEP,Dublin, Ireland,* 2004.

[22] A. E. W. Austen and W.-T. Lyn, "Relation between Fuel Injection and Heat Release in a Direct-Injection Engine and the Nature of the Combustion

Processes," *Proceedings of the Institution of Mechanical Engineers: Automobile Division,* vol. 14, p. 47–62, January 1960.

[23] A. W. C. S. &. W. M. P. Faiz, Air pollution from motor vehicles: standards and technologies for controlling emissions., World Bank Publications., 1996.

[24] M. Zheng, M. C. Mulenga, G. T. Reader, M. Wang, D. S.-K. Ting and J. Tjong, "Biodiesel engine performance and emissions in low temperature combustion," *Fuel,* vol. 87, p. 714–722, May 2008.

[25] İ. A. Reşitoğlu, K. Altinişik and A. Keskin, "The pollutant emissions from diesel-engine vehicles and exhaust aftertreatment systems," *Clean Technologies and Environmental Policy,* vol. 17, p. 15–27, June 2014.

[26] E. A. Ajav, B. Singh and T. K. Bhattacharya, "Performance of a stationary diesel engine using vapourized ethanol as supplementary fuel," *Biomass and Bioenergy,* vol. 15, p. 493–502, December 1998.

[27] J. J. Chong, A. Tsolakis, S. S. Gill, K. Theinnoi and S. E. Golunski, "Enhancing the NO2/NOx ratio in compression ignition engines by hydrogen and reformate combustion, for improved aftertreatment performance," *International Journal of Hydrogen Energy,* vol. 35, p. 8723–8732, August 2010.

[28] M. M. Maricq, "Chemical characterization of particulate emissions from diesel engines: A review," *Journal of Aerosol Science,* vol. 38, p. 1079–1118, November 2007.

[29] J. N. Chi and H. F. M. Dacosta, "Modeling and Control of a Urea-SCR Aftertreatment System," in *SAE Technical Paper Series*, 2005.

[30] B.-Q. He, S.-J. Shuai, J.-X. Wang and H. He, "The effect of ethanol blended diesel fuels on emissions from a diesel engine," *Atmospheric Environment,* vol. 37, p. 4965–4971, November 2003.

[31] A. HANSEN, "Ethanol?diesel fuel blends ?? a review," *Bioresource Technology,* vol. 96, p. 277–285, February 2005.

[32] P. Kwanchareon, A. Luengnaruemitchai and S. Jai-In, "Solubility of a diesel–biodiesel–ethanol blend, its fuel properties, and its emission characteristics from diesel engine," *Fuel,* vol. 86, p. 1053–1061, May 2007.

[33] M. Tongroon, P. Saisirirat, A. Suebwong, J. Aunchaisri, M. Kananont and N. Chollacoop, "Combustion and emission characteristics investigation of diesel-ethanol-biodiesel blended fuels in a compression-ignition engine and benefit analysis," *Fuel,* vol. 255, p. 115728, November 2019.

[34] S. A. Shahir, H. H. Masjuki, M. A. Kalam, A. Imran, I. M. R. Fattah and A. Sanjid, "Feasibility of diesel–biodiesel–ethanol/bioethanol blend as existing CI engine fuel: An assessment of properties, material compatibility, safety and combustion," *Renewable and Sustainable Energy Reviews,* vol. 32, p. 379–395, April 2014.

[35] W. G. Wang, N. N. Clark, D. W. Lyons, R. M. Yang, M. Gautam, R. M. Bata and J. L. Loth, "Emissions Comparisons from Alternative Fuel Buses and Diesel Buses with a Chassis Dynamometer Testing Facility," *Environmental Science & Technology,* vol. 31, p. 3132–3137, October 1997.

[36] M. J. RAUCKIS and W. J. MCLEAN, "The Effect of Hydrogen Addition on Ignition Delays and Flame Propagation in Spark Ignition Engines," *Combustion Science and Technology,* vol. 19, p. 207–216, April 1979.

[37] C. Stone, A. Brown and P. Beckwith, "Cycle-by-Cycle Variations in Spark Ignition Engine Combustion - Part II: Modelling of Flame Kernel Displacements as a Cause of Cycle-by-Cycle Variations," in *SAE Technical Paper Series*, SAE International, 1996.

[38] R. K. Maurya and A. K. Agarwal, "Experimental investigation of cyclic variations in HCCI combustion parameters for gasoline like fuels using statistical methods," *Applied Energy,* vol. 111, p. 310–323, November 2013.

[39] L. Nemoianu, C. Pana, N. Negurescu, A. Cernat, D. Fuiorescu and C. Nutu, "Study of the cycle variability at an automotive diesel engine fuelled with LPG," *MATEC Web of Conferences,* vol. 112, p. 10006, 2017.

[40] O. M. Ali, N. R. Abdullah, R. Mamat and A. A. Abdullah, "Comparison of the Effect of Different Alcohol Additives with Blended Fuel on Cyclic Variation in Diesel Engine," *Energy Procedia,* vol. 75, p. 2357–2362, August 2015.

[41] R. D. Misra and M. S. Murthy, "Blending of additives with biodiesels to improve the cold flow properties, combustion and emission performance in a compression ignition engine—A review," *Renewable and Sustainable Energy Reviews,* vol. 15, p. 2413–2422, June 2011.

[42] H. Huang, W. Teng, Z. Li, Q. Liu, Q. Wang and M. Pan, "Improvement of emission characteristics and maximum pressure rise rate of diesel engines fueled with n-butanol/PODE3-4/diesel blends at high injection pressure," *Energy Conversion and Management,* vol. 152, p. 45–56, November 2017.

[43] L. Zhu, C. S. Cheung, W. G. Zhang and Z. Huang, "Combustion, performance and emission characteristics of a DI diesel engine fueled with ethanol–biodiesel blends," *Fuel,* vol. 90, p. 1743–1750, May 2011.

[44] A. L. Boehman, D. Morris, J. Szybist and E. Esen, "The Impact of the Bulk Modulus of Diesel Fuels on Fuel Injection Timing," *Energy & Fuels,* vol. 18, p. 1877–1882, October 2004.

[45] C. W. Yu, S. Bari and A. Ameen, "A comparison of combustion characteristics of waste cooking oil with diesel as fuel in a direct injection diesel engine," *Proceedings of the Institution of Mechanical Engineers, Part D: Journal of Automobile Engineering,* vol. 216, p. 237–243, March 2002.

[46] K. Thakkar, S. S. Kachhwaha, P. Kodgire and S. Srinivasan, "Combustion investigation of ternary blend mixture of biodiesel/n-butanol/diesel: CI engine performance and emission control," *Renewable and Sustainable Energy Reviews,* vol. 137, p. 110468, March 2021.

[47] R. J. Donahue and D. E. Foster, "Effects of Oxygen Enhancement on the Emissions from a DI Diesel via Manipulation of Fuels and Combustion Chamber Gas Composition," in *SAE Technical Paper Series*, 2000.

[48] V. Rapp, N. Killingsworth, P. Therkelsen and R. Evans, "Lean-Burn Internal Combustion Engines," in *Lean Combustion*, Elsevier, 2016, p. 111–146.

[49] Ö. Can, İ. Çelikten and N. Usta, "Effects of ethanol addition on performance and emissions of a turbocharged indirect injection Diesel engine running at different injection pressures," *Energy Conversion and Management,* vol. 45, p. 2429–2440, September 2004.

[50] Z. Xiao, N. Ladommatos and H. Zhao, "The effect of aromatic hydrocarbons and oxygenates on diesel engine emissions," *Proceedings of the Institution of Mechanical Engineers, Part D: Journal of Automobile Engineering,* vol. 214, p. 307–332, March 2000.

[51] P. A. Boruff, A. W. Schwab, C. E. Goering and E. H. Pryde, "Evaluation of Diesel Fuel — Ethanol Microemulsions," *Transactions of the ASAE,* vol. 25, p. 0047–0053, 1982.

[52] F. Payri, J. Benajes, J. Arrègle and J. M. Riesco, "Combustion and Exhaust Emissions in a Heavy-Duty Diesel Engine with Increased Premixed Combustion Phase by Means of Injection Retarding," *Oil & Gas Science and Technology,* vol. 61, p. 247–258, March 2006.

[53] J. P. Szybist and A. L. Boehman, "Behavior of a Diesel Injection System with Biodiesel Fuel," in *SAE Technical Paper Series*, 2003.

[54] L. Xing-cai, Y. Jian-guang, Z. Wu-gao and H. Zhen, "Effect of cetane number improver on heat release rate and emissions of high speed diesel engine fueled with ethanol–diesel blend fuel," *Fuel,* vol. 83, p. 2013–2020, October 2004.

[55] H. rahimi, B. Ghobadian, T. Yusaf, G. Najafi and M. Khatamifar, "Diesterol: An environment-friendly IC engine fuel," *Renewable Energy,* vol. 34, p. 335–342, January 2009.

[56] D.-g. Li, H. Zhen, L. Xingcai, Z. Wu-gao and Y. Jian-guang, "Physico-chemical properties of ethanol–diesel blend fuel and its effect on performance and emissions of diesel engines," *Renewable Energy,* vol. 30, p. 967–976, May 2005.

APPENDIX A:

FUELS PROPERTIES AND COMPOSITION

A- 1. Fuel properties of B10

FOCUSLAB Fluid & Oil Analysis Technology

ISO 9001 : 2015 Certified

Focuslab Ltd

Customer Code : 20010
Customer Name : KMITL
Address : 3 Moo 2, Chalongkrung Road
Ladkrabang
Bangkok 10520

Test Code : 811A

Sample Information

Unit ID /
Sample Information Identification : B10
Unit type : FUEL
Oil type : DIESEL B10
Sampling Date : 22-Jun-21
Recieved Date : 22-Jun-21

Test Report Sample No 21063747

Test Description	Test Method	Test Result	Limit (a)
Apperance			
Color	Visual Inspection	Bright and Clear	Bright and Clear
Diesel Fuel			
Density at 15 C , g/cm^3	ASTM D4052	0.835	0.81 - 0.87
Cetane Index	ASTM D976	54.9	Min 50
Distillation , C	ASTM D86		
Initial Boiling Point		180.0	-
90%vol. Recovered		344.2	Max 357
Flash Point	ASTM D93	66.0	Min 52
Fatty Acid Methyl Ester, %vol	EN 14078	10.2	9 - 10
Pour Point , °C	ASTM D97	0.0	Max 10
Flow Properties			
Viscosity at 40 C , cSt	ASTM D445	3.0	1.8 - 4.1
Cleanliness			
Total Contamination , mg/kg	EN 12662	6.2	Max 24.0
Micro Carbon Residue (MCR) , %mass	ASTM D4530	<0.01	Max 0.3
Ash , %wt	ASTM D482	<0.001	Max 0.010
Total Sulfur Content , mg/kg	ASTM D5453	24.4	Max 50
Water Content , mg/kg	ASTM D6304	691	Max 200
Water and Sediment , %Vol.	ASTM D2709	<0.01	Max 0.05

Interpretation of the Test Result
- Test results are based on received fuel sample , submitted and identified by client.
- Data is provided above.

Recommendation
- No recommendation for R&D.

Remark
(a) Diesel fuel is from Thailand Diesel Specification - MOE - 2563

Tested and Issued By

Kanjana K.
Lab Technologist

Approved and Authorised by

Somchai J.
Machine Lubricant Analyst

2/57 Bangna Complex Office Tower, 12 th Fl , Soi Bangna- Trad 25, North Bangna, Bangna, Bangkok 10260, Thailand
http://www.focuslab.co.th
Tel : (66 2) 3618600-3 Fax : (66 2) 3618567

FL-5.7

FOCUSLAB™ Fluid & Oil Analysis Technology

ISO 9001 : 2015 Certified

Focuslab Ltd

Customer Code	: 20010	
Customer Name	: KMITL	
Address	: 3 Moo 2, Chalongkrung Road Ladkrabang Bangkok 10520	
Test Code	: 811A	

Sample Information

Unit ID / Sample Information Identification	:	B10
Unit type	:	FUEL
Oil type	:	not given
Sampling Date	:	22-Jun-21
Recieved Date	:	22-Jun-21

B10

Good and Qualified Diesel Fuel

A- 2. Fuel properties of B20

FOCUSLAB™ Fluid & Oil Analysis Technology

ISO 9001 : 2015 Certified

Focuslab Ltd

Customer Code : 20010
Customer Name : KMITL
Address : 3 Moo 2, Chalongkrung Road
Ladkrabang
Bangkok 10520

Test Code : 811A

Sample Information

Unit ID /
Sample Information Identification : B20
Unit type : FUEL
Oil type : DIESEL B20
Sampling Date : 22-Jun-21
Recieved Date : 22-Jun-21

Test Report Sample No 21063748

Test Description	Test Method	Test Result	Limit (a)
Apperance			
Color	Visual Inspection	Bright and Clear	Bright and Clear
Diesel Fuel			
Density at 15 C , g/cm^3	ASTM D4052	0.827	0.81 - 0.87
Cetane Index	ASTM D976	60.0	Min 50
Distillation , C	ASTM D86		
Initial Boiling Point		177.4	-
90%vol. Recovered		348.4	Max 357
Flash Point	ASTM D93	66.0	Min 52
Fatty Acid Methyl Ester, %vol	EN 14078	22.5	19 - 20
Pour Point , °C	ASTM D97	9.0	Max 10
Flow Properties			
Viscosity at 40 C , cSt	ASTM D445	3.1	1.8 - 4.1
Cleanliness			
Total Contamination , mg/kg	EN 12662	4.2	Max 24.0
Micro Carbon Residue (MCR) , %mass	ASTM D4530	<0.01	Max 0.3
Ash , %wt	ASTM D482	<0.001	Max 0.010
Total Sulfur Content , mg/kg	ASTM D5453	142	Max 50
Water Content , mg/kg	ASTM D6304	1183	Max 300
Water and Sediment , %Vol.	ASTM D2709	<0.01	Max 0.05

Interpretation of the Test Result
- Test results are based on received fuel sample , submitted and identified by client.
- Data is provided above.

Recommendation
- No recommendation for R&D.

Remark
(a) Diesel fuel is from Thailand Diesel Specification - MOE - 2563

Tested and Issued By

Kanjana K.
Lab Technologist

Approved and Authorised by

Somchai J.
Machine Lubricant Analyst

2/57 Bangna Complex Office Tower, 12 th Fl , Soi Bangna- Trad 25, North Bangna, Bangna, Bangkok 10260, Thailand
http://www.focuslab.co.th
Tel : (66 2) 3618600-3 Fax : (66 2) 3618567

FL-6.7

Page 1 of 2

FOCUSLAB™ Fluid & Oil Analysis Technology

ISO 9001 : 2015 Certified

Focuslab Ltd

Customer Code	:	20010
Customer Name	:	KMITL
Address	:	3 Moo 2, Chalongkrung Road Ladkrabang Bangkok 10520
Test Code	:	811A

Sample Information		
Unit ID /		
Sample Information Identification	:	B20
Unit type	:	FUEL
Oil type	:	DIESEL B20
Sampling Date	:	22-Jun-21
Recieved Date	:	22-Jun-21

B20	Good and Qualified Diesel Fuel
	
	

2/57 Bangna Complex Office Tower, 12 th Fl., Soi Bangna- Trad 25, North Bangna, Bangna, Bangkok 10260, Thailand
http://www.focuslab.co.th
Tel : (66 2) 3618600-3 Fax : (66 2) 3618567

FL-6.7

A- 3. Biodiesel's physical and chemical properties

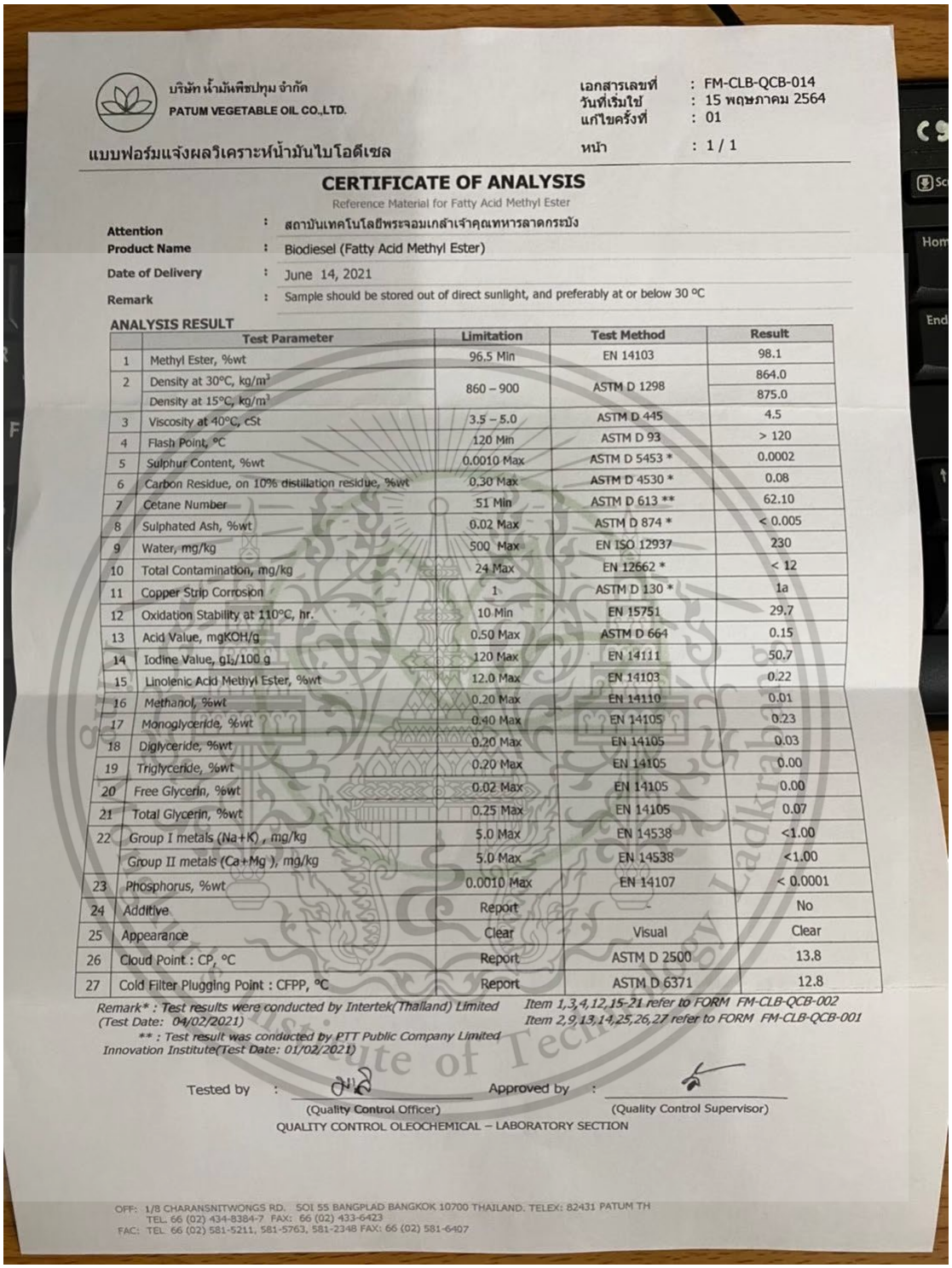

บริษัท น้ำมันพืชปทุม จำกัด
PATUM VEGETABLE OIL CO.,LTD.

เอกสารเลขที่ : FM-CLB-QCB-014
วันที่เริ่มใช้ : 15 พฤษภาคม 2564
แก้ไขครั้งที่ : 01
หน้า : 1 / 1

แบบฟอร์มแจ้งผลวิเคราะห์น้ำมันไบโอดีเซล

CERTIFICATE OF ANALYSIS

Reference Material for Fatty Acid Methyl Ester

Attention : สถาบันเทคโนโลยีพระจอมเกล้าเจ้าคุณทหารลาดกระบัง
Product Name : Biodiesel (Fatty Acid Methyl Ester)
Date of Delivery : June 14, 2021
Remark : Sample should be stored out of direct sunlight, and preferably at or below 30 °C

ANALYSIS RESULT

	Test Parameter	Limitation	Test Method	Result
1	Methyl Ester, %wt	96.5 Min	EN 14103	98.1
2	Density at 30°C, kg/m³	860 – 900	ASTM D 1298	864.0
	Density at 15°C, kg/m³			875.0
3	Viscosity at 40°C, cSt	3.5 – 5.0	ASTM D 445	4.5
4	Flash Point, °C	120 Min	ASTM D 93	> 120
5	Sulphur Content, %wt	0.0010 Max	ASTM D 5453 *	0.0002
6	Carbon Residue, on 10% distillation residue, %wt	0.30 Max	ASTM D 4530 *	0.08
7	Cetane Number	51 Min	ASTM D 613 **	62.10
8	Sulphated Ash, %wt	0.02 Max	ASTM D 874 *	< 0.005
9	Water, mg/kg	500 Max	EN ISO 12937	230
10	Total Contamination, mg/kg	24 Max	EN 12662 *	< 12
11	Copper Strip Corrosion	1	ASTM D 130 *	1a
12	Oxidation Stability at 110°C, hr.	10 Min	EN 15751	29.7
13	Acid Value, mgKOH/g	0.50 Max	ASTM D 664	0.15
14	Iodine Value, gI₂/100 g	120 Max	EN 14111	50.7
15	Linolenic Acid Methyl Ester, %wt	12.0 Max	EN 14103	0.22
16	Methanol, %wt	0.20 Max	EN 14110	0.01
17	Monoglyceride, %wt	0.40 Max	EN 14105	0.23
18	Diglyceride, %wt	0.20 Max	EN 14105	0.03
19	Triglyceride, %wt	0.20 Max	EN 14105	0.00
20	Free Glycerin, %wt	0.02 Max	EN 14105	0.00
21	Total Glycerin, %wt	0.25 Max	EN 14105	0.07
22	Group I metals (Na+K) , mg/kg	5.0 Max	EN 14538	<1.00
	Group II metals (Ca+Mg), mg/kg	5.0 Max	EN 14538	<1.00
23	Phosphorus, %wt	0.0010 Max	EN 14107	< 0.0001
24	Additive	Report	-	No
25	Appearance	Clear	Visual	Clear
26	Cloud Point : CP, °C	Report	ASTM D 2500	13.8
27	Cold Filter Plugging Point : CFPP, °C	Report	ASTM D 6371	12.8

Remark : Test results were conducted by Intertek(Thailand) Limited (Test Date: 04/02/2021)*
Item 1,3,4,12,15-21 refer to FORM FM-CLB-QCB-002
Item 2,9,13,14,25,26,27 refer to FORM FM-CLB-QCB-001
*** : Test result was conducted by PTT Public Company Limited Innovation Institute(Test Date: 01/02/2021)*

Tested by : _____ (Quality Control Officer)
Approved by : _____ (Quality Control Supervisor)
QUALITY CONTROL OLEOCHEMICAL – LABORATORY SECTION

OFF: 1/8 CHARANSNITWONGS RD. SOI 55 BANGPLAD BANGKOK 10700 THAILAND. TELEX: 82431 PATUM TH
TEL. 66 (02) 434-8384-7 FAX: 66 (02) 433-6423
FAC: TEL 66 (02) 581-5211, 581-5763, 581-2348 FAX: 66 (02) 581-6407

A- 4. Density and viscosity test result of B20E5

FOCUSLAB Fluid & Oil Analysis Technology

ISO9001:2015 Certified

FocusLab Ltd.

Customer Code : 20010
Customer Name : KMITL
Address : 3 Moo 2, Chalongkrung Road
Ladkrabang
Bangkok 10520

Test code : 604 625

Sample Information		
Unit ID / Sample Information	:	B20E5
Unit Type	:	FUEL
Oil type	:	DIESEL B20 + ETHANOL 5%
Sampling Date	:	22-Jun-21

Test Report Sample No : 21072739

Visual Inspection		Sample Pictures
Color		
Bottom		
Magnetic		

Test Description	Test Method	Unit	Test Result	Limit
Viscosity@ 40 °C	D-445	cSt	2.69	
Density 15 °C	D-4052	g/cm³	0.824	

Recommendation

Data is provided above.

Remark The result(s) issued in this report only reflected the analysis of the sample(s) submitted.
Test Result Data interpretation is not available.
Limit of test parameters are not available.

Tested and Issued By

Kanjana K.
Lab Technologist

Approved and Authorised By

Somchai J.
Machine Lubricant Analyst

Focuslab Ltd. Bangkok Thailand www.focuslab.co.th focuslab@focuslab.co.th

FL-6.8

A- 5. Density and viscosity test result of B20E10

FOCUSLAB Fluid & Oil Analysis Technology

ISO9001:2015 Certified

FocusLab Ltd.

Customer Code : 20010
Customer Name : KMITL
Address : 3 Moo 2, Chalongkrung Road
Ladkrabang
Bangkok 10520

Test code : 604 625

Sample Information		
Unit ID / Sample Information	:	B20E10
Unit Type	:	FUEL
Oil type		DIESEL B20 + ETHANOL 10%
Sampling Date	:	22-Jun-21

Test Report Sample No : 21072738

Visual Inspection		Sample Pictures
Color		
Bottom		
Magnetic		

Test Description	Test Method	Unit	Test Result	Limit
Viscosity@ 40 °C	D-445	cSt	2.49	
Density 15 °C	D-4052	g/cm³	0.822	

Recommendation

Data is provided above.

Remark : The result(s) issued in this report only reflected the analysis of the sample(s) submitted.
Test Result Data Interpretation is not available.
Limit of test parameters are not available.

Tested and Issued By

Kanjana K.
Lab Technologist

Approved and Authorised By

Somchai J.
Machine Lubricant Analyst

A- 6. Bomb calorimeter test results

Analysis Report

Sample	Biodiesel
Sample owner	King Mongkut's Institute of Technology Ladkrabang
Objective	To analyse heating value of combustion
Instrument	Automatic Bomb Calorimeter ; Leco model AC - 500
Job ID	640707-9246
Analysis Date	July 28, 2021

Results

Sample name	Heating value of combustion (MJ/kg)		
	#1	#2	Average
Biodiesel B7	45.26	45.24	45.25
Biodiesel B10	45.80	45.46	45.63
Biodiesel B20	44.89	45.01	44.95
Biodiesel B100	39.84	40.03	39.94
Biodiesel B20E5	43.90	43.99	43.95
Biodiesel B20E10	42.66	42.78	42.72
Biodiesel B20E20	40.61	40.45	40.53

(Mrs. Aree Limnirandorn)
Analyst

Analysis Report

Sample	Biodiesel and Ethanol
Sample owner	King Mongkut's Institute of Technology Ladkrabang
Objective	To analyse heating value of combustion
Instrument	Automatic Bomb Calorimeter ; Leco model AC - 500
Analysis Date	September 20, 2021

Results

Sample name	Heating value of combustion (MJ/kg)		
	#1	#2	Average
Biodiesel B10E5	44.37	44.39	44.38
Biodiesel B10E10	43.27	44.03	43.65
Biodiesel B10E20	42.60	41.50	42.05
Biodiesel B100E5	39.21	39.42	39.31
Biodiesel B100E10	37.88	38.25	38.07
Biodiesel B100E20	38.15	38.01	38.08
EthanolE100	27.88	28.22	28.05

(Mrs. Aree Limnirandorn)
Analyst

A- 7. Chemical compositions test results

EagerSmart

Method name : CHNS
Method filename : E:\...\65-002\CHNS.mth

Detection and integration parameters

Time base : (s)
Peak width : 10
Peak threshold : 1
Minimum area : 1500
Skim ratio : 10
Next sample to acquire : 19
Real time plot scale : 10
Real time plot offset : 0

Time events table

#	Time	Events type	New value
1	.1	Disable integration	
2	35	Enable integration	
3	160	Change peak threshold	.1
4	160	Change skim ratio	1
5	160	Change peak width	40
6	500.3922	Disable integration	

Calculation and report parameters

Calibration method : Linear fit
Heat Value calc. : No
CO2 Emission Factor calc. : No
Protein calc. : No
Report on : None
Peak option : Only calibrated peaks
Report format : Default
Report publisher : No
Calibration report : Yes
Concentration unit :
Stripchart format : None
Autoscalling : ---
Stripchart full scale : 10
Stripchart scale offset : 0
Stripchart initial time : 0
Stripchart end time : 600
Append for summarize : Element %
Signal to noise report : Yes
Signal peak name :
Noise evaluation from/to : 0.0-0.0(s):

Custom report

Component table

#	Component name	Ret.T.	Window	Min. %	Max.%
1	Nitrogen	47	10		
2	Carbon	67	14		
3	Hydrogen	194	60		
4	Sulphur	412	88		

Calibration factors

#	Component name	Kb	Kc
1	Nitrogen	1995673	0
2	Carbon	4763351	0
3	Hydrogen	1.488643E+07	0
4	Sulphur	2078495	0

Standard table

Sample Num.4 Sample name: STD1 (BBOT 1.5 mg)
Filename: File004 STD1 (BBOT 1_5 mg) Std name: BBOT

#	Component name	Concentration	Valid
1	Nitrogen	6.53	Yes
2	Carbon	72.58	Yes
3	Hydrogen	6.1	Yes
4	Sulphur	7.41	Yes

Sample Num.5 Sample name: STD2 (BBOT 2 mg)
Filename: File005 STD2 (BBOT 2 mg) Std name: BBOT

#	Component name	Concentration	Valid
1	Nitrogen	6.53	Yes
2	Carbon	72.58	Yes
3	Hydrogen	6.1	Yes
4	Sulphur	7.41	Yes

Sample Num.6 Sample name: STD3 (BBOT 2.5 mg)
Filename: File006 STD3 (BBOT 2_5 mg) Std name: BBOT

#	Component name	Concentration	Valid
1	Nitrogen	6.53	Yes
2	Carbon	72.58	Yes
3	Hydrogen	6.1	Yes
4	Sulphur	7.41	Yes

Sample Num.7 Sample name: STD4 (BBOT 3 mg)
Filename: File007 STD4 (BBOT 3 mg) Std name: BBOT

#	Component name	Concentration	Valid
1	Nitrogen	6.53	Yes
2	Carbon	72.58	Yes
3	Hydrogen	6.1	Yes
4	Sulphur	7.41	Yes

Operator ID/info

Operator ID :
Company name :
Column type :
Column lenght :
Date packing :
Comment :

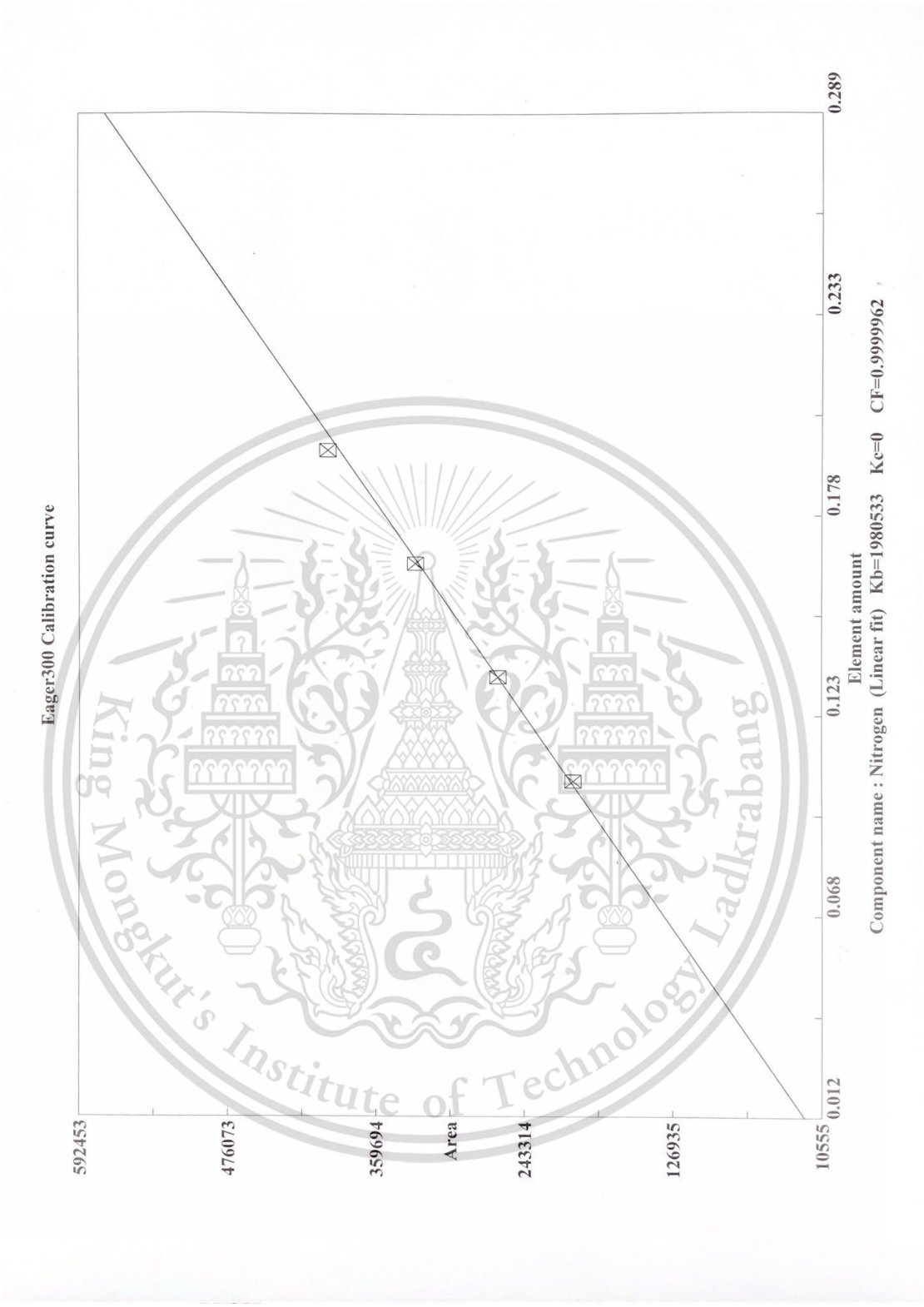

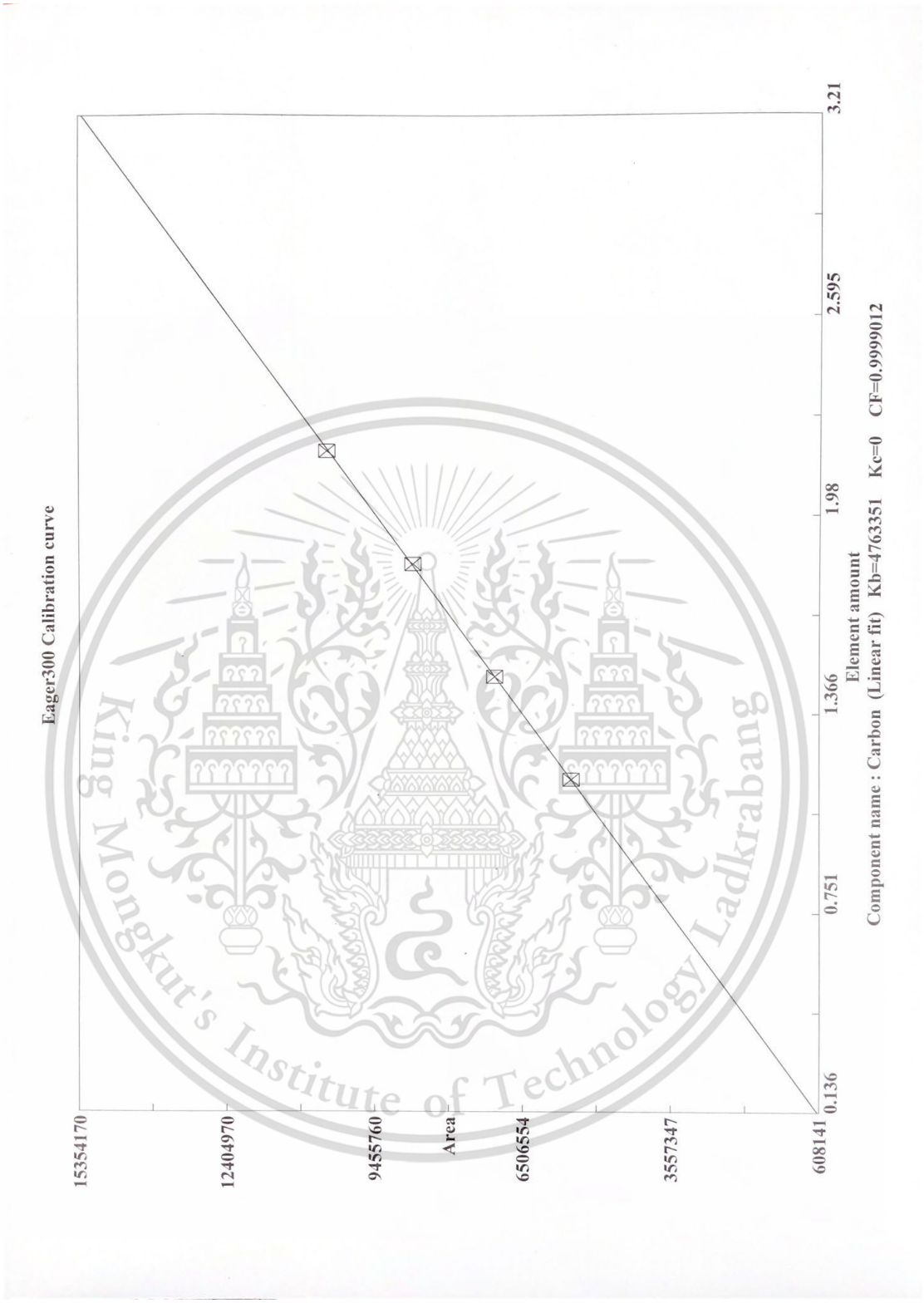

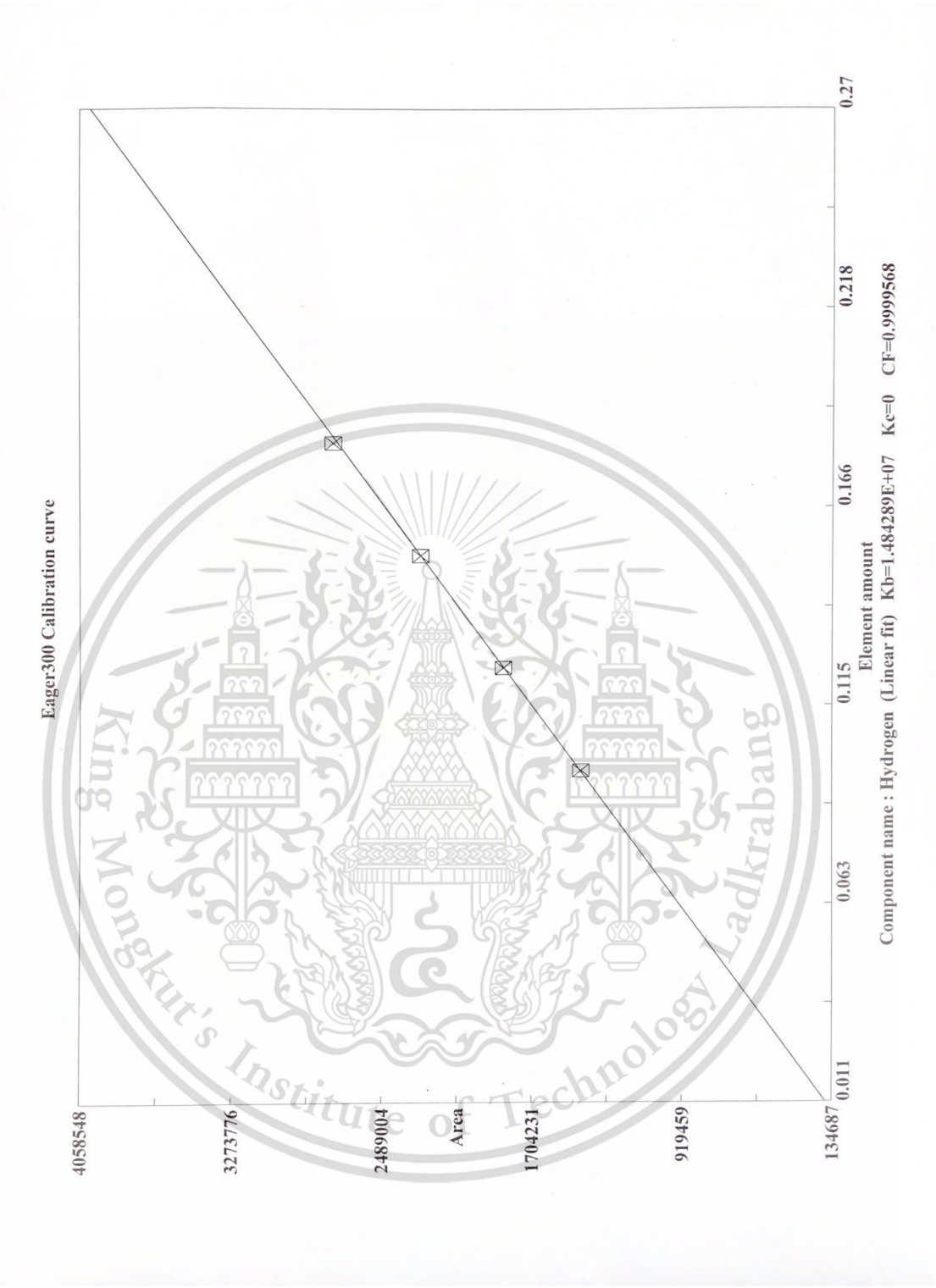

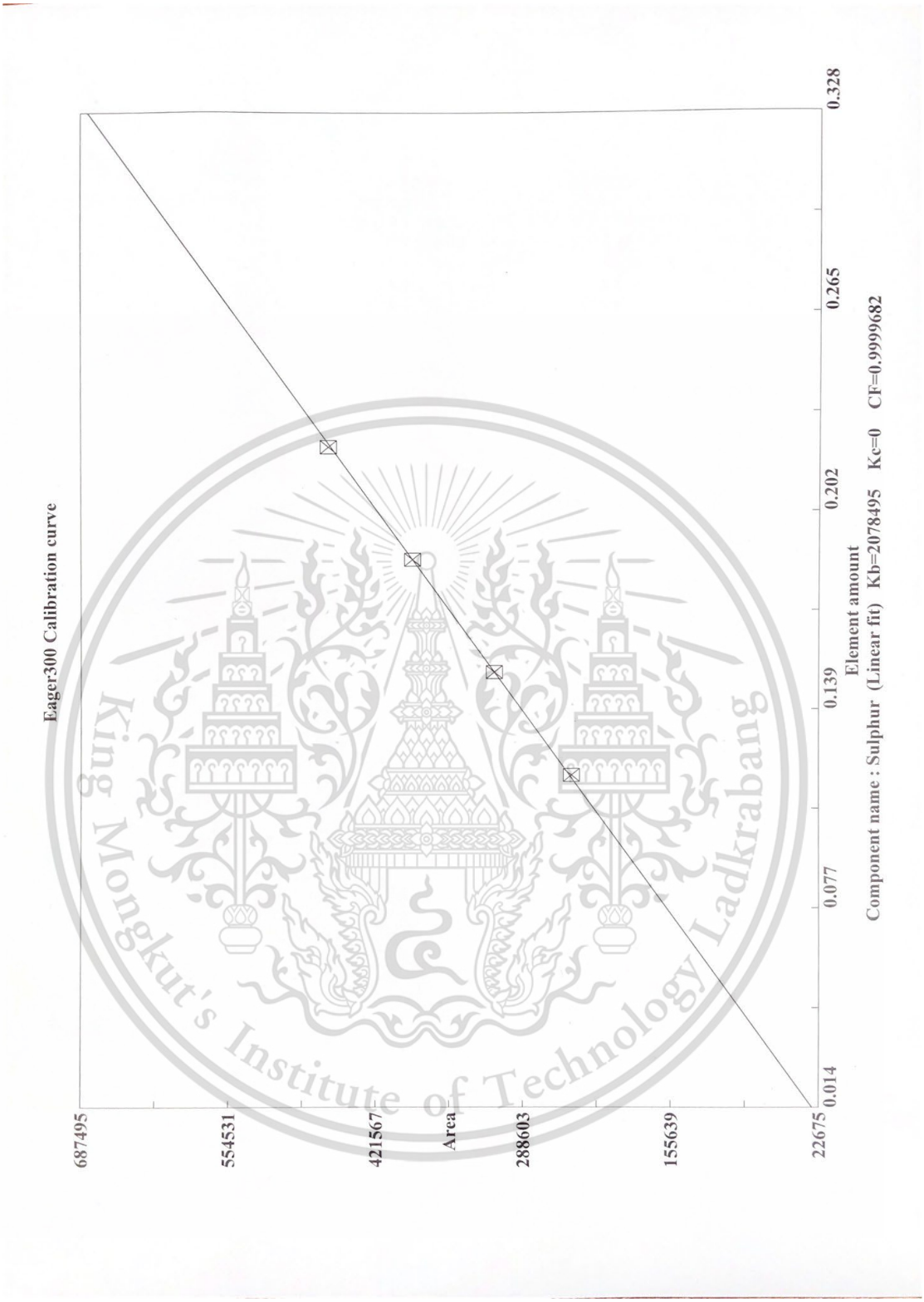

EagerSmart Summarize Results

Date : 11/08/2021 at 15:52:41
Method Name : CHNS
Method Filename : CHNS.mth

Group No : 1 Sample Name	Element % Nitrogen	Carbon	Hydrogen	Sulphur
B100_1	0	76.40828705	12.38687801	0
B100_4	0	77.04006958	12.53007603	0
B20_2	0	82.24542999	13.38155937	0
B20_3	0	82.98455048	13.52551937	0
B10_1	0	84.58450317	13.53221703	0
B10_2	0	84.74507141	13.58557034	0

6 Sample(s) in Group No : 1

Component Name	Average	Std. Dev.	% Rel. S. D.	Variance
Nitrogen	0	0.00000	0.0000	0.0000
Carbon	81.33465195	3.70018	4.5493	13.6913
Hydrogen	13.15697002	0.54714	4.1586	0.2994
Sulphur	0	0.00000	0.0000	0.0000

EagerSmart Summarize Results

Date : 11/08/2021 at 15:52:55
Method Name : CHNS
Method Filename : CHNS.mth

Group No : 1 Sample Name	Element % Nitrogen	Carbon	Hydrogen	Sulphur
B100_2	0.05251986906	76.13822174	0	0
B100_3	0.04693116993	76.21728516	0	0

2 Sample(s) in Group No : 1

Component Name	Average	Std. Dev.	% Rel. S. D.	Variance
Nitrogen	0.04972551949	0.00395	7.9472	0.0000
Carbon	76.17775345	0.05591	0.0734	0.0031
Hydrogen	0	0.00000	0.0000	0.0000
Sulphur	0	0.00000	0.0000	0.0000

APPENDIX B:

CONFERENCES PARTICIPATION

materialstoday: PROCEEDINGS

Volume 66, Part 5, 2022, Pages 2830-2835

Experimental investigation of the impact ethanol-biodiesel-diesel blended fuels on combustion, emission, and performance of compression ignition diesel engine

P. Wai [a], P. Karin [a], W. Phairote [a], N. Chollacoop [b], H. Kosaka [c], W. Po-ngen [d]

Show more

+ Add to Mendeley Share Cite

https://doi.org/10.1016/j.matpr.2022.06.524 Get rights and content

講演番号	344

文献番号	20225344

Combustion, Emission and Soot Analysis of Diesel-Biodiesel-Ethanol Blended Fuels on Common Rail Direct Injection Diesel Engine

Phyo Wai[1)] Preechar Karin[1)] Mek Srilomsak[1)] Watanyoo Phairote[1)] Nuwong Chollacoop[2)] Hidenori Kosaka[3)] and Watcharin Po-ngen[4)]

[1] *School of Engineering, King Mongkut's Institute of Technology Ladkrabang, Bangkok 10520, Thailand*
[2] *National Metal and Materials Technology Center, National Science and Technology Development Agency, Pathum Thani 12120, Thailand*
[3] *School of Engineering, Tokyo Institute of Technology, Tokyo 179-0085, Japan*
[4] *Faculty of Technical education, King Mongkut's University of Technology North Bangkok, Bangsue, Bangkok 10800, Thailand*

APPENDIX C:

PUBLICATION

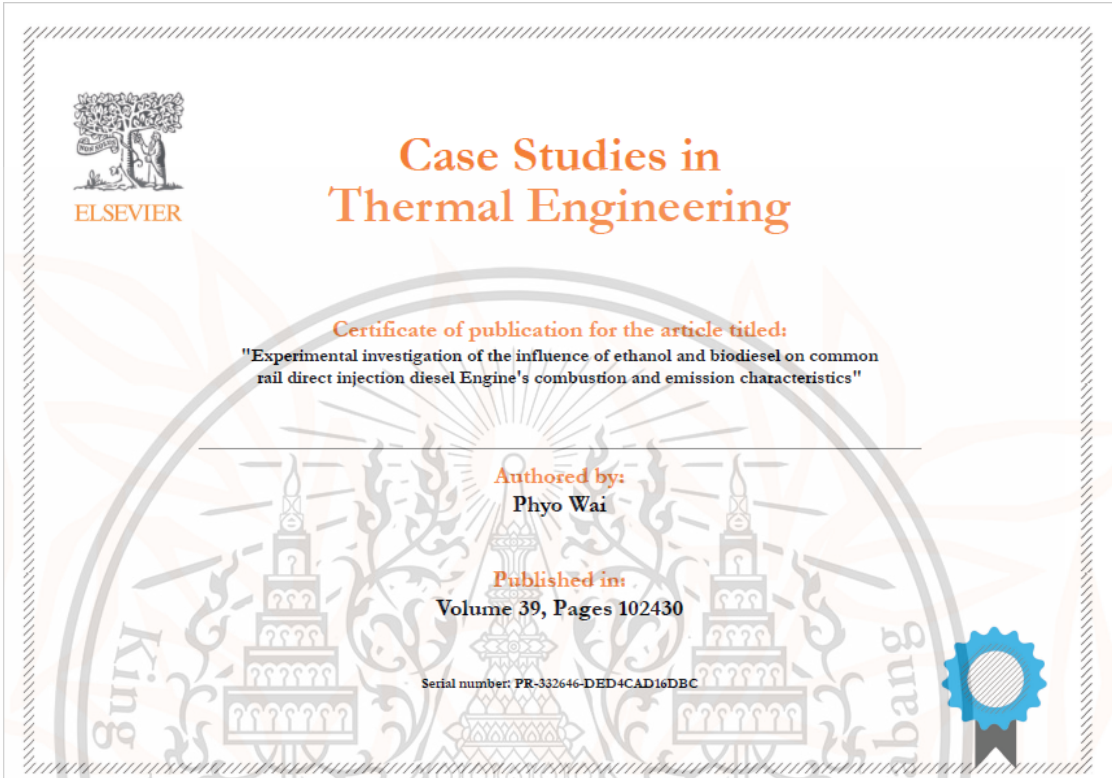

ELSEVIER

Case Studies in Thermal Engineering

Certificate of publication for the article titled:

"Experimental investigation of the influence of ethanol and biodiesel on common rail direct injection diesel Engine's combustion and emission characteristics"

Authored by:

Phyo Wai

Published in:

Volume 39, Pages 102430

Serial number: PR-332646-DED4CAD16DBC

Case Studies in Thermal Engineering 39 (2022) 102430

Contents lists available at ScienceDirect

Case Studies in Thermal Engineering

journal homepage: www.elsevier.com/locate/csite

Experimental investigation of the influence of ethanol and biodiesel on common rail direct injection diesel Engine's combustion and emission characteristics

Phyo Wai [a], Phobkrit Kanokkhanarat [a], Ban-Seok Oh [a], Veerayut Wongpattharaworakul [a], Nattawoot Depaiwa [a], Watcharin Po-ngaen [b], Nuwong Chollacoop [c], Chadchai Srisurangkul [d], Hidenori Kosaka [e], Masaki Yamakita [e], Chinda Charoenphonphanich [a], Preechar Karin [a,*]

[a] School of Engineering, King Mongkut's Institute of Technology Ladkrabang, Bangkok, 10520, Thailand
[b] Faculty of Technical Education, King Mongkut's University of Technology North Bangkok, Bangkok, 10800, Thailand
[c] National Energy Technology Center, National Science and Technology Development Agency, Pathum Thani, 12120, Thailand
[d] National Metal and Materials Technology Center, National Science and Technology Development Agency, Pathum Thani, 12120, Thailand
[e] School of Engineering, Tokyo Institute of Technology, Tokyo, 152-8552, Japan

ARTICLE INFO

Keywords:
Biodiesel
Ethanol
Diesel engine
Combustion characteristics
Particle emission

ABSTRACT

This study aims to characterize the effect of oxygenated biofuels in diesel engine combustion, thermal efficiency, and emission by blending different percentages of ethanol and biodiesel with fossil fuel derived diesel. In this research, 5% and 10% by weight of bioethanol were added to commercial B10 (10% biodiesel and 90% diesel), B20 (20% biodiesel and 80% diesel) and B100 (100% biodiesel) and experimented on using a 3 L four-cylinder common rail diesel engine. The experiment was performed under three engine speeds of 1000 rpm, 1500 rpm, and 2000 rpm with three constant engine torques of 56 Nm, 84 Nm, and 140 Nm. The results show that ethanol-biodiesel-diesel ternary blended fuels are higher in premixed combustion pressure and net heat release rate (NHRR) peaks. The cumulative heat release of ethanol blended fuels is also higher for ethanol blended fuels. The fuel consumption increased with the ethanol and biodiesel percentage in the blended fuels due to the lower heating value while the brake thermal efficiency did not decrease. It was clearly observed that the particle emission could be reduced by more than 50% when ethanol and biodiesel percentage increased.

* Corresponding author.
E-mail address: preechar.ka@kmitl.ac.th (P. Karin).

https://doi.org/10.1016/j.csite.2022.102430
Received 11 July 2022; Received in revised form 14 August 2022; Accepted 14 September 2022
Available online 15 September 2022

AUTHOR BIOGRAPHY

Author: Mr. Phyo Wai

Nationality: Myanmar

Email: 63601184@kmitl.ac.th

Education:

Master of Automotive and Advance Transportation Engineering
Faculty of Engineering, King Mongkut's Institute of Technology Ladkrabang

Bachelor of Engineering, Mechanical Engineering
Mandalay Technological University (COE)

Publications:

1) P Wai, P Karin, W Phairote, N Chollacoop, H Kosaka, W Po-ngen, "Experimental investigation of the impact ethanol-biodiesel-diesel blended fuels on combustion, emission, and performance of compression ignition diesel engine", Materials Today: Proceedings, Volume 66, Part 5, 2022, P:2830-2835, https://doi.org/10.1016/j.matpr.2022.06.524.
2) Phyo Wai, Preechar Karin, Mek Srilomsak, Watanyoo Phairote, Nuwong Chollacoop, Hidenori Kosaka, and Watcharin Po-ngen, "Combustion, Emission and Soot Analysis of Diesel-Biodiesel-Ethanol Blenaded Fuels on Common Rail Direct Injection Diesel Engine", 2022 JSAE Annual Congress (Spring), 2022.
3) Phyo Wai, Phobkrit Kanokkhanarat, Ban-Seok Oh, Veerayut Wongpattharaworakul, Nattawoot Depaiwa, Watcharin Po-ngaen, Nuwong Chollacoop, Chadchai Srisurangkul, Hidenori Kosaka, Masaki Yamakita, Chinda Charoenphonphanich, and Preechar Karin, "Experimental investigation of the influence of ethanol and biodiesel on common rail direct injection diesel Engine's combustion and emission characteristics", Case Studies in Thermal Engineering, Volume 39, 2022, https://doi.org/10.1016/j.csite.2022.102430.